Government of **Western Australia**
Department of **Mines and Petroleum**

RECORD 2013/11

GEOLOGICAL SETTING OF MINERAL DEPOSITS IN THE SOUTHERN CROSS DISTRICT — A FIELD GUIDE

compiled by
MP Doublier



Geological Survey of Western Australia

Centre for EXPLORATION TARGETING

CLIFFS

St Barbara Limited

WESTERN AREAS NL
ABN 68 091 049 357

Government of **Western Australia**
Department of **State Development**

Record 2013/11

GEOLOGICAL SETTING OF MINERAL DEPOSITS IN THE SOUTHERN CROSS DISTRICT — A FIELD GUIDE

compiled by
MP Doublier

Perth 2013

Geological Survey of Western Australia

MINISTER FOR MINES AND PETROLEUM
Hon. Bill Marmion MLA

DIRECTOR GENERAL, DEPARTMENT OF MINES AND PETROLEUM
Richard Sellers

EXECUTIVE DIRECTOR, GEOLOGICAL SURVEY OF WESTERN AUSTRALIA
Rick Rogerson

REFERENCE
The recommended reference for this publication is:
Doublier, MP (compiled by) 2013, Geological setting of mineral deposits in the Southern Cross district — a field guide: Geological Survey of Western Australia, Record 2013/11, 55p.

National Library of Australia Card Number and ISBN 978-1-74168-547-3

Grid references in this publication refer to the Geocentric Datum of Australia 1994 (GDA94). Locations mentioned in the text are referenced using Map Grid Australia (MGA) coordinates, Zone 50. All locations are quoted to at least the nearest 100 m.

Published 2013 by Geological Survey of Western Australia
This Record is published in digital format (PDF) and is available online at <www.dmp.wa.gov.au/GSWApublications>.

Further details of geological products and maps produced by the Geological Survey of Western Australia are available from:
Information Centre
Department of Mines and Petroleum
100 Plain Street
EAST PERTH WESTERN AUSTRALIA 6004
Telephone: +61 8 9222 3459 Facsimile: +61 8 9222 3444
www.dmp.wa.gov.au/GSWApublications

Contents

Figures

Tables

Geological setting of mineral deposits in the Southern Cross district — a field guide

compiled by
MP Doublier

with contributions from
MP Doublier, N Thébaud[1], J Collins[1], T Angerer[1], W Witt[2], S Shenton[3], SG Hagemann[1], CL Kirkland, DR Mole[1], TC McCuaig[1], SS Romano, and MTD Wingate

Preface

The Southern Cross district in the Yilgarn Craton is a historic mining area with significant economic gold, nickel and iron deposits. These deposits share the characteristic that their formation is closely linked with the structural setting of the Southern Cross greenstone belt at regional or deposit scale, or both.

This field guide describes operating gold, nickel and iron mines at Koolyanobbing, Marvel Loch and the Forrestania area and investigates their structural and stratigraphic context. It also describes several outcrops that represent examples of structural styles and rock types common in the area.

Much of the new data presented here are the outcome of ARC Linkage Project LP100100647: Tectonic evolution and lode gold mineralization in the Southern Cross district, Yilgarn Craton: a study of the Meso- to Neo-archean missing link. We also gratefully acknowledge support from St Barbara Ltd, Western Areas NL, and Cliffs Natural Resources.

Yilgarn Craton

Introduction

by MP Doublier

The Yilgarn Craton of Western Australia is a Paleo- to Neo-archean craton composed of various terranes that can be distinguished based on geochemical, geochronological and stratigraphic criteria (Fig. 1; Cassidy et al., 2006).

1 Centre for Exploration Targeting, The University of Western Australia, 35 Stirling Highway, M006, Crawley WA 6009

2 The Walter Witt Experience, 122 Edward Street, Bedford WA 6052

3 St Barbara Limited, 1205 Hay Street, West Perth WA 6005

The South West and Narryer Terranes contain the overall lowest proportion of greenstones and are the only terranes where widespread granulite facies metamorphism is exposed. Together with the Youanmi Terrane, they form the western Yilgarn, which is separated from the Eastern Goldfields Superterrane by the crustal-scale Ida Fault (Drummond et al., 2000).

The Youanmi Terrane and the Eastern Goldfields Superterrane contain substantial greenstone belts, which are separated by granite and gneiss. The Youanmi Terrane comprises the Murchison and Southern Cross Domains, and the Eastern Goldfields Superterrane is subdivided, from west to east, into the Kalgoorlie, Kurnalpi, Burtville and Yamarna Terranes (Cassidy et al., 2006; Pawley et al., 2012).

Isotopic data

Isotopic data reveal differences in the crustal evolution of the different crustal blocks: Sm–Nd model ages are younger in the Eastern Goldfields Superterrane, and overall older and more heterogeneous in the western Yilgarn, with the oldest model ages mainly observed in the Narryer Terrane (Fig. 2; Champion and Cassidy, 2007). The Sm–Nd results are in accordance with more recent Lu–Hf data (Fig. 3). Zircons from the Youanmi Terrane are typically characterized by negative εHf values, which suggests that the sources to the host magmas have undergone crustal reworking. In contrast, the mainly positive εHf values from the Eastern Goldfields Superterrane indicate juvenile source input (Wyche et al., 2012; Mole et al., 2011).

Taken together, the isotopic evidence supports the proposal that the Youanmi Terrane forms part of a proto-Yilgarn Craton, to which the elements of the Eastern Goldfields Superterrane were accreted (i.e. Czarnota et al., 2010).

Supracrustal rock record

The oldest supracrustal rocks identified in the Yilgarn Craton are from the Narryer Terrane, where Rasmussen

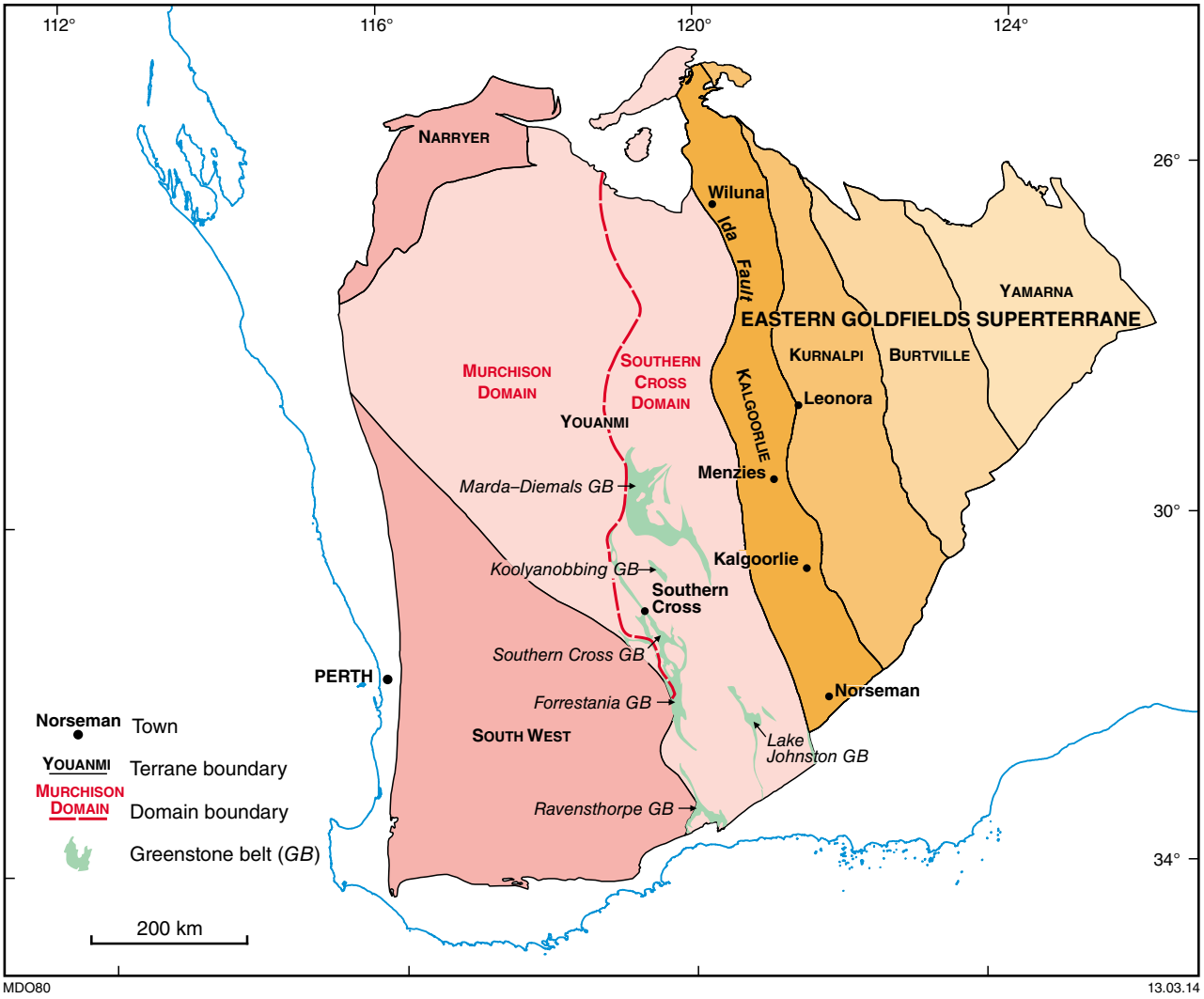

Figure 1. Terrane subdivision of the Yilgarn Craton after Cassidy et al. (2006), modified by Pawley et al. (2009); from Wyche et al. (2012)

et al. (2010) dated secondary xenotime and monazite in banded iron-formation (BIF) at c. 3080 Ma, which provides a minimum depositional age for these rocks.

Supracrustal rocks from the South West Terrane are typically preserved as isolated greenstone belts (Wilde, 2001). The rock record includes quartzites with old detrital zircons, similar to those in the Narryer and Youanmi Terranes, but with a different provenance (Pidgeon et al., 2010). However, there are also supracrustal rocks that range in age from 2715 to 2670 Ma (Wilde and Pidgeon, 1986; Allibone et al., 1998).

The spatial distribution and timing of greenstone formation in the Youanmi Terrane and the Eastern Goldfields Superterrane has recently been summarized by Pawley et al. (2012). In Fig. 4, the Youanmi Terrane is represented by the Murchison Domain, for which a detailed regional stratigraphy has been established (e.g. Van Kranendonk and Ivanic, 2009). The Southern Cross Domain will be discussed separately (see section 'Southern Cross Domain'). Apart from the easternmost Yamarna Terrane, which is relatively poorly exposed, all terranes record an early phase of greenstone deposition ≥2900 Ma, and a hiatus in greenstone deposition between c. 2900 Ma and >2820 Ma (Pawley et al., 2012; Van Kranendonk et al., 2013). From this time onwards, the record between the Youanmi Terrane and the Eastern Goldfields Superterrane is different in character, except for the Burtville Terrane, which shows affinities with the Youanmi Terrane. Between c. 2820 and 2710 Ma, three greenstone groups were deposited in the Murchison Domain in (ultra)mafic to felsic cycles with breaks in magmatism reflected by deposition of BIF (Van Kranendonk et al., 2013). The oldest of these cycles (Norie Group) is synchronous to the emplacement of large, layered mafic–ultramafic igneous complexes such as the Windimurra and Narndee Igneous Complexes of Ivanic et al. (2010). It is notable that these complexes are located within a corridor of young Sm–Nd model ages (Fig. 2). Greenstones and mafic intrusions ranging from

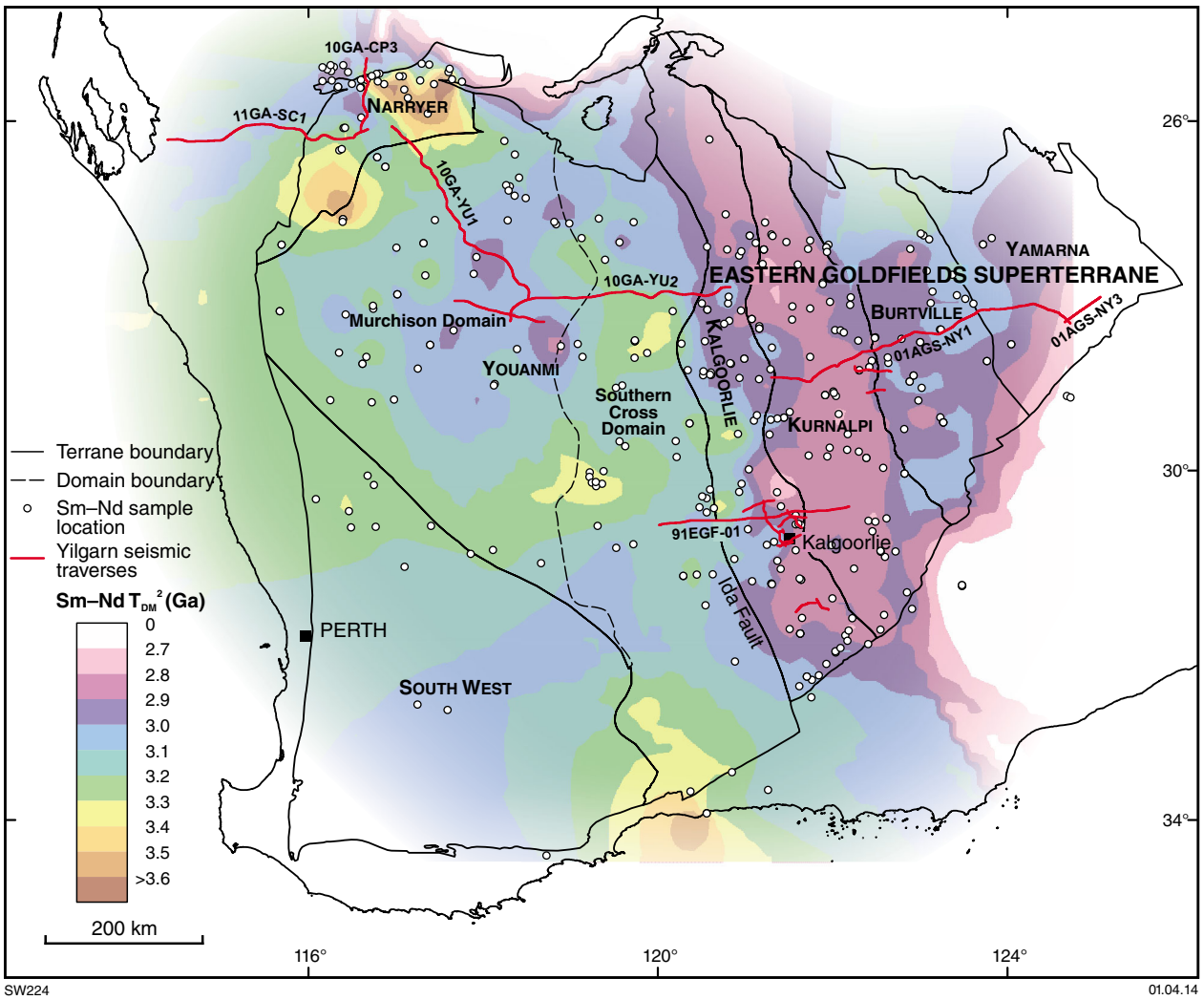

Figure 2. Two-stage Sm–Nd depleted-mantle model age map of the Yilgarn Craton. Modified after Champion and Cassidy (2007) by Wyche at al. (2012)

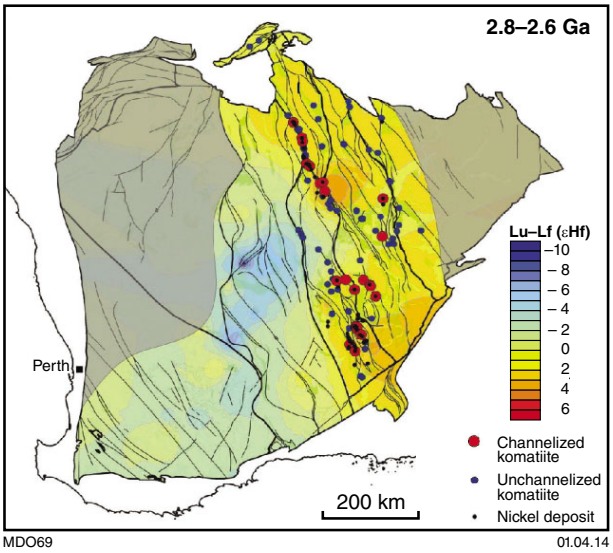

Figure 3. Lu–Hf isotope map of the Yilgarn Craton for the 2800–2600 Ma εHf time slice, together with the distribution of channelized/unchannelized komatiite flows of that age (after Mole et al., 2011)

2815–2785 Ma have also been described in the Burtville Terrane (Pawley et al., 2012). This rock record has been interpreted to reflect a mantle plume event at 2820–2790 Ma (Ivanic et al., 2010; Van Kranendonk et al., 2013).

Widespread greenstone deposition in the Kalgoorlie and Kurnalpi Terranes at 2720–2710 Ma shows some time overlap with the Glen Group of the Murchison (2735–2710 Ma). The Kalgoorlie Terrane greenstone stratigraphy has been subdivided into a 2710–2690 Ma tholeiitic to komatiitic Kambalda Sequence (Krapež and Hand, 2008), which is attributed to a second, major plume event (Campbell and Hill, 1988). The Kambalda Sequence is overlain by the Kalgoorlie Sequence. The latter mainly consists of felsic volcanic and volcaniclastic rocks, and conglomerates, which have been attributed by Squire et al. (2010) to two depositional cycles. The older cycle deposited between c. 2690 and 2670 Ma is the Black Flag Group, which hosts economically important dolerite bodies such as the Golden Mile Dolerite. The second cycle includes the Merougil Group, which was deposited between c. 2670 and 2658 Ma. The supracrustal rocks of the Kurnalpi Terrane include 2720–2700 Ma mafic volcanic rocks and calc-alkaline complexes and 2692–2680 Ma bimodal (basalt–rhyolite) volcanic complexes and associated intrusive and sedimentary rocks (Barley et al., 2008).

The Kurrawang Formation is the youngest sedimentary unit (2658–2655 Ma) and consists of polymictic conglomerates and sandstones (Squire et al., 2010). These rocks, commonly called 'late basins' (Krapež et al., 2008), overlie all other greenstones in the Eastern Goldfields Superterrane.

Granite magmatism

Granites and granitic gneisses occupy about 75% of the Yilgarn Craton and the rock record is overwhelmingly dominated by the youngest period of magmatism between c. 2720 and 2620 Ma (Figs 4 and 5). This record is biased due to the increasingly poor preservation potential of granite bodies with increasing age during periods of crustal reworking, a process which is evident from the isotopic record and granite geochemistry (Champion and Cassidy, 2002). Inherited zircon grains have proven invaluable in helping to decipher periods of magmatism and crustal melting. Recent compilations of magmatic and inherited granite geochronology show that, although granites and gneisses older than c. 2800 Ma are poorly preserved (Pawley et al., 2012), granite magmatism of this age and older is well documented by the inherited zircon record (Mole et al., 2012; Van Kranendonk et al., 2013). Although some magmatic events can be recognized across the whole of the Yilgarn Craton, other

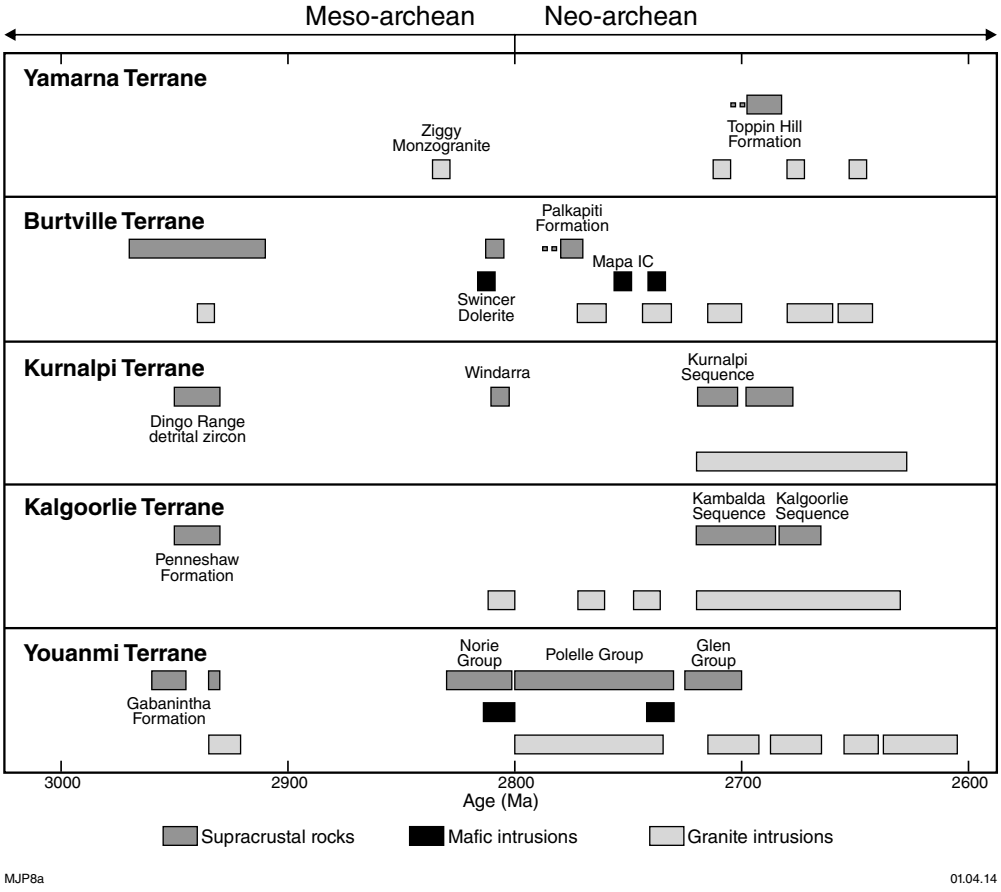

Figure 4. Simplified time–space plot of the major greenstone and granite events for the Youanmi (mainly Murchison) and Eastern Goldfields Superterrane (after Pawley et al., 2012). Note that the 'granite intrusions' do not include the detrital/inherited zircon record.

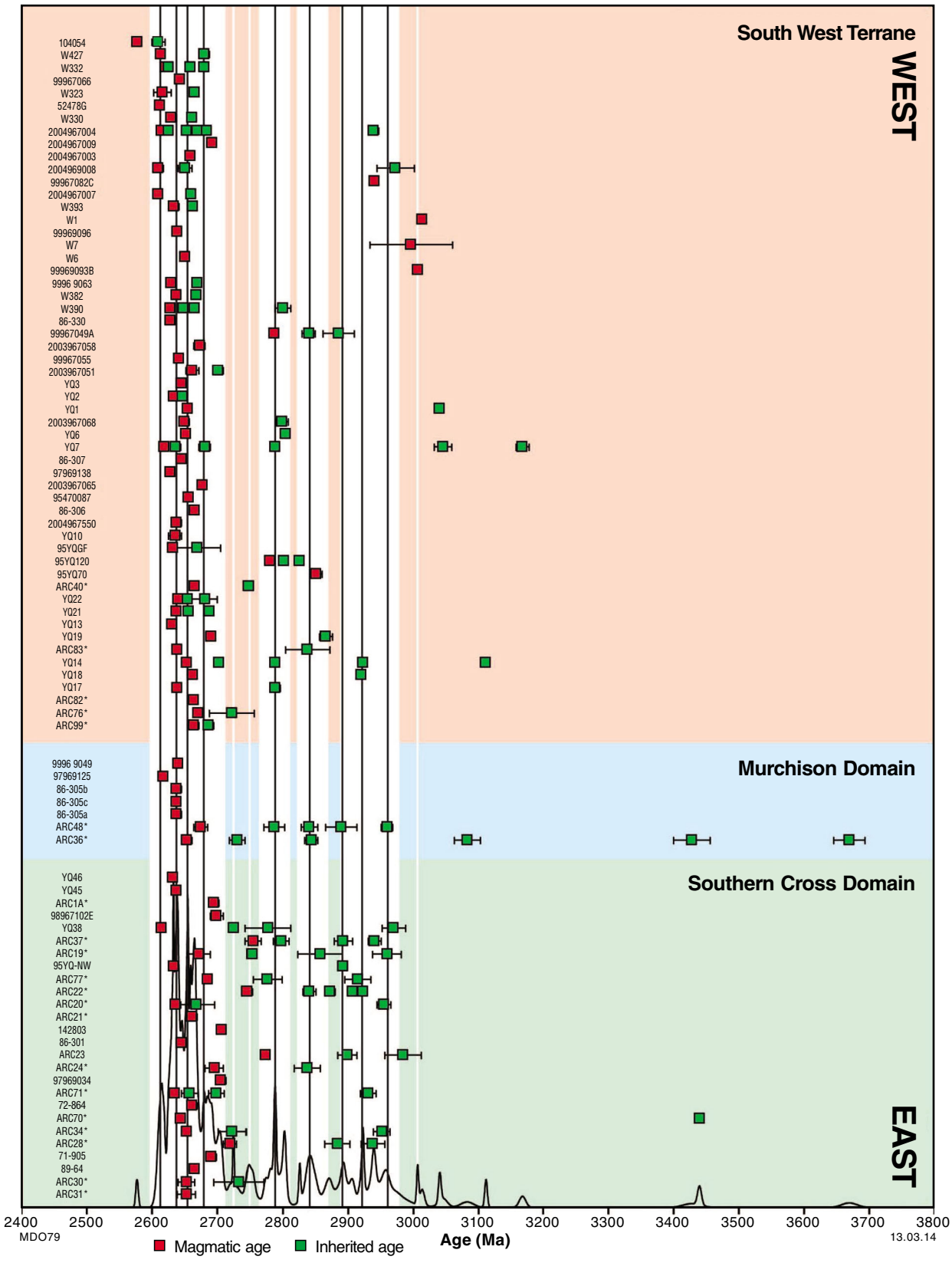

Figure 5. Time–space plot of granitization within the Southern Cross and southern-most Murchison Domains and the South West Terrane (after Mole et al., 2012)

magmatic pulses may vary between crustal blocks, or are restricted to certain areas. For example, a hiatus of magmatism between c. 2890 and 2830 Ma is observed in the Murchison Domain (Van Kranendonk et al., 2013), a period where felsic magmatism in the Southern Cross Domain and the South West Terrane is well documented (Mole et al., 2012). Typically, the periods of extensive greenstone formation, which some authors have linked to mantle plume events (Van Kranendonk et al., 2013), are accompanied by granitic magmatism. This magmatism is either contemporaneous with greenstone deposition (Eastern Goldfields Superterrane), or slightly delayed with respect to the commencement of greenstone deposition (Murchison Domain; Van Kranendonk et al., 2013).

Based mainly on data from the Youanmi Terrane and the Eastern Goldfields Superterrane, the Yilgarn granites have been subdivided into five groups using geochemical, petrological and geochronological criteria (Champion and Sheraton 1997; Champion and Cassidy, 2002): i) high-Ca granites; ii) low-Ca granites; (iii) high-HFSE (high high field strength elements) granites; (iv) mafic granites; and (v) syenites. The dominant group is the high-Ca group in all provinces, which typically comprises more than 50% of the recognized granites, followed by the low-Ca granites. Both groups may form more than 80% of the granites within the respective areas (Champion et al., 2002). The authors show that the timing of the different groups varies across the craton, with the Eastern Goldfields Superterrane being distinctly different from the Youanmi Terrane (Fig. 6; Champion et al., 2002). From a petrogenetic point of view, the widespread distribution of the low-Ca granite magmatism between c. 2650 and 2630 Ma is a very important event for the tectonic evolution of the craton: the geochemical character of these granites is most consistent with melting under moderate pressures (<10 kbar) from reworked continental crust (Champion and Cassidy, 2002). Granites of such affinities are usually found in regions undergoing extension or attenuation, or regions above mantle hot spots (Champion et al., 2002). This is remarkably different from the typically older high-Ca granites, which indicate melting at higher pressures (10–15 kbar), either deep within a thickened crust, or possibly from melting of a subducting slab (Champion and Cassidy, 2002) — both scenarios linked to contractional tectonics. Hence, the transition from high-Ca to low-Ca granite magmatism possibly reflects a (craton-scale) change in the overall tectonic environment (Champion and Cassidy, 2002).

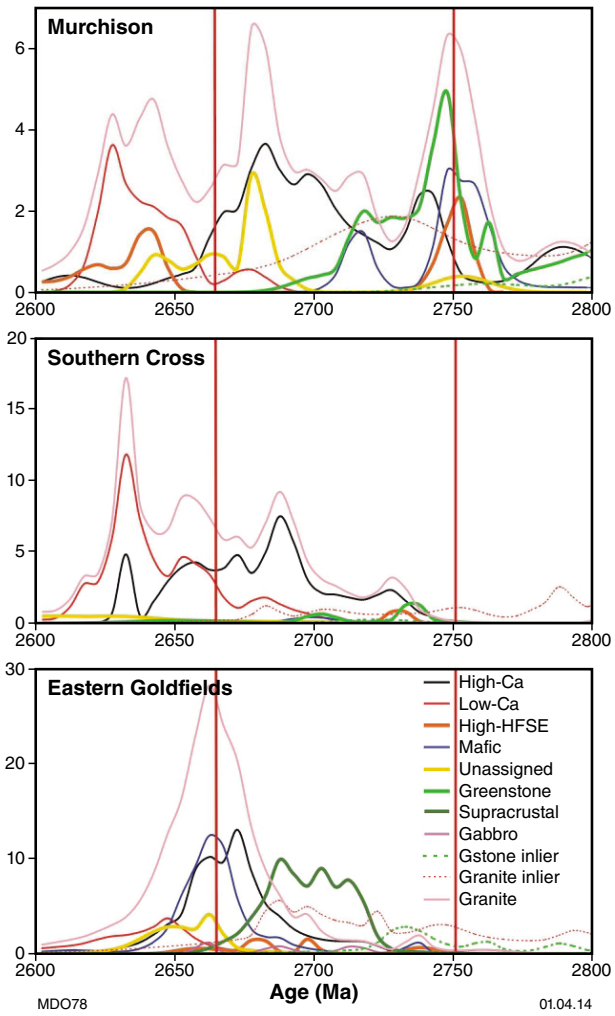

Figure 6. Frequency plots illustrating the variations of the different granite groups through time in the Youanmi Terrane and the Eastern Goldfields Superterrane (after Champion et al., 2001)

Southern Cross Domain

by MP Doublier, N Thébaud, DR Mole, and SS Romano

Stratigraphy

Compared to adjacent terranes and domains, most of the upper crustal record in the Southern Cross Domain lacks suitable rocks for geochronology (i.e. felsic volcanic rocks), and hence establishment of a stratigraphy over much of the area has proven difficult. In what follows, a brief description of the lithostratigraphy, together with a compilation of existing geochronological constraints, is provided for several greenstone belts in the central and southern part of the domain. In all the greenstone belts, the rocks are metamorphosed to at least greenschist facies, and for clarity the 'meta' prefix is omitted.

The central Southern Cross Domain (Marda–Diemals greenstone belt)

In the northern Southern Cross Domain, the lowest exposed part of the greenstone succession is represented by quartzites or quartz-rich sedimentary rocks, which typically contain old detrital zircons up to c. 4350 Ma, and are either in faulted contact with, or intruded by, younger granites (Wyche et al., 2004).

In the Marda–Diemals greenstone belt (Fig. 1) in the central part of the domain, Chen et al. (2003) described two greenstone successions, which are considered as representative for wider parts of the northern Southern Cross Domain (Riganti et al., 2010). The lower succession consists of a lower association dominated by basalt, overlain by a middle association characterized by a thick unit of chemical sedimentary rocks (i.e. BIF and chert), and an upper association with a higher proportion of komatiitic basalt, intercalated shales and gabbros in the Diemals area (Fig. 7). There are no direct depositional ages on the lower succession, but an upper age constraint is provided by a gabbroic sill (Grass Flat Gabbro), which intruded into cherts and overlying komatiitic basalts at c. 2796 Ma (GSWA 185990, Wingate et al., 2011).

The upper succession is formed by the c. 2732 Ma Marda Complex (GSWA 168960, Nelson 2001) and the Diemals Formation, which both rest uncomformably upon the lower succession. The lower part of the former consists of conglomerates, sandstones and siltstones and is conformably overlain by rhyolite, andesite and subordinate dacite (Fig. 8; Chen et al., 2003). The Diemals Formation contains various clastic sedimentary rocks (Fig. 8). A westward-fining grain size in the lower part of the formation has been taken to indicate an alluvial to fluviatile depositional environment in the eastern part and a lacustrine to shallow-marine environment in the western part (Chen et al., 2003; Morris et al., 2007). While the conglomerates in the lower part of the succession have a compositional affinity with the greenstones, the sedimentary rocks in the upper part record a substantial contribution from granitic rocks, and immature lithic sandstones suggesting rapid deposition in an unstable

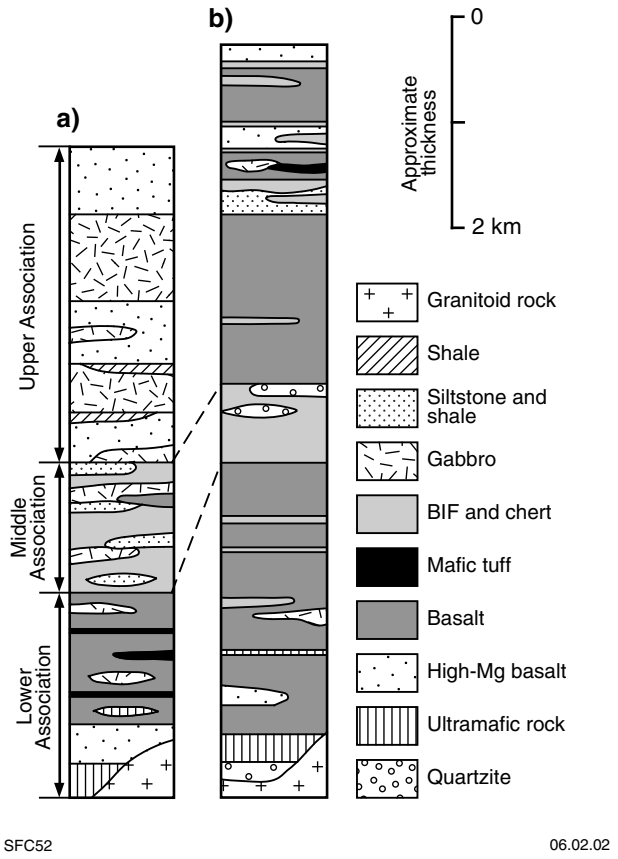

Figure 7. Lithostratigraphic columns of the lower greenstone sequence in the (a) Diemals area; (b) the Bungalbin–Marda area (after Chen et al., 2003)

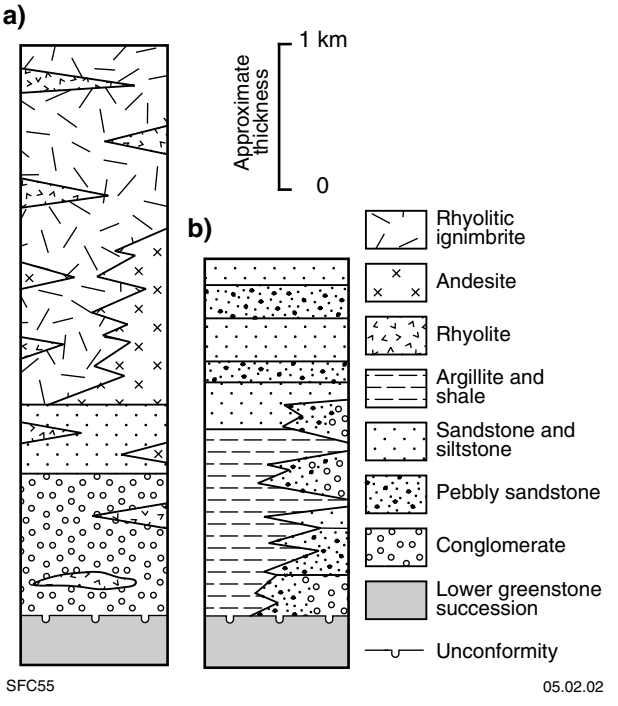

Figure 8. Lithostratigraphic columns of the (a) Marda Complex; (b) Diemals Formation (after Chen et al., 2003)

tectonic environment (Chen et al., 2003; Morris et al., 2007). Analysis of detrital zircons from a sandstone of the Diemals Formation yielded a range of SHRIMP U–Pb ages and a likely maximum depositional age of c. 2701 Ma (GSWA 185988, Wingate et al., 2012a), which indicates that deposition of the Diemals Formation was younger than formation of the Marda Complex.

Koolyanobbing greenstone belt

The age of the Koolyanobbing greenstone belt to the south of the Marda–Diemals greenstone belt is unconstrained. The greenstone sequence does not include equivalents of either Marda Complex or Diemals Formation and recent work by Angerer et al. (2012) suggests the existence of four magmatic cycles separated by BIF horizons (see section 'Locality 3').

The southern Southern Cross Domain

Based on ages of felsic intrusive rocks ('porphyries') within the lower parts of the greenstone succession, the Southern Cross – Forrestania and the Lake Johnston greenstone belts have been interpreted to be older than 2900 Ma (Wang et al., 1996; Mueller and McNaughton, 2000). Current collaborative work between the Geological Survey of Western Australia (GSWA) and the Centre for Exploration Targeting (CET) has provided increasing evidence that the supracrustal rocks of these greenstone belts are at least partly younger than c. 2900 Ma. The rocks of this area have been typically metamorphosed in the amphibolite facies.

Lake Johnston greenstone belt

A stratigraphy for the Lake Johnston greenstone belt in the southeastern part of the domain, first proposed by Gower and Bunting (1976), was recently refined by Heggie et al. (2012) and Romano et al. (2010). The lowest part of the stratigraphy is represented by the Maggie Hays Formation, which consists of a thick package of basalt in its lower part, overlain by a sequence of mafic volcaniclastic rocks, hyaloclastites and thin lava flows, interbedded with minor quartz-rich sedimentary rocks (Fig. 9; Romano et al., 2010). The package is intruded by numerous dolerite dykes, quartzofeldspathic sills, and by sills of the mafic–ultramafic intrusive rocks of the Lake Medcalf Igneous Complex, which is mainly exposed in the southern part of the belt. The overlying Honman Formation grades from dacitic to rhyolitic volcanic to volcaniclastic rocks into a clastic sedimentary package. At the top of the Honman Formation is a prominent package of dominantly chemical sedimentary rocks with quartzite, chert and BIF. Intrusive and extrusive ultramafic rocks and komatiites within and above the Honman Formation are likely a separate formation (Romano et al., 2013). One of the intrusive units, the 'Central Ultramafic Unit' (Heggie et al., 2012; Buck et al., 1998), hosts the Maggie Hays nickel deposit. The uppermost unit of the succession is the Glasse Formation, which is dominated by massive basalt (Fig. 9).

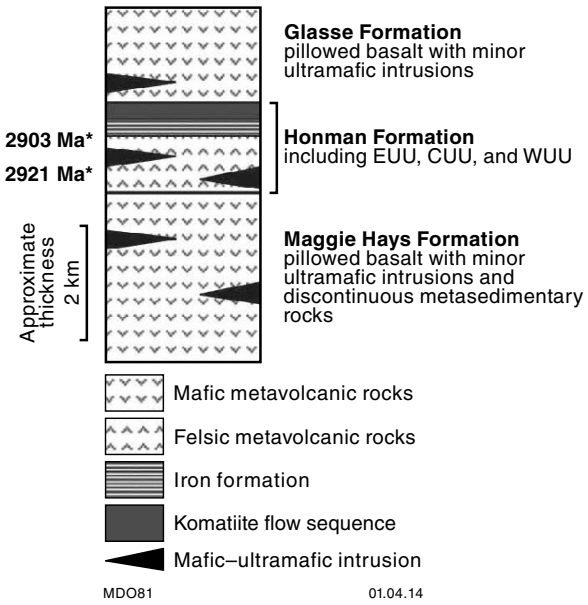

Figure 9. Lithostratigraphy of the Lake Johnston greenstone belt (modified from Heggie et al., 2012)

Felsic volcaniclastic rocks of the Honman Formation yielded a maximum depositional age of c. 2873 Ma (SHRIMP U–Pb; Thébaud et al., 2009; Romano et al., in revision), which is substantially younger than the previous age constraints obtained on porphyritic felsic rocks from the Honman Formation dated at c. 2912 and 2903 Ma (Wang et al., 1996). The authors interpreted a young (c. 2858 Ma) zircon age component in Wang et al. (1996) to reflect a metamorphic event. This interpretation has been challenged by Romano et al. (2010), who pointed out that Th/U ratios of zircons are not conclusive evidence of metamorphic growth. Regardless, the upper part of the Honman Formation and overlying Glasse Formation must have been deposited after 2873 Ma.

If, as proposed by Heggie et al. (2012), the ultramafic units within the Honman Formation are intrusive equivalents of the effusive komatiites on top of the Honman Formation, these new geochronological data suggest that the effusive komatiites and intrusive ultramafic rocks and associated mineralization are younger than 2873 Ma (Romano et al., 2010). A minimum age for the entire succession is given by intrusive granites at c. 2770 Ma (Romano et al., 2010).

Southern Cross – Forrestania greenstone belt

A detailed stratigraphy for the Southern Cross greenstone belt and the Forrestania greenstone belt, which represents its lateral continuity to the south, is difficult to establish due to its complex structural framework. The sequence of the former broadly consists of a lower volcanic succession, up to 5 km thick, overlain by at least 2 km of clastic sediments (Fig. 10). The lower part of the volcanic succession consists of tholeiitic and komatiitic

basalt, and the upper part is dominated by komatiites and other ultramafic rocks. Several thin units of BIF are interbedded with the volcanic rocks, and minor amounts of gabbro have intruded the sequence. The basal part of the sedimentary package is represented by black mudstone ('black shale'), which is overlain by a mixed succession of psammitic and pelitic units, and minor quartzite and conglomerate.

Based on SHRIMP U–Pb ages of zircons from 'altered quartz porphyry sills' (Mueller and McNaughton, 2000) at the Southern Star (c. 2934 Ma; interpreted as a magmatic age) and Copperhead deposits (c. 2912 Ma; interpreted as a minimum age), it was until recently thought that the Southern Cross greenstones were deposited prior to 2900 Ma. However, a new SHRIMP U–Pb zircon age from the sedimentary succession, west of the Hopes Hill mine, indicates a maximum depositional age of c. 2700 Ma (Thébaud et al., in prep.). This date suggests that at least the upper part of the stratigraphy is considerably younger than 2900 Ma, and possibly an equivalent of the Diemals Formation in the Marda–Diemals greenstone belt.

Like the Southern Cross greenstone belt, the stratigraphy of the Forrestania greenstone belt is affected by structural complexity. The rock record comprises a lower volcanic/magmatic component and an upper sedimentary succession (Chin et al., 1984), which represents the lateral continuation of the upper succession at Southern Cross (Gee, 1995). The lower succession is predominantly mafic but contains at least four units of komatiitic rocks, partly intercalated with BIF (Perring et al., 1997) and clastic sediments. A recent study of the geochemistry of ultramafic units in the Southern Cross greenstone belt suggests that not all units within the Forrestania belt have obvious correlatives in the Southern Cross greenstone belt (Thébaud and Barnes, 2012). This could indicate a different stratigraphic component within the Forrestania belt. This is supported by the observation that clastic sediments are intercalated within the lower sequence (see section on Flying Fox deposit in 'Locality 1' for an example), although the contact relationships are not always clear, and contacts with the magmatic rocks are at least partly tectonic. A sample from the Spotted Quoll mine in the Forrestania greenstone belt yielded a maximum depositional age of c. 2832 Ma (Doublier et al., 2012) that, although substantially older than the maximum depositional ages from the Southern Cross sediments (Thébaud and Miller, 2009), also indicates sedimentation (and presumably mafic–ultramafic magmatism) after c. 2830 Ma.

Ravensthorpe greenstone belt

The Ravensthorpe greenstone belt is the southernmost belt in the Southern Cross Domain and consists of three tectonostratigraphic units with a complex tectono-metamorphic history (Witt, 1998, 1999): during an accretionary event, the Ravensthorpe 'Terrane' and the Cocanarup greenstones were thrust eastward over the Carlingup 'Terrane'. The supracrustal Archean rock record differs between the units (e.g. Witt, 1997).

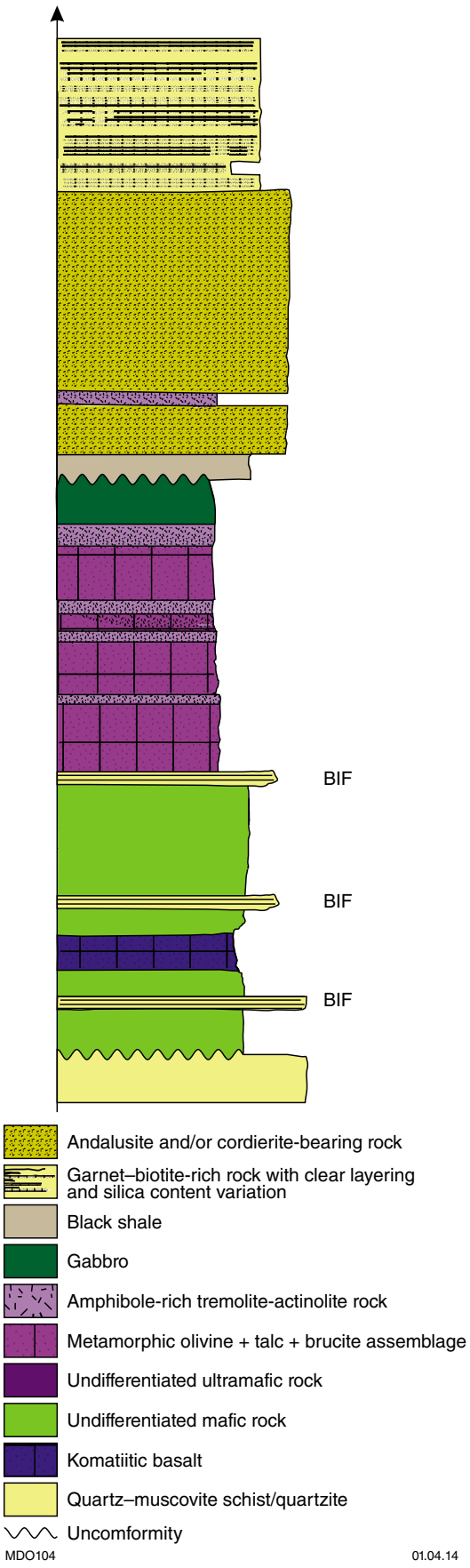

Figure 10. Lithostratigraphy of the central Southern Cross greenstone belt (after Thébaud and Miller, 2009)

The Ravensthorpe 'Terrane' consists of the Manyutup Tonalite Complex and the Annabelle Volcanics, which are dominated by andesitic to dacitic agglomerates and tuffs, and minor basalts. The Cocanarup greenstones are dominated by sedimentary rocks with minor BIF and mafic and ultramafic rocks. For the Carlingup 'Terrane', Witt (1997) proposed a formal stratigraphy (Fig. 11). In this scheme, shales, siltstones, lithic sandstones and several BIF units of the Chester Formation are in faulted contact with the overlying Bandalup Ultramafics. The upper part of the stratigraphy is formed by the Maydon Basalt and the sedimentary Hatfield Formation, which contains minor dacitic volcanic and volcaniclastic rocks. The stratigraphic relationship between the tectonostratigraphic units, as well as the stratigraphic context of the Ravensthorpe greenstone belt within the Southern Cross Domain is uncertain. However, a rhyolite from the Carlingup 'Terrane', which could not be assigned to a formal unit, yielded a U–Pb zircon date of c. 2958 (Nelson, 1995). This date is interpreted as the age of deposition, and indicates that at least parts of the sequence are older than 2900 Ma. This is the only result from the supracrustal rocks of the Ravensthorpe greenstone belt; hence correlations with other greenstone belts remain speculative.

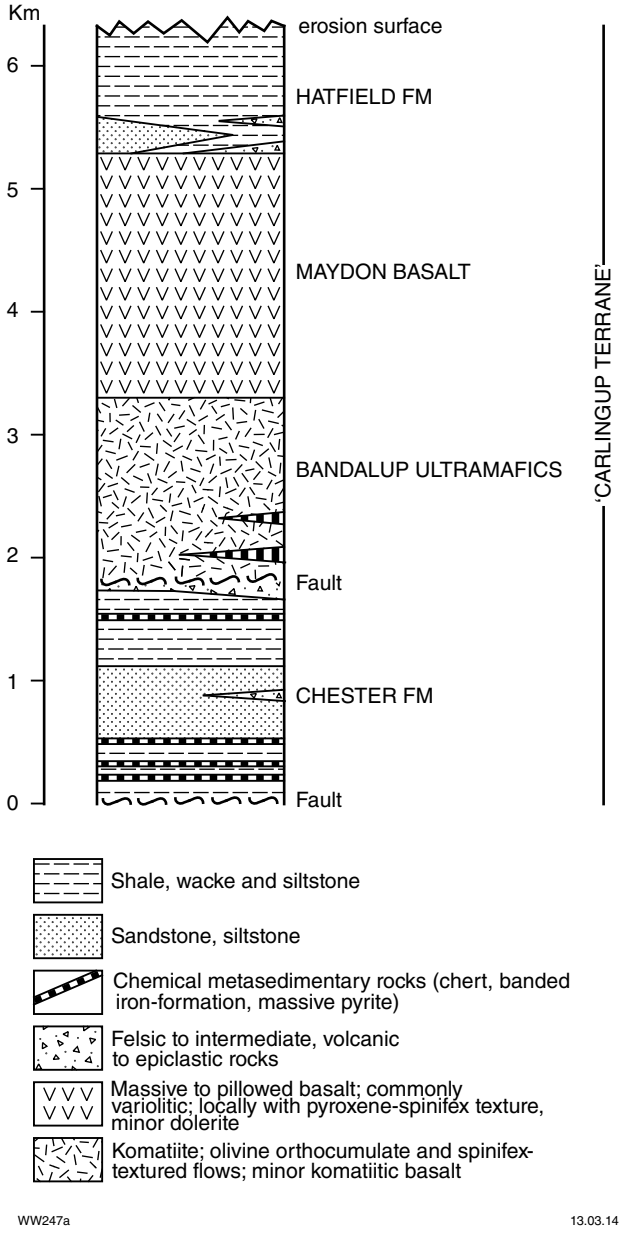

Figure 11. Lithostratigraphy of the Carlingup 'Terrane' (after Witt, 1998)

Structural evolution of the Southern Cross greenstone belt

by MP Doublier, N Thébaud, DR Mole, and SS Romano

The Southern Cross – Forrestania greenstone belt in the southern Southern Cross Domain is about 300 km long. A prominent feature of the regional geology is the preservation of several granite–gneiss domes: the Ghooli, Mt Rankin and Parker domes. The greenstones within the belt are mainly metamorphosed in the amphibolite facies and the metamorphic grade decreases away from the granite–greenstone contacts (Fig. 12; e.g. Ahmat, 1986; Dalstra et al., 1999). The Ghooli dome is the largest and best studied of the dome structures. It is a composite granite–gneiss dome and, based on the foliation pattern, Dalstra et al. (1998) distinguished three subdomes. These are, from north to south: the Hamersley dome, the Lake Deborah (half-) dome, and the Ghooli dome (Fig. 13). The main foliation in the greenstones largely trends subparallel to the dome-greenstone contacts, as does the marginal foliation within the dome structures. The main structural grain trends north-northwesterly.

The structural inventory and evolution of the area has been studied by several authors (e.g. Bloem et al., 1994, 1997; Dalstra and Ridley, 1995; Dalstra et al., 1998; Witt et al., 2001). The area underwent polyphase deformation and the different views on the deformation history have been summarized in Fig. 14 (Witt et al., 2001). Although the schemes are broadly similar, several differences are evident. The only other region where the early north–south compressional event, proposed by Witt et al. (2001), has been described is the Marda–Diemals belt to the north (Dalstra and Ridley, 1995; Chen et al., 2003). Also, Bloem et al. (1997) interpreted doming to be synchronous with their D_2 folding during east–west compression, whereas Witt et al. (2001) suggest that doming postdates folding (D_1 and D_2 in their scheme), based on the observation that F_2 folds are reoriented at the northern end of the Parker dome. Although the structural inventory is complex in detail, the sequence of deformation events can be roughly summarized as follows:

- Early deformation ('D_1'): thrusting and formation of large-scale upright to recumbent folds during north–south compression. As mentioned above, this deformation is still a subject of debate (Witt et al., 2001; Bloem et al., 1994, 1997).

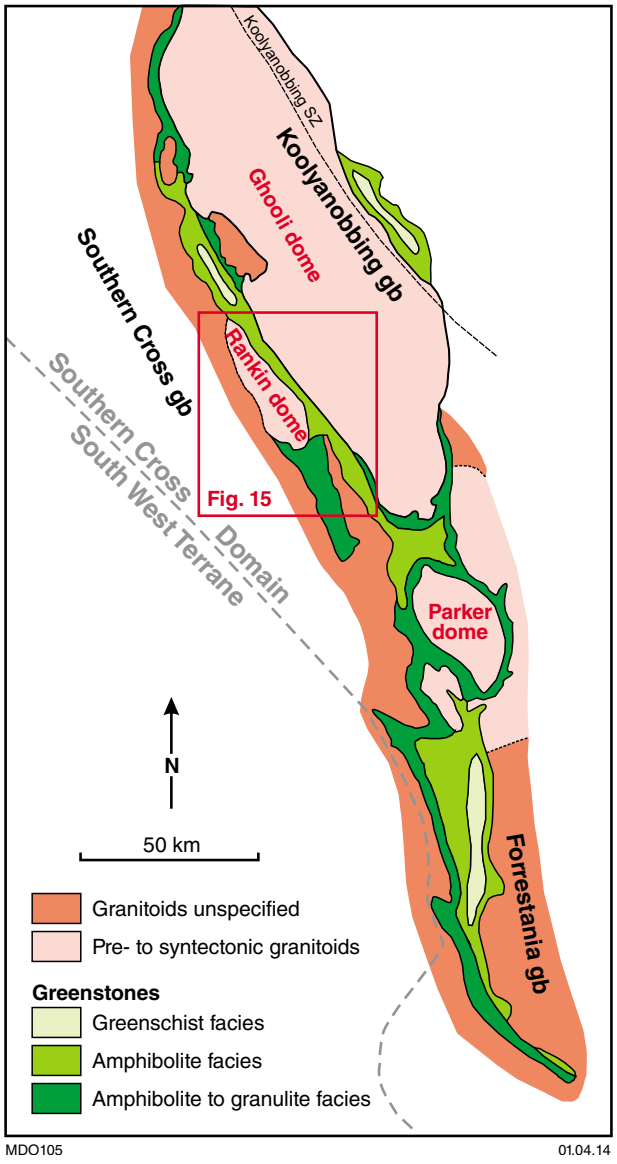

Figure 12. Metamorphic pattern and dome structures in the Southern Cross – Forrestania greenstone belt (summarized after Ahmat, 1986; Keats, 1991; Dalstra et al., 1998; Mueller et al., 2004)

- D_2: small to large scale (first order at km scale), tight to isoclinal, similar folds, with north-northwesterly trending axial planes and variable plunges. The regional foliation (S_2) is attributed to this deformation event.
- D_3: tightening of earlier folds, formation of F_3 folds (Bloem et al., 1997; Witt et al., 2001). Strain partitioning and formation of ductile shear zones, commonly subparallel to S_2 and bedding.
- D_4: formation of brittle–ductile faults: sinistral (270–290°) and dextral (030–050°) shear senses.

As well as timing, the mechanism of doming is a matter of debate. Several authors favour diapirism as the main driving force for the doming, synchronous to regional east-northeast–west-southwest directed shortening (Bloem et al., 1997; Dalstra et al., 1998). Alternatively, the granite domes have been interpreted as thrust sheets of limited thickness, with the domal pattern caused by fold interference (Witt et al., 2001).

The polyphase deformation and doming led to an overall complex geology, which is well illustrated in the area covered by the Southern Cross 1:100 000 map sheet (Fig. 15). In this area, two separate greenstone branches converge towards north. The belt varies substantially in thickness, with a 'bottleneck' north of Southern Cross township. Some large-scale folds are preserved. Major shear zones separate lithotectonic segments and may cause the termination of substantial rock packages. As shown in cross-section (Fig. 16), the lithologies and shear zones have an overall steep orientation. Potential field modelling suggests that the greenstone sequence is cut at depths of 2–3 km by granites of the post-2640 Ma suite. Related pegmatoidal sills and dykes are common in some deposits (see 'Timing of gold mineralization' below).

Some of the shear zones focus fluid flow and mineralization. Particularly important are the mineralized Corinthia–Treasury Shear Zone and the corridor to the west, which is marked by a horizon of BIF. This area is coincident with what has been termed the Corinthia–Frasers Shear Zone in earlier literature (Bloem et al., 1994, 1997) and is host to a whole range of gold deposits (Fig. 17).

The structural evolution of the Koolyanobbing and Forrestania areas is described in the respective sections below.

Felsic magmatism of the Ghooli dome

by MP Doublier, N Thébaud, DR Mole, MTD Wingate, and CL Kirkland

The Ghooli dome and surrounding areas record a protracted history of magmatic activity, from c. 2775 to 2625 Ma (Dalstra et al., 1998; Qiu et al., 1999; Mueller and McNaughton, 2000; Mole et al., 2012; Wingate et al., 2012b; Thébaud et al., in prep.). Within the dome, the spatial distribution of granite crystallization ages (Fig. 18) forms a concentric pattern with ages less than 2700 Ma northwest of Koolyanobbing, in the Lake Deborah subdome from Dalstra et al. (1998), surrounded by older rocks (>2700 Ma) in the northern, western and southern parts. This distribution of magmatic ages is consistent with the foliation pattern, suggesting that the Lake Deborah subdome represents a 'half-dome' (Fig. 13; Dalstra et al., 1998). The concentric age pattern of the dome is cut by the Koolyanobbing Shear Zone, suggesting that the shear zone postdates the doming process. The shear zone itself is intruded by the c. 2656 Ma, post-kinematic Lake Seabrook granite (Qiu et al., 1999), which provides a minimum age for the doming (Fig. 19).

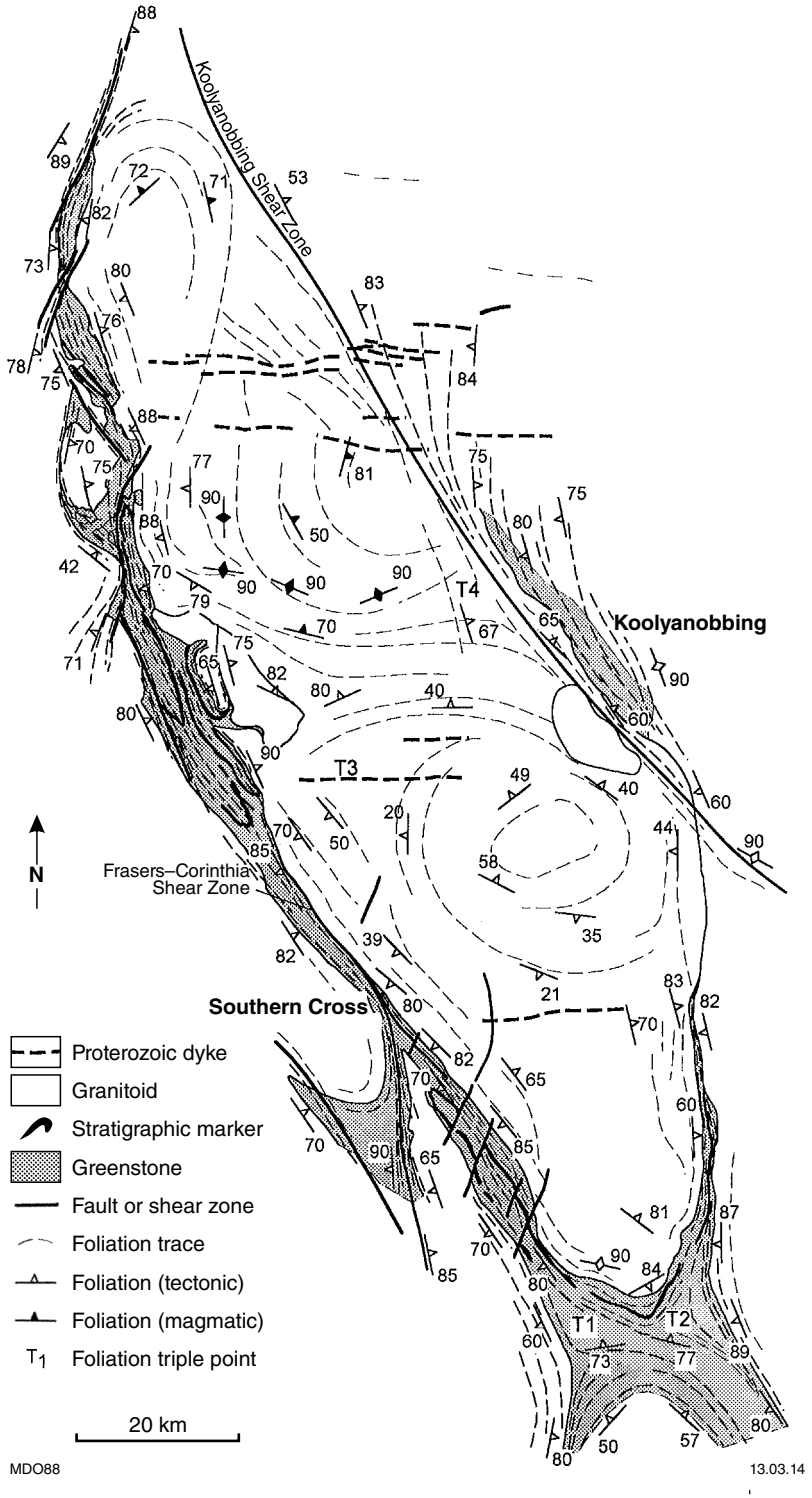

Figure 13. Regional structural map of the Ghooli dome and surrounding greenstone belts (after Dalstra et al., 1998)

Proposed new scheme	Bloem et al. (1997)	Dalstra and Ridley (1995)	Bloem et al. (1994)
D_1 North–south compression: Low-angle thrust faults and recumbent folds. F_1 folds locally preserved (e.g. gently plunging folds in Lakes Domain and Parker Domain) but S_1 is largely transposed by S_2, except in the Banker Saddle		**D_1 North–south compression:** East–west, tight, upright folds (Marda) and recumbent, isoclinal folds (Diemals)	
D_2 East–west compression: Tight to isoclinal, upright to recumbent folds. On the west side of the Ghooli dome, F_2 folds are oriented NW to NNW and fold axes are subhorizontal. On the north side of the Parker dome, F_2 folds are oriented ENE and fold axes plunge steeply. Macroscopic F_1/F_2 interference folds in Polaris Domain, Banker Saddle	**D_1** Tight to isoclinal folds with NW axial planar foliation and variable plunges	**D_2 East–west compression:** Upright north–south folds (oldest deformation in the Southern Cross belt)	**D_1** Upright, tight folds with NW axial planes, plunge shallowly NW at Southern Cross
D_3 Continued east–west compression contemporaneous with emplacement of Ghooli and Parker domes: Tightening of F_1 and F_2 folds as strain is partitioned around granitoid domes. NNW upright folds in the Banker Saddle (e.g. Lakes domain)	**D_2** Open folds with 50–70°SE plunge between Ghooli and Parker domes; zones of ductile shear parallel to S_1 and bedding, shallow to moderate plunging L_2 (includes Frasers–Corinthia Shear Zone); sinistral shear bands (290–300°); dextral shear bands (000–030°)	**D_3** NE–SW dextral ductile shear zones (Evanston) N–S normal ductile shear zones (Jackson) E–W sinistral, reverse brittle–shear ductile zones (Marda)	**D_2** Tightening of D_1 folds; ductile shear zones (320–340°); sinistral shear bands (290–300°); dextral shear bands (000–030°)
D_4 Continued east–west compression: Partitioning of strain around the Ghooli and Parker domes. Thrusting of the Parker Domain and Lakes Domain over the Moonargidding Domain and the Jilbadji Domain, respectively. WNW sinistral, brittle–ductile faults, especially near the SW corner of the Ghooli dome	**D_3** Brittle–ductile faults; sinistral (270–290°) and dextral (030–050°) shear bands	**D_4** Small-scale brittle faults (NW–SE and NNE–SSW)	**D_3** Brittle–ductile faults; sinistral (270–290°) and dextral (030–050°) shear bands

MDO87 01.04.14

Figure 14. Correlation of deformation histories for the Southern Cross greenstone belt (after Witt et al., 2001)

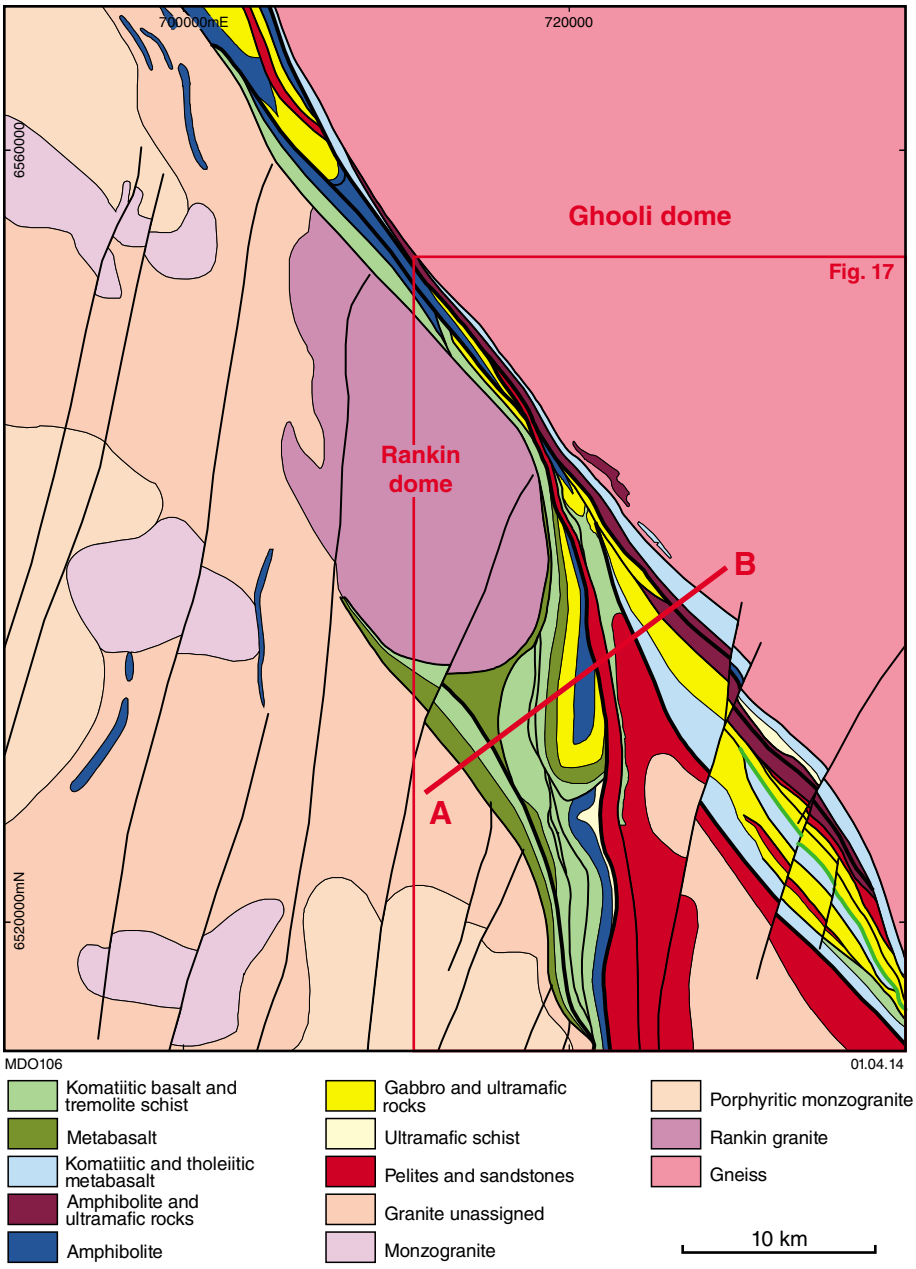

Figure 15. Simplified interpreted bedrock geology of the Southern Cross 1:100 000 map sheet

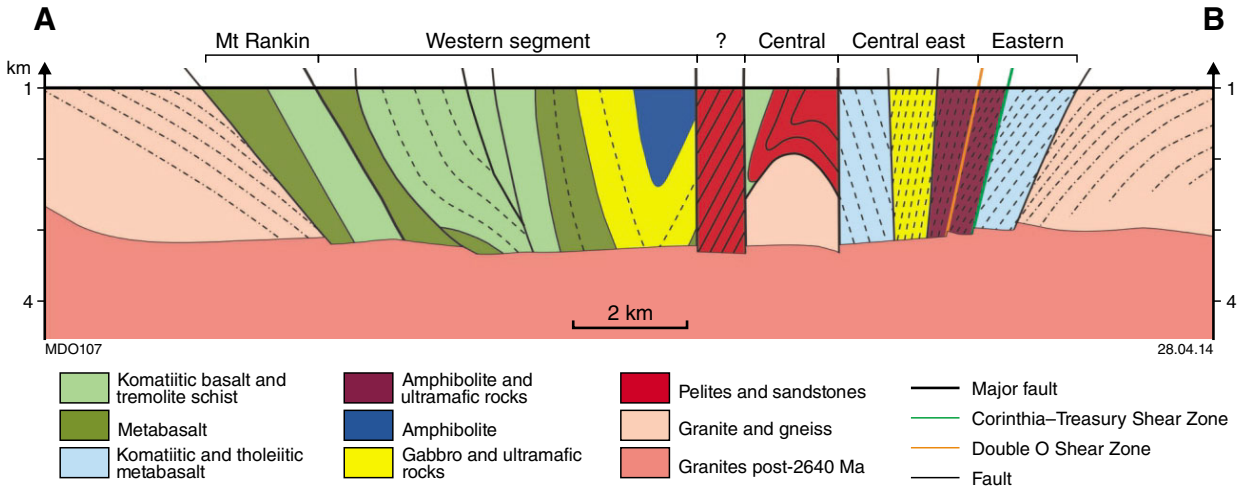

Figure 16. Diagrammatic cross-section through the Southern Cross greenstone belt south of Southern Cross

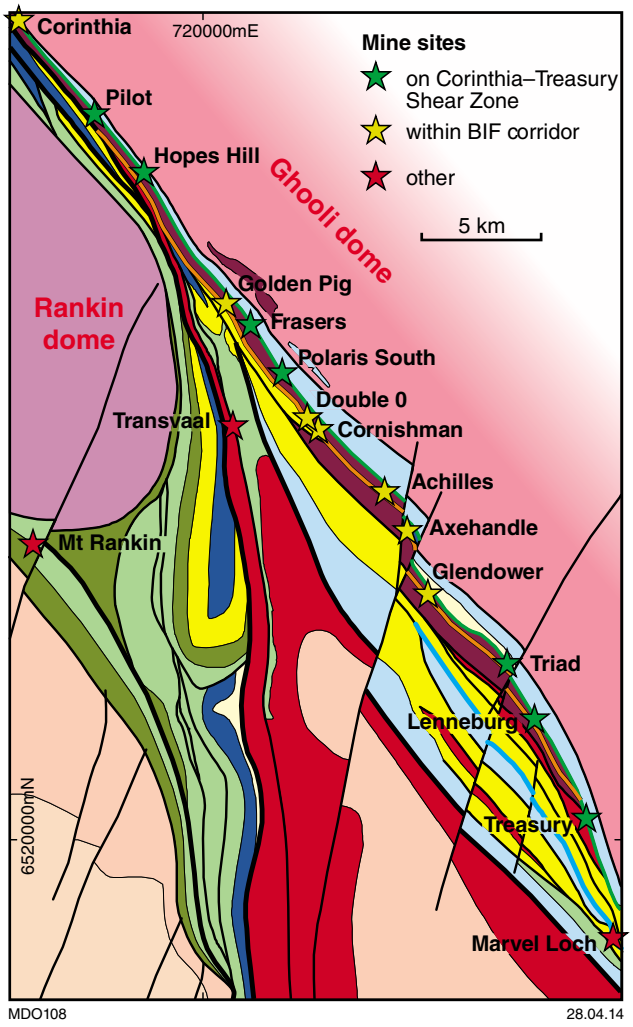

Figure 17. Simplified interpreted bedrock geology of the Southern Cross area, highlighting the positions of gold deposits with respect to shear zones

A maximum age for the doming is provided by the young sedimentary rocks (c. 2700 Ma). These rocks exhibit the main greenstone deformation, which is interpreted to either predate or be synchronous with the doming process (Witt et al., 2001; Bloem et al., 1997).

Granites younger than 2635 Ma have been detected across the area, and are synchronous with gold mineralization (see 'Timing of gold mineralization' below). Both their emplacement and the mineralization postdate the doming (and the main deformation) by at least 20 Ma.

The geochronological data also reveal some differences between the Ghooli dome and its surroundings. The older granites and gneisses within the dome range between c. 2775 and 2700 Ma (Fig. 19). Granites of this age have so far not been found in the surrounding granite terrain.

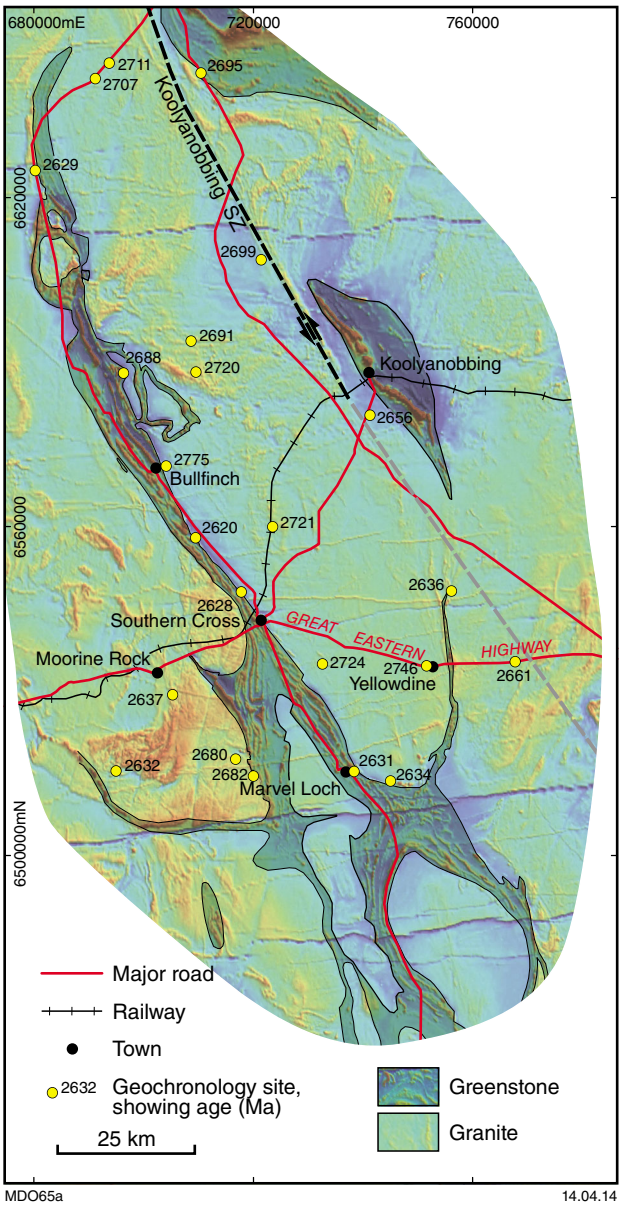

Figure 18. Magmatic ages and locations of geochronology samples from granites and gneisses in the Southern Cross area

Apparently, the Ghooli dome exposes older (deeper?) crustal levels. Within the dome, a period of increased magmatic activity is observed between c. 2725 and 2680 Ma. Similar ages are well known from other parts of the Yilgarn Craton (Fig. 4).

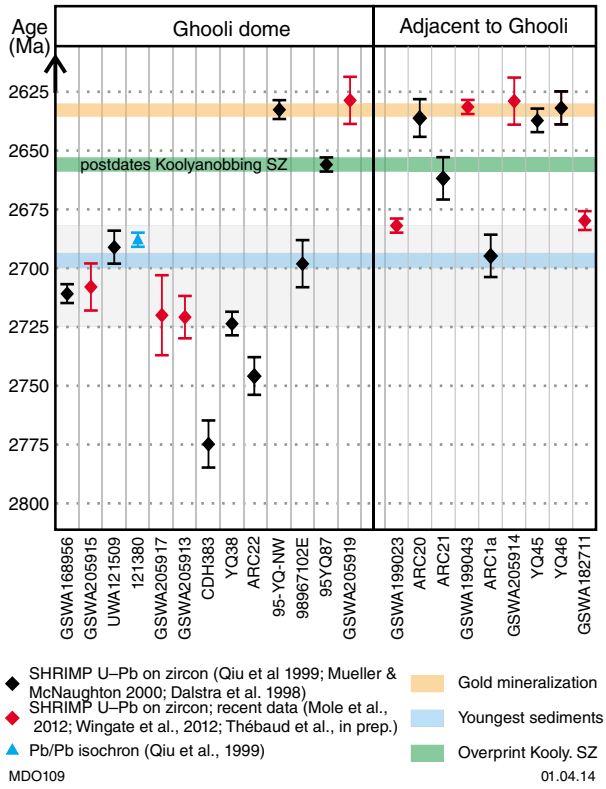

Figure 19. Compilation of geochronology data from the Southern Cross area, with respect to gold mineralization and dome emplacement

Styles of gold mineralization

by W Witt (for Sons of Gwalia)

The Southern Cross greenstone belt is a traditional gold-mining area, and contains numerous historical and more recent deposits (for an overview, see Keats, 1991). Detailed observations from various deposits in the Southern Cross district allow us to distinguish two styles of gold mineralization in the Southern Cross greenstones.

Model 1 deposits are shear-hosted deposits in which mineralized veins are folded conformably within the ductile fabric of the shear zone (Figs 20 and 21). They are commonly located on the contacts between komatiitic basalt–ultramafic rocks and either sedimentary or mafic rocks. Several deposits of this type are located along a shear zone (Corinthia–Treasury Shear Zone) close to the

western margin of the Ghooli dome. They include Frasers, Polaris South, Pilot, Hopes Hill, Triad and Treasury (Fig. 17). Other deposits of this type are located on other ductile shear zones and include Marvel Loch, Transvaal and Yilgarn Star (Witt et al., 2001).

Model 2 deposits are brittle-vein deposits hosted by BIF, in which the veins cut and therefore postdate bedding, metamorphic banding and folding (Figs 22 and 23). An important corridor with this style of deposit lies along a specific BIF unit to the west of the Corinthia–Treasury Shear Zone. Deposits include Golden Pig, Cornishman, and Glendower, and possibly Lenneburg and Corinthia in the north. This area (i.e. the mineralized Corinthia–Treasury Shear Zone and the corridor which hosts Model 2 deposits to the west) is coincident with what has been termed the Corinthia–Frasers Shear Zone in earlier literature (Bloem et al., 1994, 1997). In Model 2 deposits, rheological contrasts between competent iron-formation and weak hangingwall ultramafic and footwall-altered mafic schist promoted brittle fracture within the iron formation. Fracture may also have been promoted where the BIF is intersected by north-northeasterly striking faults (Fig. 17; e.g. Achilles, Axehandle). Other Model 2 deposits within the Southern Cross greenstone belt include Great Victoria, Nevoria, and Mount Rankin and Jaguar in the westernmost part of the belt (Fig. 17; Keats, 1991).

Geochronological constraints on gold mineralization

by MP Doublier, N Thébaud, MTD Wingate, and CL Kirkland

The timing of gold mineralization in the Southern Cross area has been the subject of several isotopic investigations. A first age constraint was provided by Bloem et al. (1995), who dated crystallization of a weakly deformed pegmatite from the Corinthia deposit at 2620 ± 6 Ma (Pb–Pb isochron age). These authors suggested that the pegmatite was affected by the latest shearing along the Corinthia–Treasury Shear Zone and, based on structural criteria, that the formation of the shear zone was synchronous with gold mineralization. They interpreted the c. 2620 Ma date to reflect either gold mineralization, or at least the minimum age for that mineralization (Fig. 24).

A direct age for the mineralization was provided by Mueller et al. (2004), who dated an allanite inclusion in garnet (TIMS U–Pb) at 2635.7 ± 1.2 Ma. The dated mineral assemblage was interpreted to form part of a metasomatic ('skarn') ore coeval with gold mineralization. This result is within error of a scheelite–almandine Pb–Pb isochron date from the same deposit (2630 ± 13 Ma; Mueller at al., 2004). The Nevoria orebodies are cut by pegmatites derived from underlying granite. The granite postdates the mineralization, and is dated at 2634 ± 4 Ma (SHRIMP U–Pb zircon; Qiu et al., 1999).

A drillcore sample from a metamonzogranite dyke at Marvel Loch yielded a SHRIMP U–Pb zircon crystallization age of 2631 ± 3 Ma (GSWA 199043, Wingate et al., 2012b). The granite, which is largely undeformed and crosscuts the regional foliation in the greenstones, develops a solid state fabric near the Marvel Loch Shear Zone. It is interpreted to have been emplaced during the final stage of ductile deformation along this shear zone, which is the principal host structure to the Marvel Loch deposit. Granites, similar to those dated, are widespread in the deposit and are interpreted to be late syn- to post-mineralization (Mueller, 1991).

Collectively, the data indicate a mineralization event between c. 2635 and 2630 Ma, synchronous with the granite magmatism and the final ductile shearing along the Marvel Loch Shear Zone. A second mineralization event, about 10 million years later, might be inferred from the Corinthia deposit, although the timing relationship between the dated pegmatite and mineralization is ambiguous (Bloem et al., 1995). Older mineralization events cannot at present be ruled out.

A period of thermal activity, magmatism and fluid flow younger than c. 2635 Ma is suggested by a metadolerite sample from the Transvaal deposit. Zircons from this metadolerite have low Th/U ratios (<0.2), which could indicate a metamorphic (i.e. non-magmatic) origin or competition during igneous crystallization with a thorium-sequestering phase.

Locality descriptions

A geographic overview of the field trip localities is shown in Figure 25.

Locality 1: the Flying Fox Ni–Cu–PGE komatiite-hosted deposit, Forrestania greenstone belt

by J Collins and TC McCuaig

Geological setting

The Flying Fox nickel deposit is located in a narrow curvilinear belt bounded by gneiss and intruded by granitoid rocks located in the Forrestania greenstone belt, Youanmi Terrane within the Archean Yilgarn Craton of Western Australia (Perring et al., 1996; Frost, 2003; Fig. 26). The belt is located about 350 km east-southeast of Perth, and is the southern extension of the Southern Cross greenstone belt, Southern Cross Domain, Youanmi Terrane in the Archean Yilgarn Block (Cassidy et al., 2006; Chin et al., 1984; Gee, 1979; Porter and McKay, 1981). The belt trends in a northerly direction over a length of 250 km and ranges in width from 5 to 30 km.

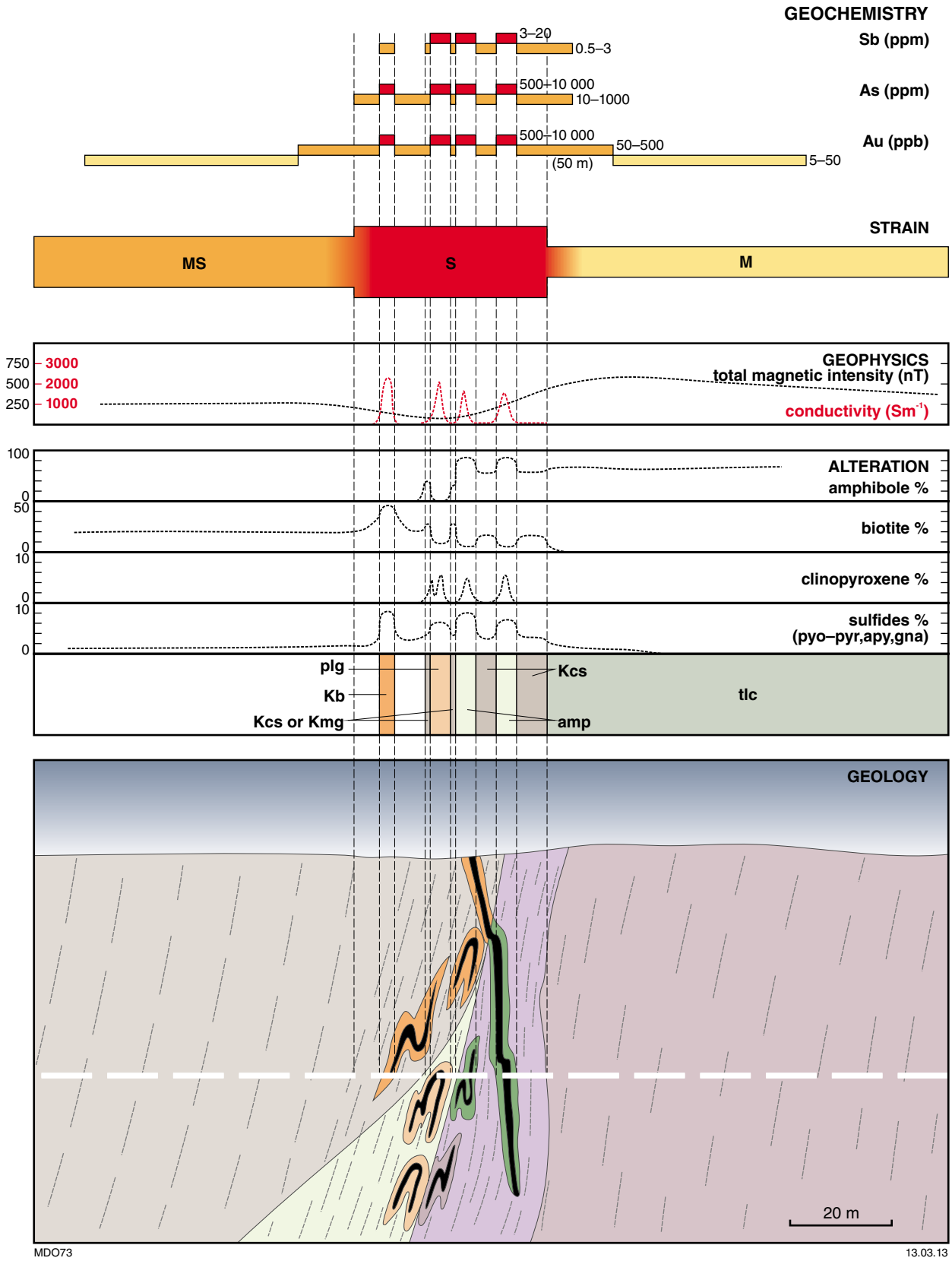

Figure 20. Vector diagram of a generic Model 1 deposit, displaying various geochemical, mineralogical and structural parameters across a Model 1 shear-zone-hosted deposit

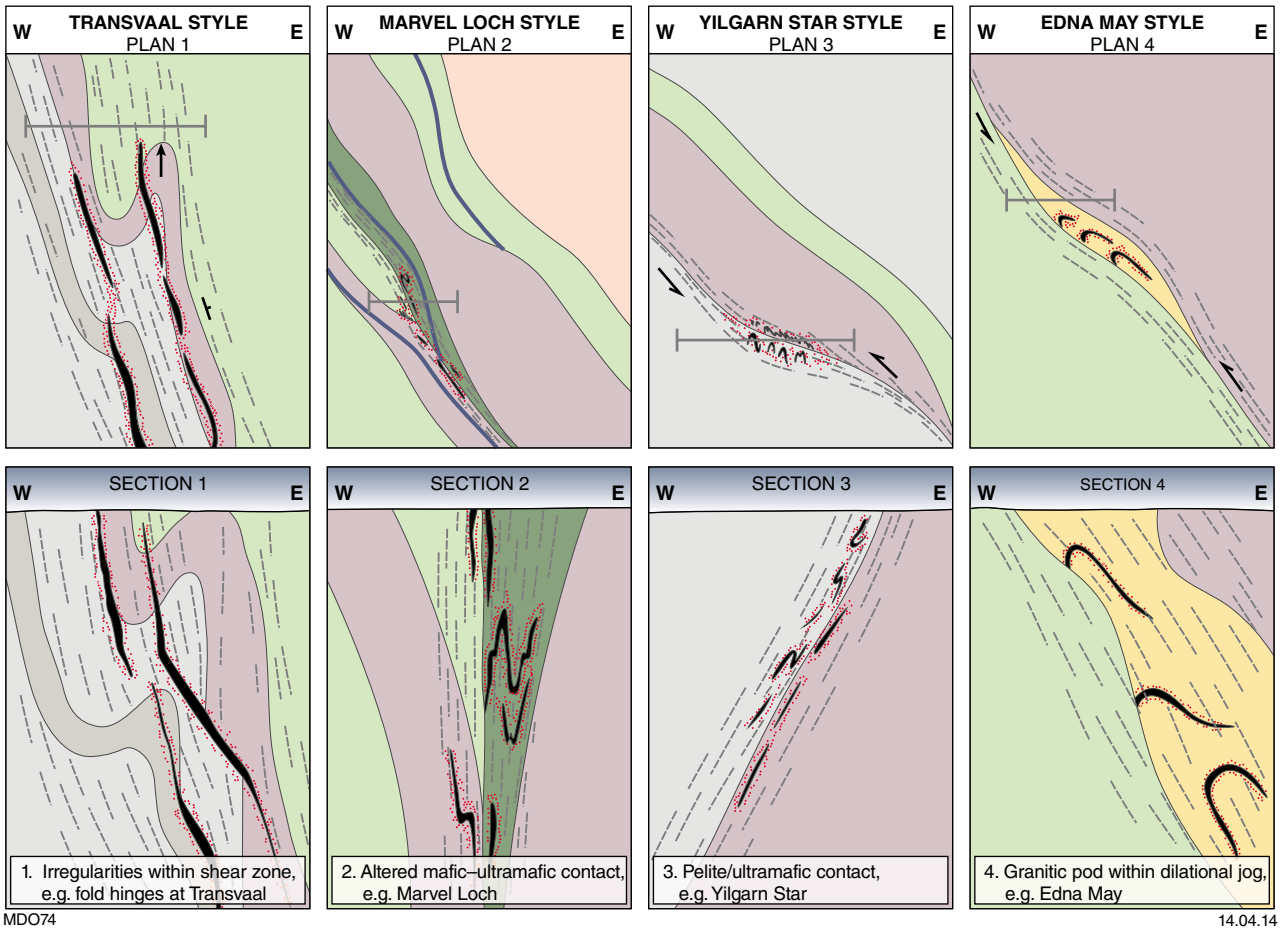

Figure 21. Examples of, and variations within, Model 1 style deposits illustrating the (1) Transvaal, (2) Marvel Loch, (3) Yilgarn Star and (4) Edna May deposits

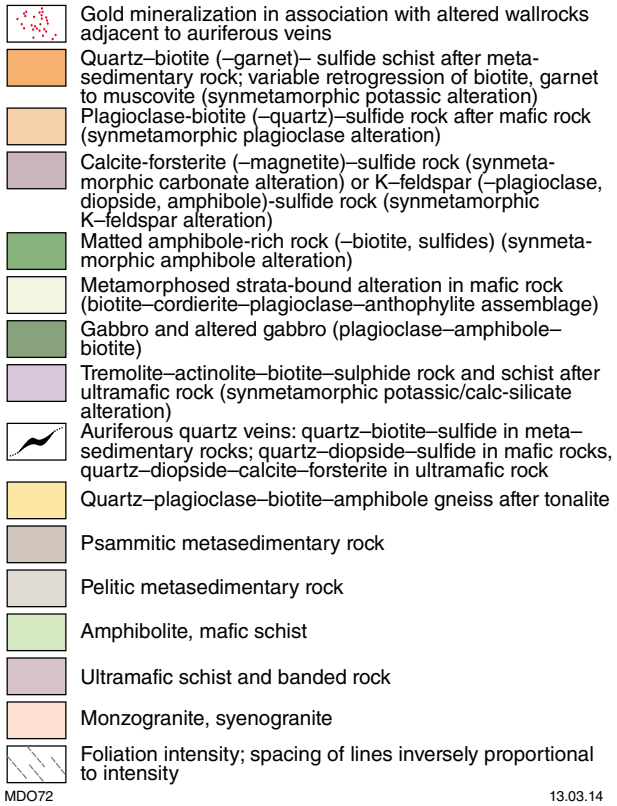

Legend for Figs 20 and 21

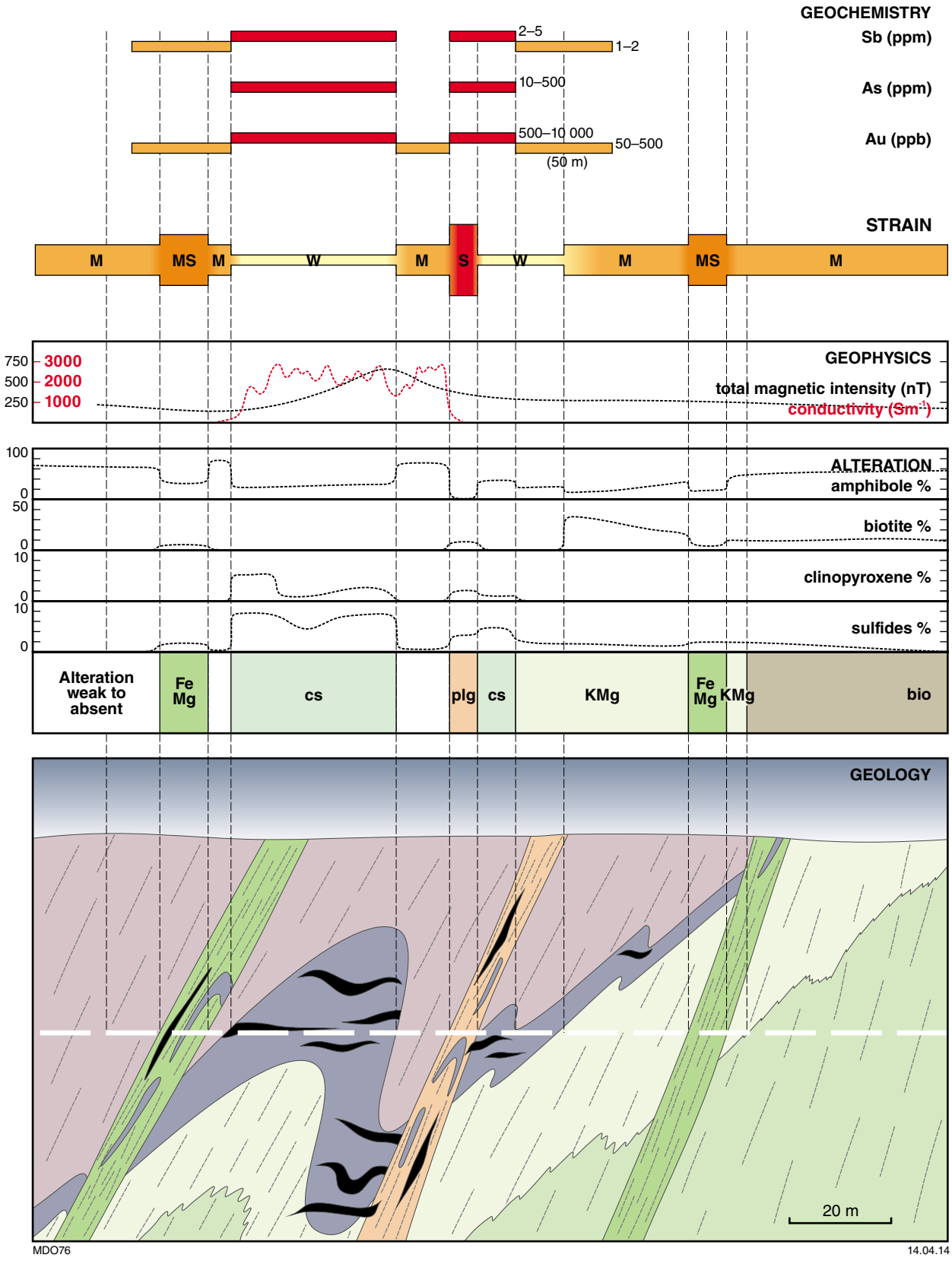

Figure 22. **Vector diagram of a generic Model 2 deposit, displaying various geochemical, mineralogical and structural parameters across a Model 2 brittle vein deposit**

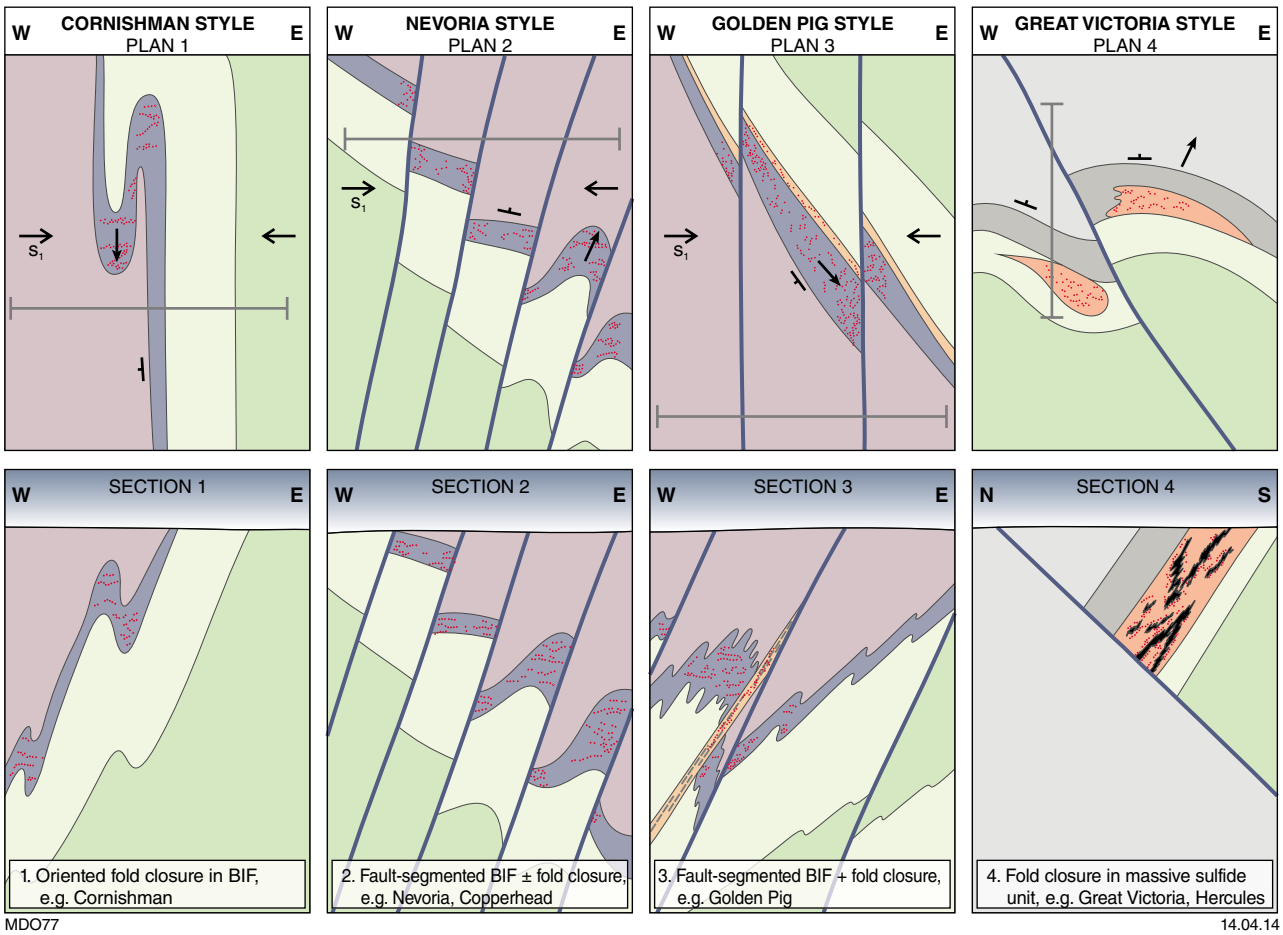

Figure 23. Examples of, and variations within, Model 2 style deposits illustrating the (1) Cornishman, (2) Nevoria, (3) Golden Pig and (4) Great Victoria deposits

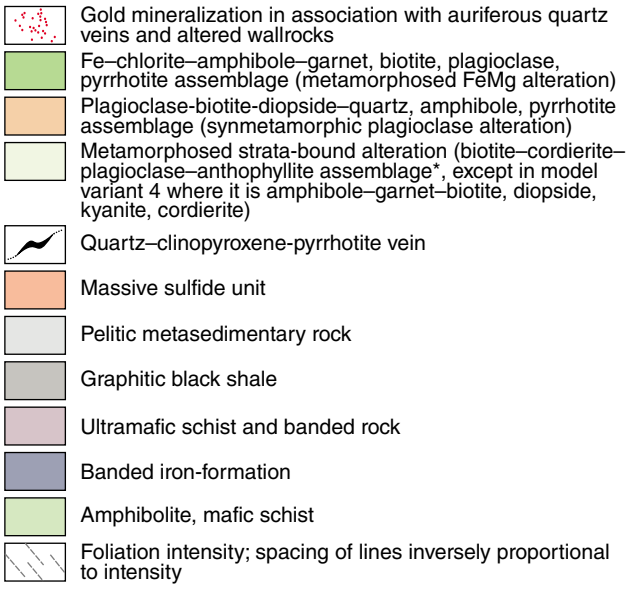

Legend for Figs 22 and 23

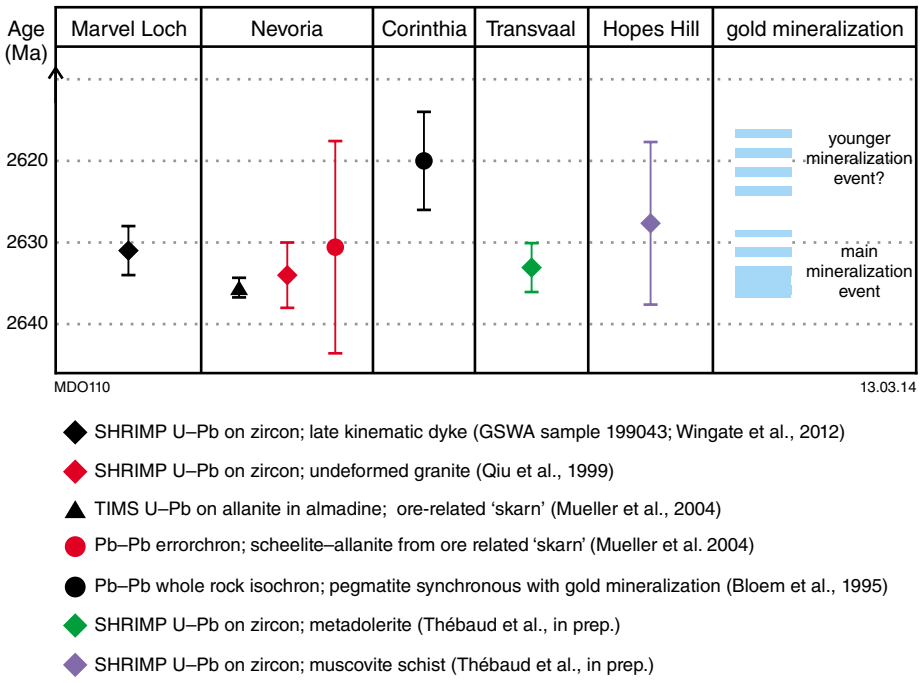

Figure 24. Time–space chart of available geochronology relevant to the timing of gold mineralization in the Southern Cross greenstone belt

The stratigraphy of the Forrestania greenstone belt consists of two successions: a) a lower succession of at least four sequences of predominantly tholeiitic and komatiitic metavolcanic rocks intercalated with BIF, sulfidic chert layers, and localized felsic metasedimentary units; and b) an upper succession of fine-grained, clastic metasedimentary rocks (pelitic to psammitic schists) with minor BIF horizons, which is located in the centre of the belt (Porter and McKay, 1981; Chin et al., 1984; Frost, 2003). Enclosing the greenstone belt is a terrain comprising deformed and recrystallized granitoids and gneisses that have been intruded by younger, undeformed plutons of granite and adamellite. A series of easterly trending Proterozoic dykes of the Widgiemooltha dyke swarm, intrude and crosscut all Archean successions (Frost, 2003; Perring et al., 1995).

Six ultramafic belts recognized in the Forrestania area are the Western, Mid-Western, Takashi, Central fold, Mid-Eastern, and Eastern, with the Flying Fox deposit located in the Western ultramafic belt (Perring et al., 1995, 1996). The Eastern ultramafic belt is continuous over the entire strike of the Forrestania greenstone belt, in contrast to the other five belts, which have interpreted strike lengths of between 10 and 40 km (Frost, 2003). Subeconomic nickel concentrations are common in the southern half of the Forrestania greenstone belt including at the Seagull, Rat Bat, South Ironcap, Liquid Acrobat, and Beautiful Sunday prospects. However, economic nickel sulfide deposits are restricted to the Eastern and Western belts, with only one occurrence in the Central belt (Antimony Nickel NL — low-grade disseminated nickel sulfide). To date, no economic nickel sulfides have been discovered in the Mid-Western, Takashi, and Mid-Eastern ultramafic belts (Frost, 2003).

Lithostratigraphy and regional metamorphism

The stratigraphy at the Flying Fox deposit is interpreted to represent an east-younging succession of four distinct lithological packages that are interpreted to be conformable (Figs 27 and 28): a) quartzofeldspathic sedimentary rocks (footwall sedimentary rocks) intercalated with minor basaltic rocks; b) a cumulate-rich compound komatiite flow sequence (terminology of Barnes, 2006) grading upwards from olivine–tremolite rocks (ortho- and mesocumulates) to tremolite–chlorite rocks (noncumulates) consistent with the A and B zones definitions of Pyke at al. (1973). The cumulate komatiites host an irregular halo of disseminated sulfides that directly overlies the massive sulfides; c) a komatiite–basalt thin-flow facies sequence, where noncumulate komatiites and high-magnesium basalts (tremolite–actinolite rocks) dominate; and d) biotite–garnet schist (hangingwall sedimentary rocks) occupying the central portion of the Forrestania greenstone belt (Collins et al., 2012a; Fig. 26).

The Forrestania greenstone belt has experienced upper amphibolite facies metamorphism with peak metamorphic conditions, interpreted by Porter and McKay (1981), estimated at 655 ± 30°C and 4.0 ± 1.0 kbar. Regional metamorphism resulted in widespread textural destruction;

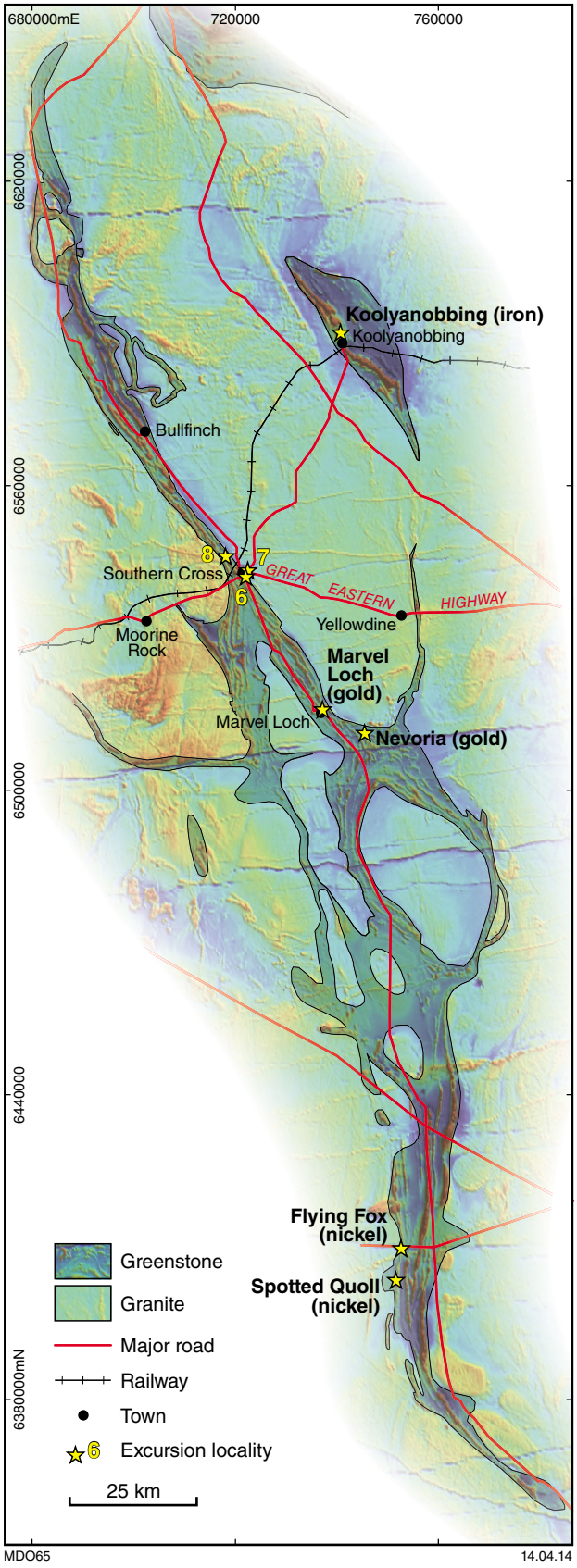

Figure 25. Excursion localities on a simplified geological map and RTP aeromagnetic image

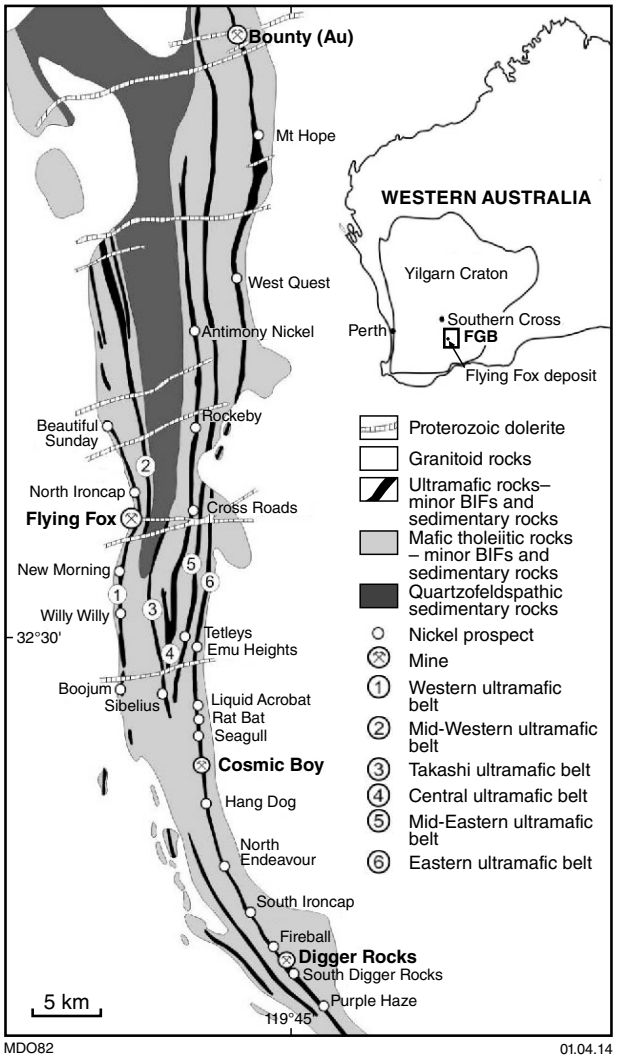

Figure 26. Simplified geological map of the Forrestania greenstone belt (FGB) showing the distribution of the ultramafic belts and locations of nickel prospects and mines, including the Flying Fox nickel deposit (modified after Perring et al., 1997)

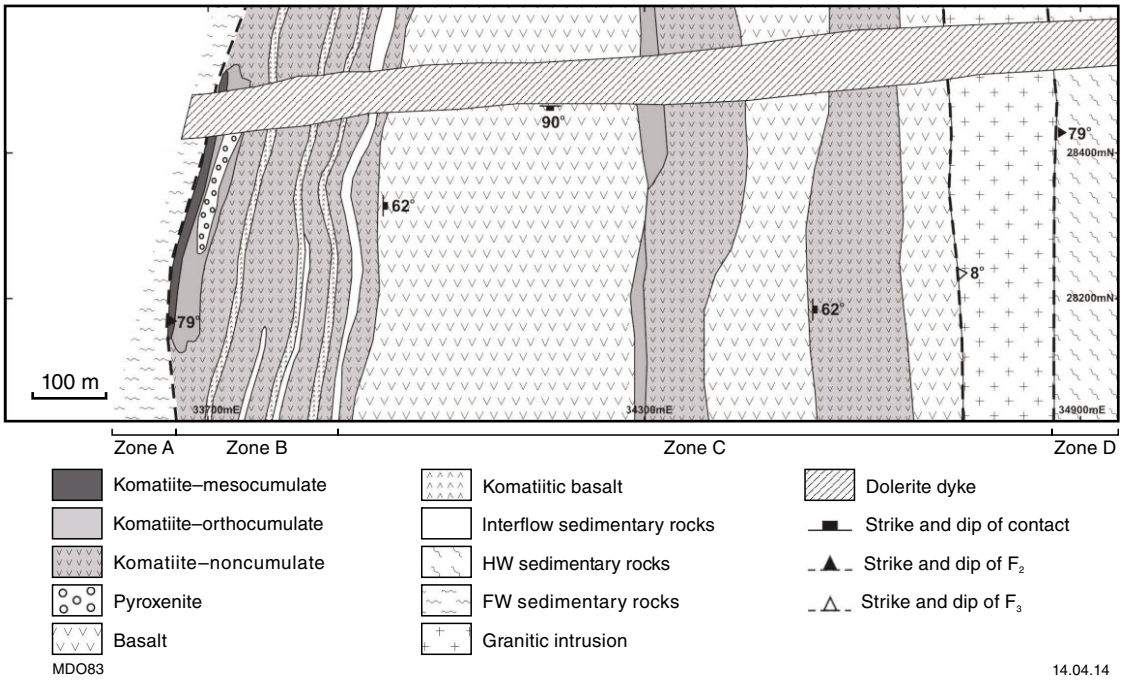

Figure 27. Geological plan map showing the distribution of rock types, nickel sulfide ore shoots, and major structures at the Flying Fox deposit. Lithological contacts and structural elements are projected from drillholes to c. 1350 mRL (120 m below surface), as granitic rocks dominate from 1350 mRL to surface. Detailed geology is limited along the eastern margins as wedge drilling from parent holes is concentrated at depth. The division of lithological packages (zones A–D) has been notated on the plan view map which is correlative to the lithological packages in Figure 28 (modified after Perring et al., 1997).

however, some diagnostic textures (e.g. olivine- and pyroxene-spinifex textures in komatiites, olivine adcumulates, sedimentary bands in BIF) and structures (e.g. pillow rims in basalts) have been preserved in low-strain domains (Perring et al., 1997).

Mining history and production

The Flying Fox deposit was discovered in 1977 at the end of the late 1960s to early 1970s nickel boom, and Outokumpu Mining Australia Pty Ltd subsequently mined the deposit during 1994–97 producing about 240 kt @ 3.2% Ni. Three exploration holes (about 700 m each in length) were drilled in 1994–95 to test for a potential fault-offset ore position (now identified as T1) located about 300–350 m east of the ore shoot. One drillhole intersected disseminated nickel sulfides, whereas the other two drillholes intersected a barren contact. Although strong geophysical anomalies were indicated, they were not considered of sufficient interest to warrant follow-up drill testing (Frost et al., 2006). In 2002 Western Areas NL resurveyed and reinterpreted the stratigraphy and structural overprint of the deposit, which led to a significant new discovery, whereby the first concealed ore shoot T1 was defined in 2004. Drilling has successfully delineated a current mineral resource of 2 415 700 t of ore at an average grade of 4.76% nickel.

Deformation

Deformation at the Flying Fox deposit has been interpreted from observations in diamond drill core that intersects the ore zone, host rocks, and surrounding country rocks, and from mapping of underground exposure of the T0 and T1 ore shoots (Collins et al., 2012a; Fig. 29). A series of five clearly defined deformation events have been interpreted based on integrated observations of fabrics and block movements from the thin section to mine scale. The D_1 to D_3 structures in this deformation scheme are interpreted to be the product of progressive deformation.

During D_1 to $D_{2a–b}$, the coaxial and noncoaxial deformation at the komatiite–sulfide and footwall sedimentary rock contact has flattened and sheared the sulfides along and off-contact. During the D_3 event, the main ore body was faulted and offset up to a maximum of 350 m by flat-lying thrusts, resulting in the current location of the ore shoots (Fig. 28). The D_4 event is characterized by the emplacement of the granitic magma postpeak metamorphism during extension, which resulted in dilation along the footwall sedimentary contact creating a brittle–ductile fault and displacing the underlying stratigraphy.

The dilation of the granitic magma has created the T0 and T4 ore shoots, whereas the T5 pipe ore shoot resulted from entrainment and relocation of a portion of the T5 ore

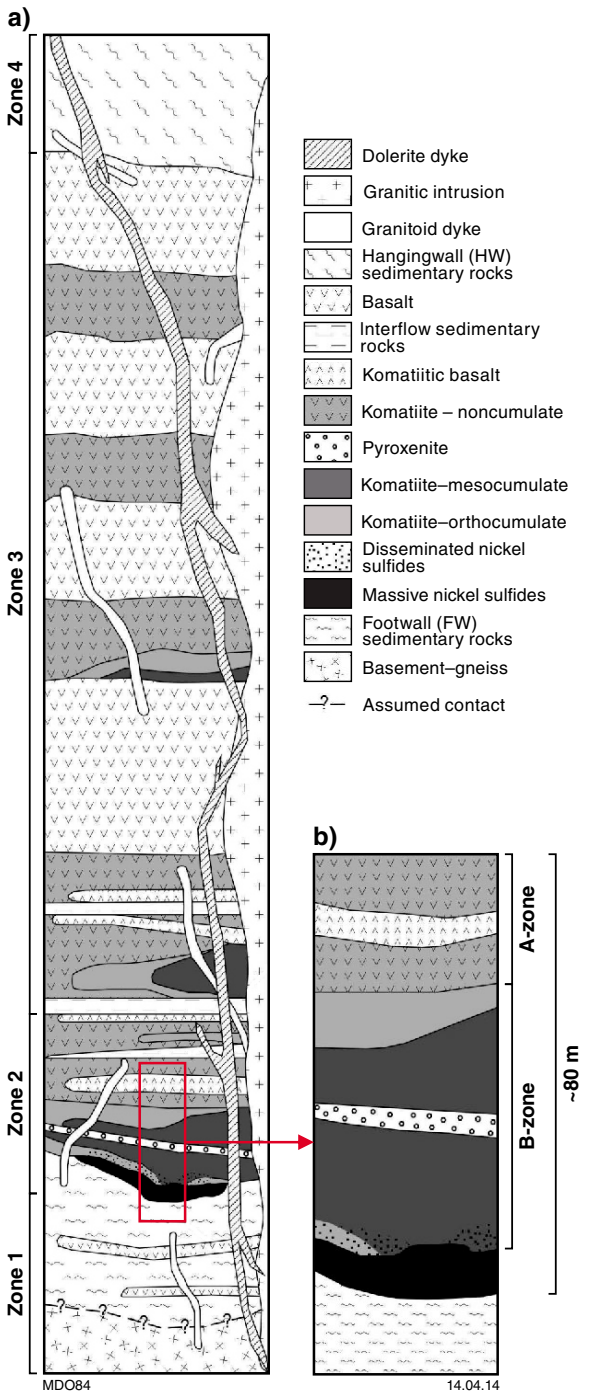

Figure 28. Lithostratigraphic profile through the Flying Fox deposit based on diamond drillhole interpretation. The basal komatiites are interpreted to be a differentiated channel flow, where A- and B-zones are identified (as defined by Pyke et al., 1973). The differentiated channel flow is directly overlain by an interflow sedimentary unit separating this zone from an overlying komatiite–basalt succession, which is intercalated with interflow sedimentary rocks and komatiitic basalts. The massive sulfides are concentrated along the footwall sedimentary and basal komatiite contact and are directly overlain by discontinuous zones of disseminated sulfides within the cumulate komatiitic rocks. The granitic rocks comprise at least eight types and crosscut the stratigraphy. All Archean rocks are crosscut by the Proterozoic dolerite dyke.

shoot by granitic magma about 20 m to the east along a flat-lying thrust. The granitic rocks locally incorporated the sulfide ore during this event, which has created the atypical granite-hosted nickel sulfides (Fig. 28). Although the sulfides were mobilized during deformation, the massive ore is currently positioned at the base of the high-Mg komatiites (differentiated komatiites, A and B zone observed; Figs 28 and 30) and is directly overlain by disseminated sulfides, which indicates that, in general, the ore shoots have been mobilized locally off their primary contact. Textures and mineralogy of alteration assemblages identified by Collins et al. (2012a) indicate that fluid flow was coeval with sulfide remobilization (Table 1).

Nickel sulfide mineralization

Nickel sulfide mineralization at the Flying Fox deposit, described and interpreted in Collins et al. (2012b), takes the form of a typical Type 1 sulfide-rich contact mineralization associated with a number of Type V sulfide-rich ore shoots that occur in faults and shear zones (Lesher and Keays, 2002; Barnes, 2006). Mineralization is located as thin, tabular high-grade ore shoots, which, for the most part, directly underlie the lowermost komatiitic unit in the stratigraphy (Figs 27 and 28). The ore is tectonically dismembered into 11 discrete ore shoots that make up T0, T1/T2, T4, T5, T6/T7, and the original Flying Fox ore shoot. The ore shoots are thin (generally 2–5 m wide) and comprise varying proportions of massive, breccia, and vein/stringer sulfides. The Flying Fox deposit as a whole is a high-grade deposit with the majority of economic resources accounted for by massive sulfides.

Layering of ore types typical of komatiite-hosted deposits (Naldrett, 1973), comprising massive sulfides overlain by matrix-textured and disseminated sulfides, is not observed at the Flying Fox deposit. However, thin discontinuous zones of disseminated sulfide, for example the T5 disseminated ores, often directly overly massive sulfides. The matrix-textured ores — which are observed at deposits including the Lunnon Shoot at Kambalda (Ewers et al., 1972), Alexo (Naldrett, 1973), and Kattiniq in the Raglan belt (Barnes et al., 1982; Lesher, 2007) — are absent at Flying Fox, and commonly ore types occur in isolation from each other and from the komatiite host rock, especially in areas of extreme structural dislocation (Collins et al., 2012a).

The T0, upper T1, T4, and upper T5 ore shoots are located on the footwall sedimentary and granitic rock contact that rolls from shallowly east dipping to a steeper 60° to the east (Fig. 30). The lower portion of T1 and T5, and T2 ore shoots are located at the base of the komatiites directly overlying the footwall sedimentary rocks and dip between 70 and 90° to the east (Fig. 30). Some nickel sulfide mineralization associated with T1/T2 and T5 is located off-contact in fault splays within the footwall sedimentary rocks. The upper part of the T5 ore shoot has a pipe-like geometry, and is almost entirely enveloped by granite–pegmatite (Fig. 30). The T5 ore shoot is the largest defined of the ore shoots discovered to date and is still open at depth.

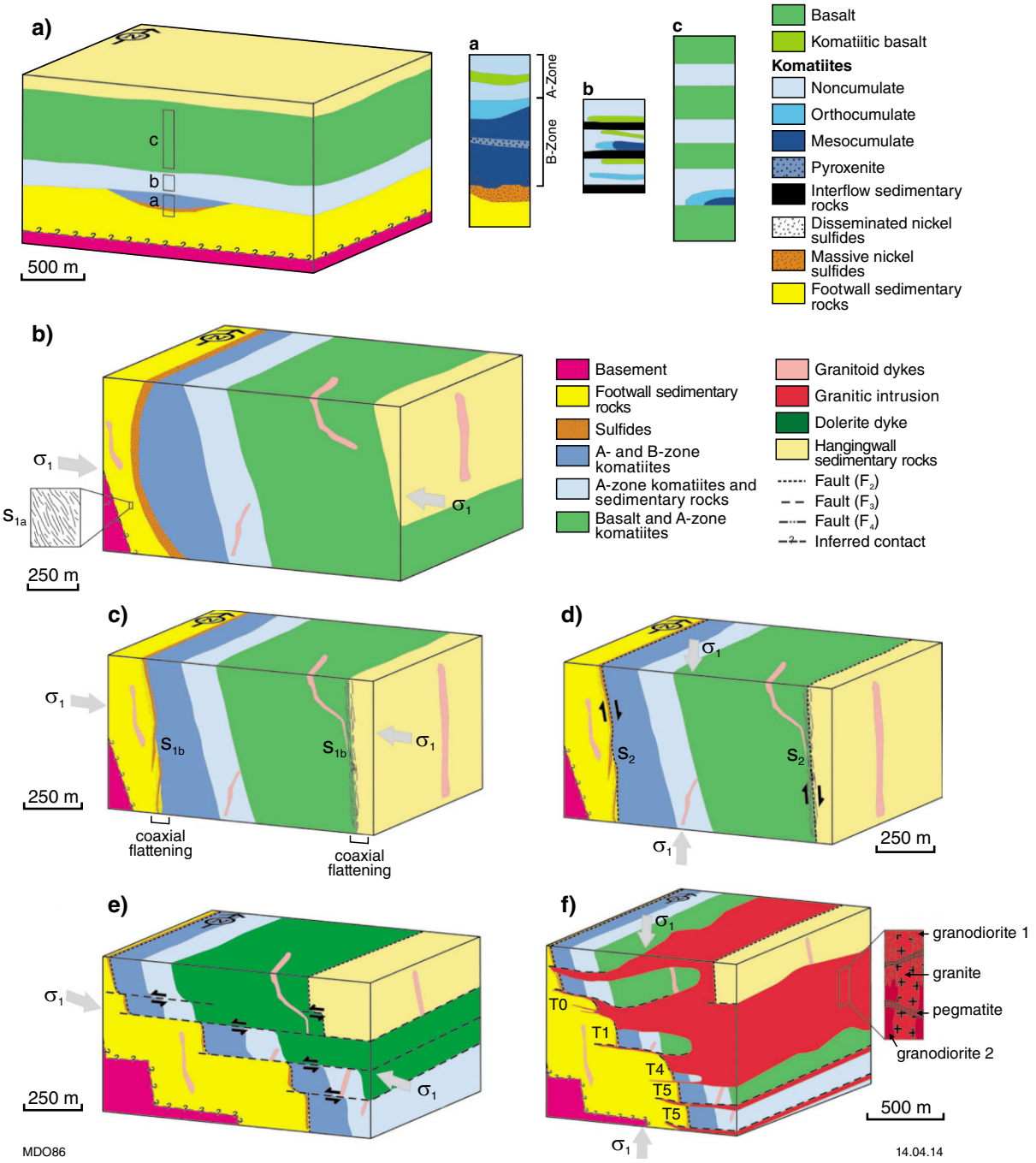

Figure 29. **Block models showing integrated history of the Flying Fox deposit, including volcanism, deformation, and magmatism: a) D_0: primary volcanism producing nickel sulfide mineralization in an interpreted trough structure. Basement contact is inferred, and all stratigraphy was essentially horizontal when extruded/deposited; b) D_{1areg}: east–west compression resulted in tilting of the stratigraphy (60° towards the east). Granitic dyke intrusions syn- to post-D_{1a}; c) D_{1b}: continued east–west compression resulted in coaxial flattening along footwall sedimentary rock – komatiite and hangingwall sedimentary rock – basalt contacts which resulted in the nickel sulfides being squeezed off contact into the footwall sedimentary rocks; d) D_{2FF}: rotation in σ1 (northwest–southeast) resulted in the coaxial flattened zones becoming shear zones with a normal sense of movement; e) D_{3FF}: rotation in σ1 back to east–west shortening resulted in flat-lying shear zones, dipping 5–10° towards the southeast, that offset the ore shoots and stratigraphy; f) D_4: east–west compression ceased and extension commenced. Granitic magma (no less than five pulses) intruded along and exploited the D_3 shear zones, dilating at triple points to create the T0 and T4 ore shoots. The T0 ore shoot was dissected by granitic magma fingering through the ore, resulting in slight rotation of the ore shoot and an apparent offset towards the west (i.e. in the direction of granitic movement). A portion of the T5 ore shoot was ripped off and entrained in the granitic magma, forming a pipe-like shoot offset up to tens of metres to the east.**

Table 1. An integrated chronology of events at the Flying Fox deposit including the timing of metamorphism, magmatism, and sulfide remobilization with associated hydrothermal alteration assemblages (D_{Reg} = deformation events observed regionally, D_{FF} = deformation events observed at Flying Fox; am – amphibole, bt – biotite, cal – calcite, cb – carbonate, chl – chlorite, di – diopside, fuc – fuchsite, grt – garnet, ms – muscovite, pn – pentlandite, py – pyrite, qtz – quartz, ser – sericite, sil – sillimanite)

Event	*Deformation*	*Metamorphism*	*Magmatism*	*Nickel sulfides*	*Hydrothermal alteration*
D_{0Reg}	Ultramafic and mafic volcanism and sediment deposition			Nickel mineralization synchronous with komatiite emplacement	Sea floor alteration of basalts and possibly komatiites resulting in dp–grt–qtz–cb veins
D_{1aReg}	E–W compression tilting the stratigraphy producing a dominant foliation (S1a) dipping 62° towards 92°	Prograde metamorphism (upper amphibolite facies) and contact metamorphism (associated with the granitoid dykes)	Intrusion of granitoid dykes late D1a		
D_{1bFF}	Continued E–W compression has resulted in coaxial flattening at the basalt/hangingwall sedimentary rock contact and footwall sedimentary rock and massive sulfide/komatiite contact defined by a steep foliation (S1b) dipping 72° towards 92°	↓		Sulfides revert to Mss and squeeze along S1b fabric and off-contact	fuc in FW sedimentary rocks and sulfides, alteration haloes around stringer/vein sulfides, py–pn intergrowths, di–cb–am–qtz–grt veins in basalt and hangingwall sedimentary rocks aligned with S1b
D_{2FF}	E–W extension (localized) resulting in dip-slip shearing along the coaxial flattened zones displaying normal offset	Continued prograde metamorphism		Continued remobilization during shearing	di–cb–am–qtz ± grt alteration in the basalt associated with F3 shear
D_{3FF}	E–W compression resulted in NNE–SSW striking thrusts (F3) that offsets the ore body by up to 250 m, defined by a shallow foliation (S3) dipping 8° towards 94°, and a crenulation cleavage	↓		Sulfides smeared along F3 shears, S3 foliations and fold hinge of crenulation cleavage	
D_{4FF}	E–W extension resulting in two brittle–ductile faults (F4) at the contact between the granitic rocks and the footwall sedimentary rocks (T0 and T4) dipping 60° towards the east	Retrograde metamorphism and contact metamorphism (associated with granitic rock intrusion)	Intrusion of granitic rocks creating the two F4 faults	Sulfides entrained in granitic rock creating breccia sulfides, smeared along F4 fault planes, offset into the footwall sedimentary rocks, and encapsulated by granite (T5)	chl alteration of granite, qtz veining, fel phenocrysts in the granite altered to sericite, py–pn intergrowths in sulfides, bt rimming stringer sulfides, fuc in granite and sulfides
D_{5FF}	Brittle faulting observed in all rock types	Contact metamorphism (associated with dolerite dyke intrusion)	Intrusion of E–W trending dolerite dyke		chl–cal–ser coating F4 -faults

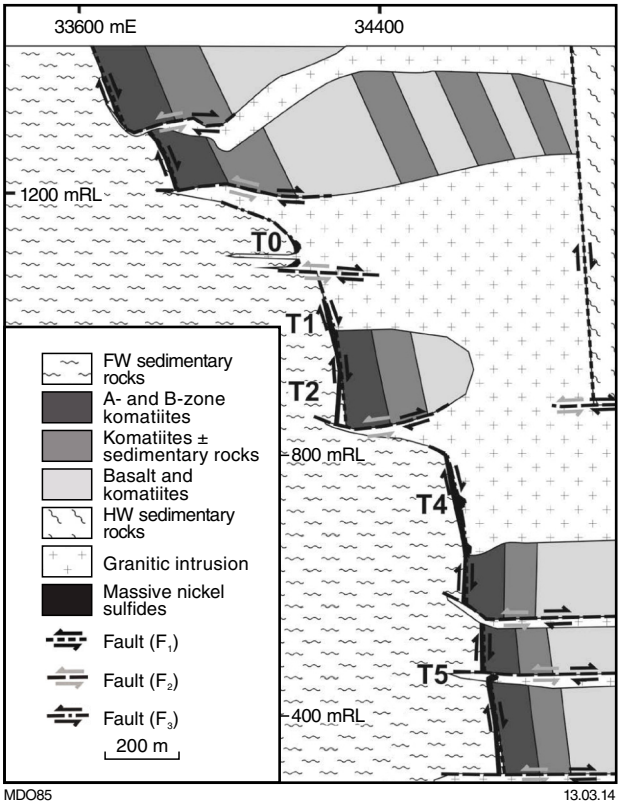

Figure 30. Simplified north-facing schematic cross-section through the Flying Fox deposit illustrating the location of the T0, T1, T2, T4, and T5 ore shoots in relation to stratigraphy. Note that the massive sulfide ore shoots are dominantly located between the footwall sedimentary rock and komatiite, or footwall sedimentary rock and granite contacts, and that the stratigraphy is steeper at these contacts. The flat-lying faults show a dominant reverse motion but revert to normal motion during later extension when the granitic rocks intruded.

Locality 2: Spotted Quoll nickel mine – Forrestania greenstone belt

by Western Areas NL

The Spotted Quoll deposit is located about 6 km to the south of the Flying Fox deposit in the Western ultramafic belt of the Forrestania Nickel Project (Fig. 26).

The geological setting of the openpit Spotted Quoll deposit is complex. Nickel mineralization is hosted in a strongly mineralized shear zone hidden below a granite dyke (Fig. 31). It is inferred that the sulfides have been sheared and remobilized in their present location. The local stratigraphy is heterogeneous, and includes ultramafic rocks, basalts and various sediments, including minor BIFs (Table 2). The stratigraphic age of the sequence is not well known. However, metasedimentary rocks from the lower part of the Spotted Quoll succession yield a maximum depositional age of 2832 ± 13 Ma, which indicates sedimentation younger than c. 2900 Ma (Doublier et al., 2012).

The first ore from Stage 1 underground mining (Fig. 32) was delivered in November 2011, and production of 10 000 tpa nickel during Stage 1 is expected. As of June 2012, the ore reserve estimate was 3.095 Mt @ 4.2% nickel containing 131 360 t nickel, which remains open at depth. This corresponds to a mine life of greater than 10 years.

Locality 3: synorogenic and weathering-related BIF-hosted high-grade iron ore in the Yilgarn Craton: the Koolyanobbing K and satellite deposits, Western Australia

by T Angerer and SG Hagemann

Introduction

The structural control of high-grade iron ore (58–68 wt% Fe) hosted in banded iron-formation (BIF) is considered to be one of the most important factors that influence the location and geometry of ore deposits (Dalstra and Rosière, 2008, and references therein). However, the details of ore formation processes and the relative timing of deformation and iron oxide enrichment is still contentious for most known iron ore deposits globally, mainly because of the lack of absolute geochronological constraints. This has led to contrasting structural and genetic models, which have been summarized recently by Dalstra (2011). Syngenetic models propose that syn-sedimentary or diagenetic structures, such as extensional faults or boudinage (Findlay, 1994) led to lithofacies variations or diagenetic modification of BIF and the production of chert-free iron formation (e.g. Lascelles, 2007). In hypogene models, hydrothermal fluid flow associated with deformation is interpreted to be important for the localization of iron oxide mineralization in low mean stress zones within and adjacent to structures (e.g. Dalstra and Rosière, 2008). Stress regimes in which iron ore formed can be variable, in such as compressional (Powell et al., 1999), extensional (Taylor et al., 1981), and transpressional/tensional (Angerer and Hagemann, 2010) settings have been proposed for specific deposits. Hypogene–supergene models are now proposed for a multitude of iron ore deposits in various geological settings to explain their multistage, structurally controlled upgrading processes (e.g. Barley et al., 1999; Taylor et al., 2001; Thorne et al., 2004). Ancient or recent supergene goethite upgrade facilitates existing structures as high-permeability zones for the movement of groundwater, causing either leaching of gangue and redistribution of Fe in the lateritic and saprolitic zone (Ramanaidou, 2009), or pseudomorphic goethite replacement of gangue in probably deeper zones of groundwater circulation (Morris et al., 1980; Morris, 1985).

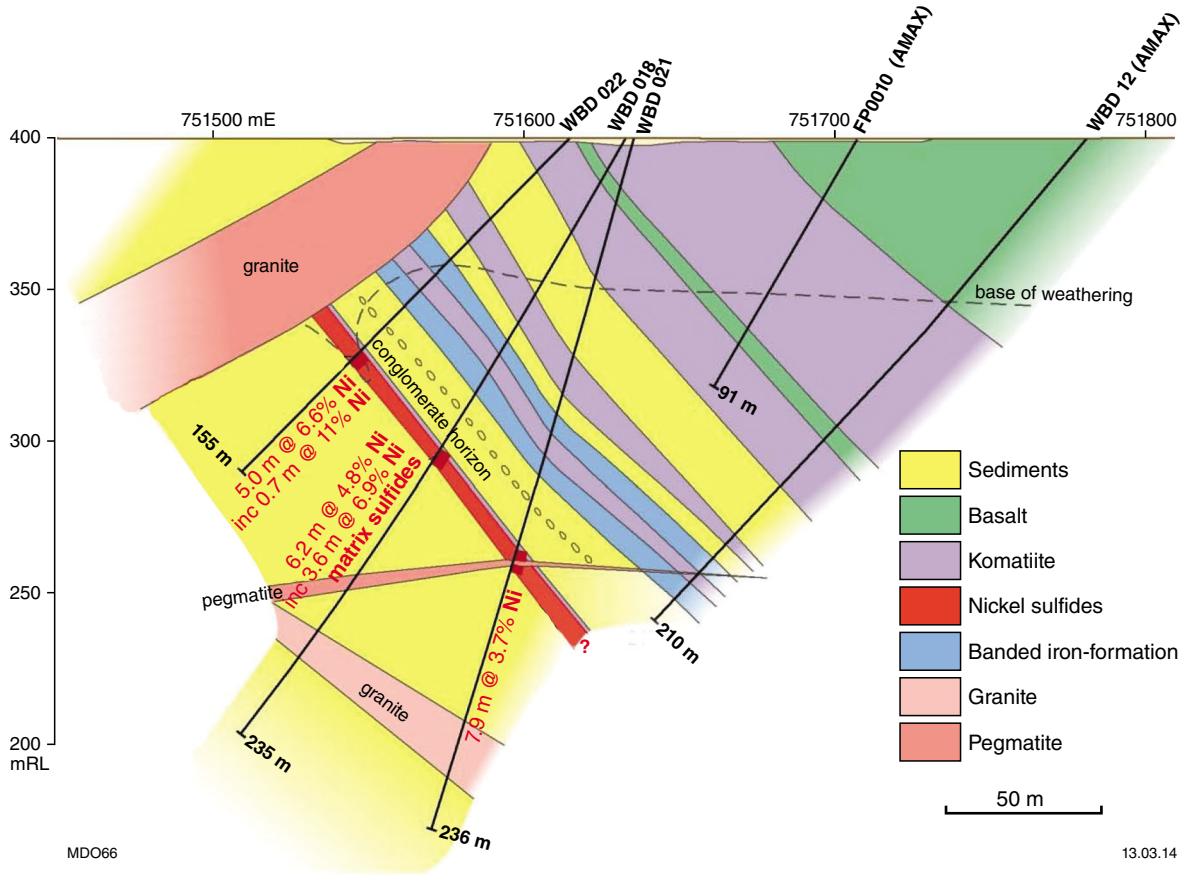

Figure 31. Diagrammatic section through the Spotted Quoll deposit (Forrestania), illustrating distribution of the rock types

Table 2. Local stratigraphy of the Spotted Quoll deposit

Geological unit	*Description*	*Sub-units*	*Approx. width (m)*
Footwall sediments	Quartz–sillimanite–mica +/- garnet sediments	Amphibolitic sediment, chert	>500m
Spotted Quoll ore zone(s)	Pyrite–violarite (supergene), Pyrrhotite–pyrite–violarite–pentlandite (transition), Pyrrhotite–pentlandite–pyrite (primary). Chalcopyrite- and arsenic-bearing phases incl. niccolite, gersdorfite	Massive, matrix, breccia, stringer and disseminated sulfide in enclosing amphibolitic sediments and ultramafics	<15m, two ore horizons in northern zone, one in southern zone
Host sedimentary sequence	Mostly silicic sediments in footwall and hangingwall of ore zone, with minor altered ultramafic. Strong banding and interlayering of sedimentary units	Amphibolitic sediment, BIF, felsic sediments. Debris flows and conglomerate located 10–15 m above ore zone	20–30 m
Hangingwall ultramafic	Dominantly massive amphibole-rich komatiite with porphyro-blastic metamorphic olivine. Minor olivine-rich ultramafic	Two main units of intercalated silicic sediments. Minor komatiitic basalt	120–150 m
Basalt	Actinolite-chlorite basalt		70–90 m
Graphitic, sulfidic sediments	Black to grey (graphitic) shale to siltstone with abundant iron sulfides +/- carbonate alteration	Black shale, sulfidic shale, siltstone, massive sulfide, massive carbonate	50–60 m
Eastern ultramafic	Actinolite–chlorite komatiite with metamorphic olivine		60 m
Eastern basalt	Actinolite–chlorite basalt		60 m
Eastern sediments	Quartz–mica sediments and schists		>200 m

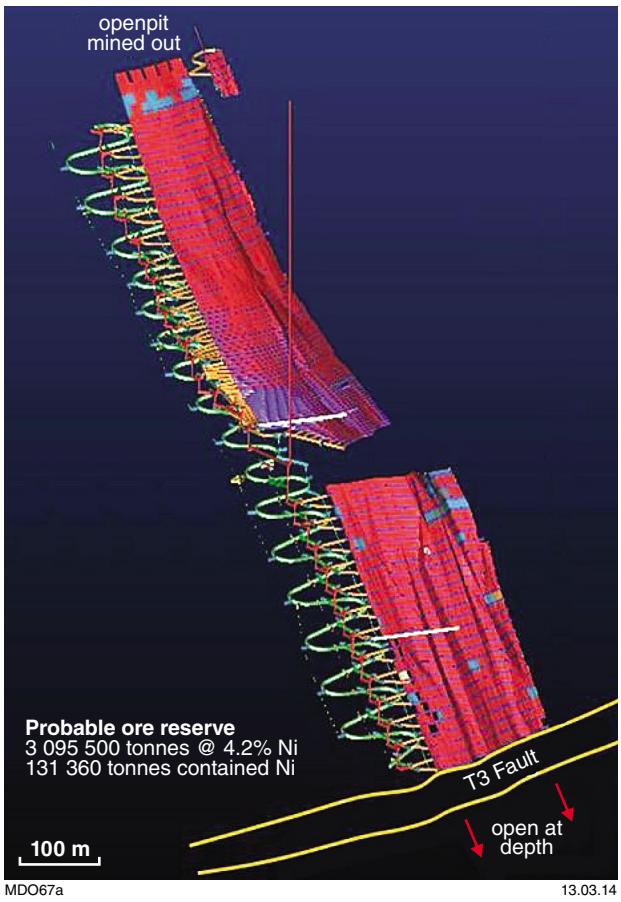

Figure 32. 3D model of the Spotted Quoll mine site showing the open pit, and underground stages 1 and 2

Many Archean greenstone belts in the Youanmi and Murchison Terranes, Yilgarn Craton, host BIF (~30% Fe), some of which contain high-grade magnetite-, hematite- or goethite-rich ore deposits (58–68% Fe) of about 10 Mt to more than 200 Mt in size. In recent years, numerous small- to medium-sized exploration and mining companies are focusing on understanding controls on greenstone belt-hosted iron ore and exploiting the increasing number of delineated resources (Greentree and Lord, 2007; Cooper and Flint, 2009). As a result, several industry-sponsored studies of greenstone belt-hosted iron deposits in the Yilgarn Craton have been, or are currently being, undertaken by the Centre for Exploration Targeting in order to understand 'iron upgrade' processes, timing of mineralization with respect to the terrain history, structural control, and fluid sources, as well as generating new targets (a brief and meanwhile slightly outdated summary given by Angerer et al., 2010). BIF-related high-grade magnetite-, hematite-, and goethite-rich ore deposits Archean granite–greenstone belts of the Yilgarn Craton are described for the Weld Range (Duuring and Hagemann, 2012b, a), Jack Hills Matthew Ridge (Maskell et al., in press), and Windarling (Angerer et al., 2013). The present article summarizes the results of a study on the structural controls and mechanisms of ore formation in the Koolyanobbing iron ore deposits (Angerer and Hagemann, 2010; Angerer et al., 2012).

Geological setting of the Koolyanobbing deposits

The Koolyanobbing greenstone belt (KGB) in the Southern Cross Domain, 350 km east of Perth, contains seven known deposits with a total pre-mining iron ore reserve of about 200 Mt (Portman, 2008). The main deposit, K pit, with a pre-mining resource of more than 100 Mt of high-grade iron ore is assumed to be the largest known single deposit in the Yilgarn (Fig. 33). The KGB is composed of the about 3.0 Ga lower greenstone succession, which mainly consists of tholeiitic basalt flows and pillows and minor basic tuffs, komatiites, and several BIF units. A subdivision of mafic volcanic events in the KGB into four distinct lithostratigraphic subsequences (Fig. 34) has been proposed by Angerer et al. (2012). This division into subsequences 1 to 4 (S1 to S4) is based on the occurrence of four major mafic volcanic sequences divided by three inter/postvolcanic periods, recorded as greenstone belt-wide BIF sedimentation, which therefore mark the top of each sequence. The ultramafic rocks in the sequences, based on whole-rock high field strength elements, preserve both aluminium-depleted and -undepleted komatiites and continental lithospheric mantle contaminated boninites. Such a co-magmatism of both lava types can be interpreted as the result of the interaction of a mantle plume (source of komatiite) in a geodynamic subduction zone (source of boninite) setting (Angerer et al., in 2012).

The following deformation sequence in the KGB has been established by Angerer and Hagemann (2010) and is also summarized in Fig. 35: a) a D_1 produced mostly horizontal westerly to southwesterly trending small-scale folds in the BIF units. The D_{1a} (recumbent isoclinal) and D_{1b} (open to tight, upright to vergent) have been produced probably within one progressive deformation event that also produced minor D_{1b} thrusts; b) the D_2, probably related to the emplacement of the surrounding granitoid domes, such as the Ghooli dome, tilted the lower succession and D_1 folds from a roughly horizontal position into the steep east-northeasterly dipping or plunging position. The KGB represents one single fold limb showing locally internal parasitic D_{2a} folds with varied fold hinge orientation. The D_{2b} is a progressive deformation subsequent to D_{2a}, mainly involving reverse shearing and folding of chlorite schists and talc-altered BIF, and predominantly reverse faulting of lithological boundaries; c) ductile strike-slip movement took place during D_3 along the boundary to granitoids/gneisses that formed the Koolyanobbing Shear Zone; d) brittle strike-slip movement during D_4 led to tectonic duplication accommodated by horizontal duplexes and reverse faults; e) a late-stage brittle segmentation and reactivation of existing faults is attributed to D_5.

The D_1 structures formed in a north–south to northwest–southeast compressional regime, whereas all D_2 to D_4 deformation events were generated during an east–west compression and were expressions of the main orogenic event in the central Yilgarn Craton. The deformation sequence in the KGB is in accordance to the proposed evolution in the Southern Cross Domain (Dalstra, 1995; Chen et al., 2001; Chen et al., 2004).

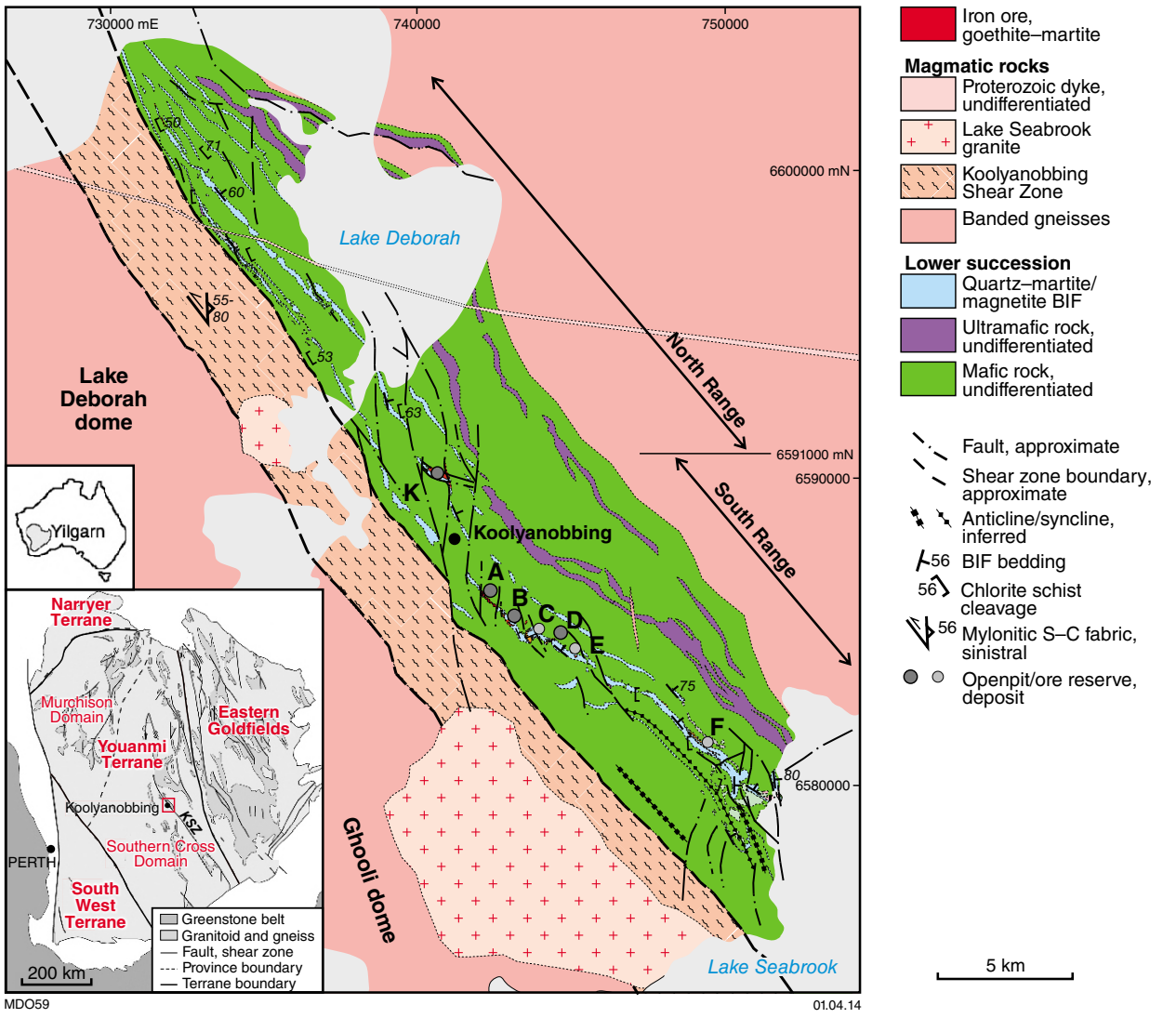

Figure 33. Overview maps: simplified geological map of the Koolyanobbing greenstone belt (KGB); insets: Yilgarn Craton with its location in Australia (modified after Angerer and Hagemann, 2010)

The K deposit

The K deposit is located in the central part of the KGB, about 1.5 km north of the town of Koolyanobbing (Fig. 33). The host rock of the K deposit is a quartz–magnetite–martite BIF unit. The footwall and the hangingwall of the BIF sequence consist of chlorite schists with internal decametre-wide lenses of massive metabasalts and ?metatuffites. A 50–70 m thick lens of stratigraphic massive pyrite is located between the footwall mafic rocks and the BIF (Figs 36 and 37). The quartz–magnetite BIF displays considerable compositional variation in the south and southeastern pit walls, from carbonate–magnetite to talc–magnetite BIF. The BIF in the K deposit is structurally thickened to about 230 m due to: a) east- to southeast-plunging metre- to decametre F_{2a}-folds, the latter displaying S-, Z-, and M-shapes and fold axial planes that dip steeply towards the north-northeast to northeast; b) a large-scale sinistral duplex and imbricate fan system (with a western and eastern lithon), which is indicated by en echelon, steeply north-northeasterly to east-northeasterly dipping D_4-faults that are parallel to, and crosscutting, the BIF unit at a low angle. D_5-faults crosscut the D_4-duplex and -imbricate fan structures, or reactivate older faults.

The iron ore in the K deposit ore body can be subdivided into four distinct zones: a) a goethite–martite–specularite zone represents the main ore body and extends from the original surface to about 70 m below the current surface; b) a martite–specularite–goethite zone is situated generally below the first zone and includes the western and eastern lithons; c) thin pure specularite or quartz–specularite breccia zones are D_4-duplex and -imbricate fan hosted; d) a magnetite zone (Guarin Jr et al., 2009) in the south wall and in the central part of the openpit characterized by medium-grade quartz–, talc–, and carbonate–magnetite BIF enveloping magnetite ore bodies. The main magnetite

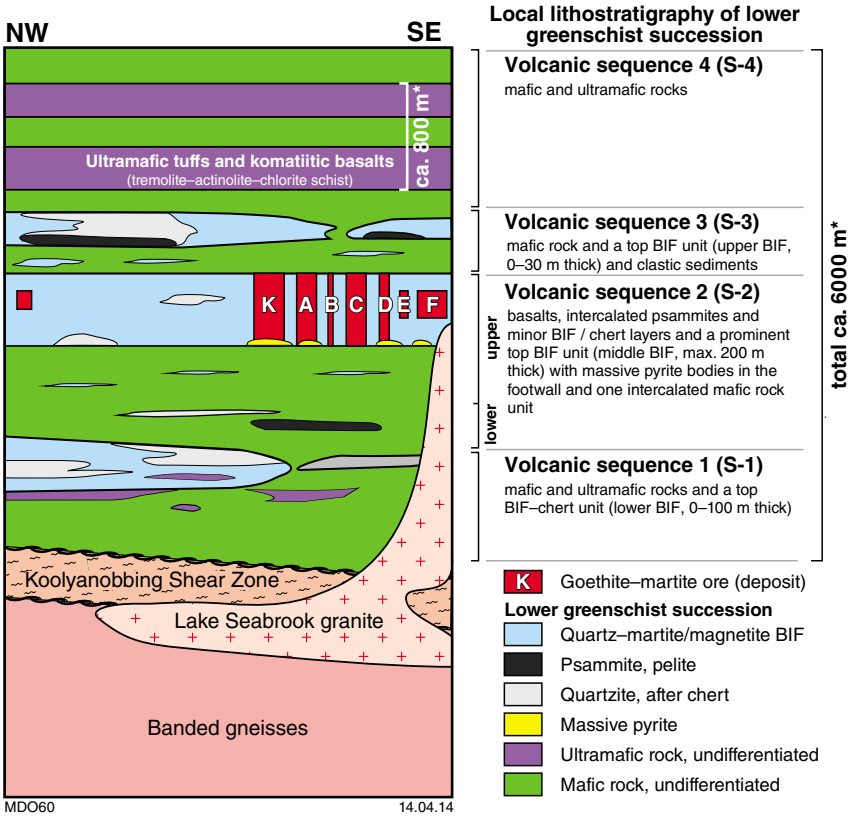

Figure 34. Stratigraphic column of the Koolyanobbing greenstone belt, with division of the four volcanic sequences (modified after Angerer and Hagemann, 2010)

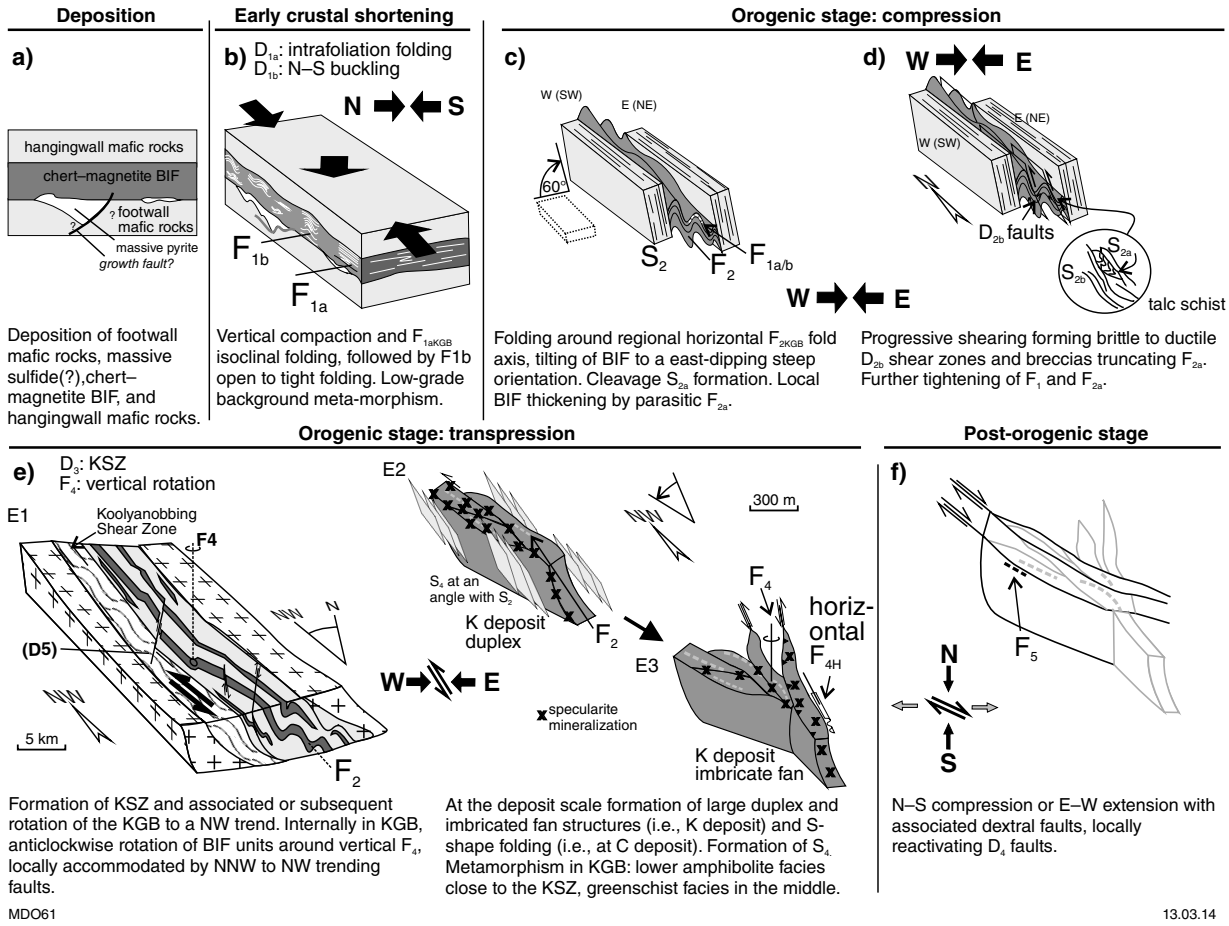

Figure 35. Structural model of the Koolyanobbing greenstone belt (modified after Angerer and Hagemann, 2010)

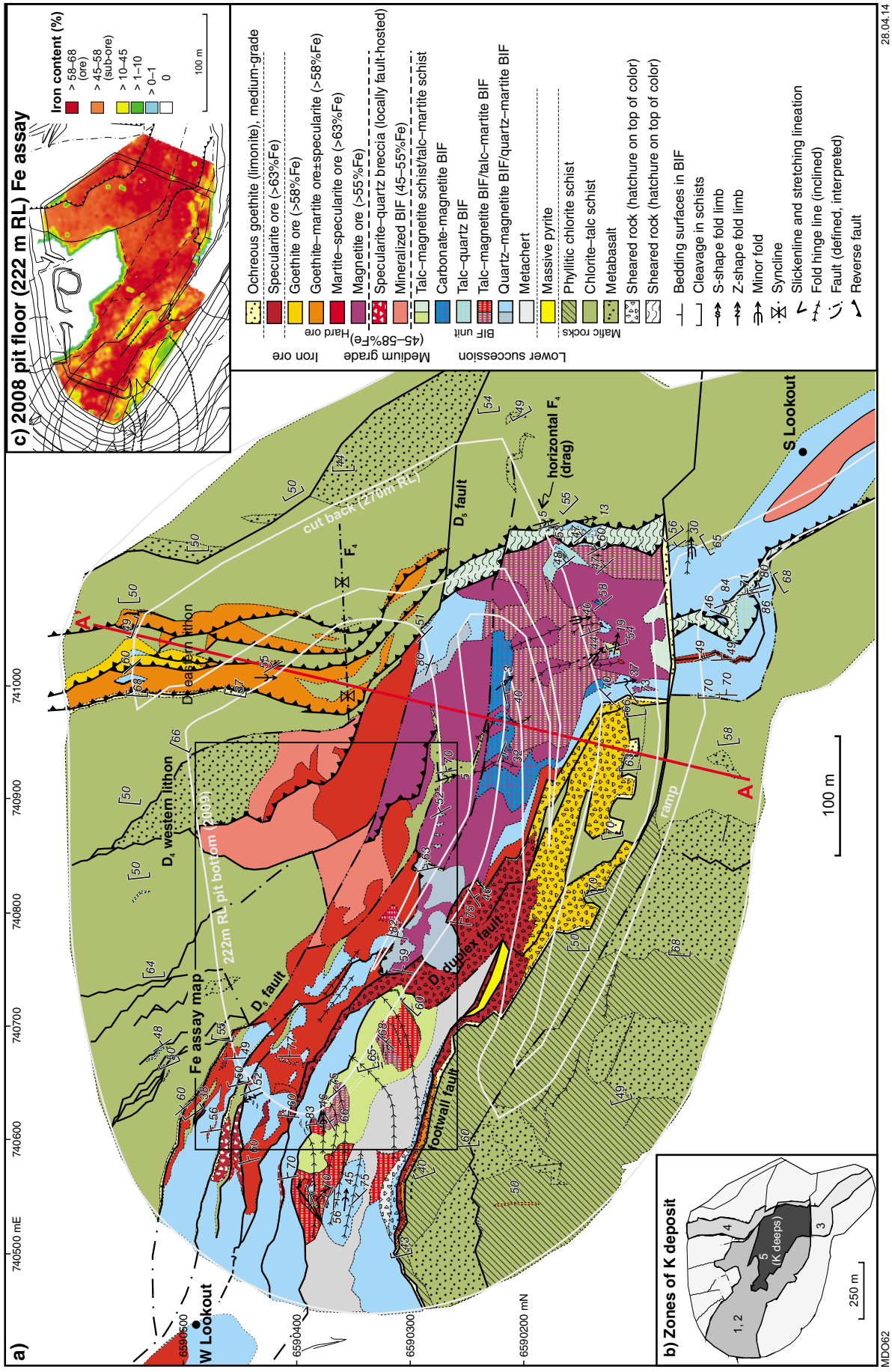

Figure 36. Geological map of the K deposit (pit outline of mid 2008). The red line indicates cross-section shown in Figure 37. The two lookouts are indicated by black filled circles (modified after Angerer and Hagemann, 2010)

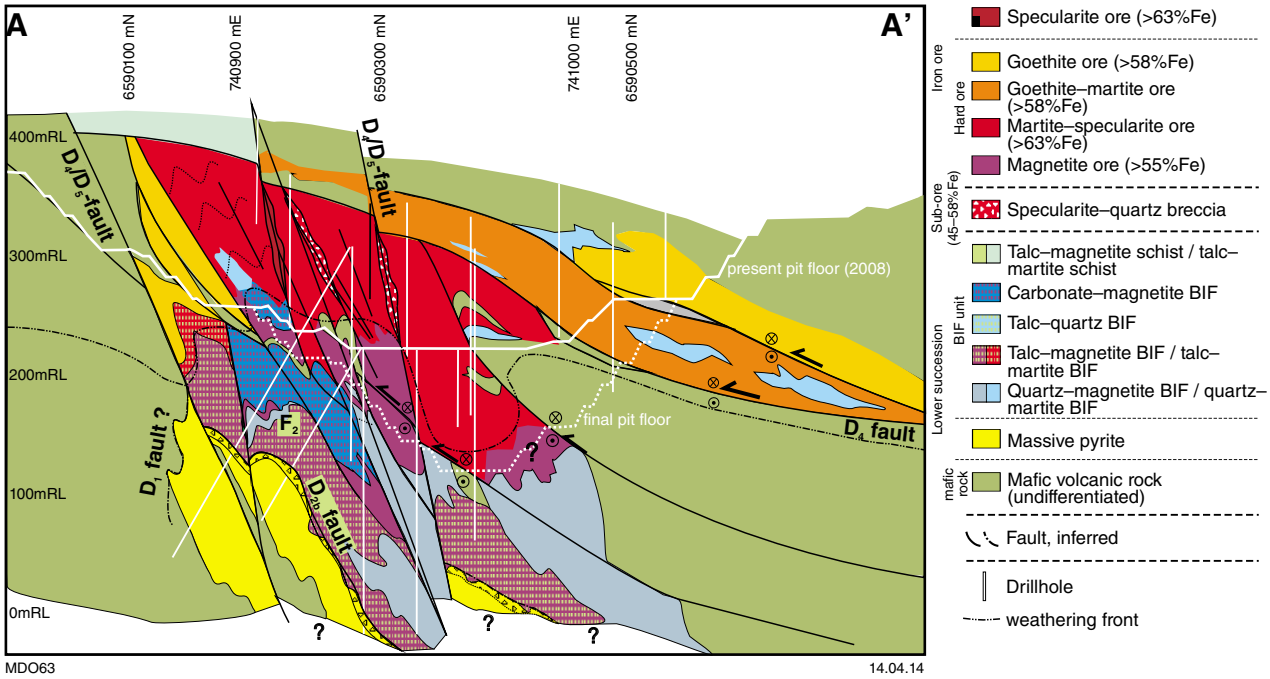

Figure 37. Cross-section of the K deposit. Location is shown by the red line in Figure 36 (modified after Angerer and Hagemann, 2010)

ore zone is located either underneath the martite ore body, or is juxtaposed against it by steeply dipping D_4/D_5 faults.

Goethite–martite–specularite ore is laminated (partly vuggy) or massive. With a higher content of (typically coarse crystalline) specularite in the ore, the laminated texture tends to be obliterated. Magnetite ore is texturally similar, and appears to be the unweathered precursor of martite ore.

Ore-forming stages

In the K deposit, four hypogene ore formation stages have been identified and related to specific Archean deformation events. A fifth stage is the recent supergene, that is, weathering-related, modification of pre-existing hypogene ore.

Ore stage 1: siderite and Fe-magnesite replacement alteration

Iron ore stage 1 is an early Fe–Mg(±Ca?) metasomatism that caused local alteration of quartz–magnetite BIF to Fe-rich carbonate–magnetite BIF, replacing silica layers (Fig. 38a). Carbonates are mostly siderite and Fe–magnesite. Iron is added to the BIF host rock; hence, carbonate alteration is an important ore-forming stage. Because carbonates are structurally weaker and easier to dissolve than quartz at very low temperature, ore stage 1 'prepared' BIF for subsequent strain localization and coupled dissolution of carbonate gangue during ore stage 2.

The structural control of this carbonate–talc alteration is impossible to reconstruct because subsequent deformation (D_2–D_4) and alteration were so intense in the deposit that the geometry of the alteration zone has been obliterated. The relative timing of ore stage 1 may be as early as diagenetic; however, quartz in zones of incomplete replacement shows recrystallized textures and this suggests that replacement postdated early metamorphic D_1.

Ore stage 2: residual magnetite enrichment during D_2–D_4

Iron ore stage 2 includes the formation of laminated magnetite ore and magnetite ore breccia. Magnetite ore bodies are located predominantly in tight D_{1b}/D_2-folded zones, which strike subparallel to the BIF unit, that is, north-northwesterly to west-northwesterly and plunge is moderately steep. Considering the thinned limbs consisting of residual magnetite layers (Fig. 38b), dissolution of carbonate during tight folding is likely to be the mechanism of ore formation. As a consequence of gangue dissolution, microporosity increased and caused magnetite microlayers to disintegrate forming fine-grained cataclasis zones intercalated with the mechanically more stable magnetite mesolayers in laminated and breccia ore. By overprinting relationships, the minimum age for the magnetite ore formation in the K deposit is constrained by the onset of D_4.

The proximal talc–carbonate and intermediate carbonate zones surrounding magnetite ore indicate their close genetic relationship to ore. The close spatial relation between talc and magnetite ore may be explained by two, not necessarily excluding, processes: a) selective mobilization of pre-existing talc by mechanical or by solution transfer, occurring in high mean stress zones such as tight fold limbs; or b) reaction of dissolved Mg from selectively mobilized magnesite in areas of residual quartz-rich magnetite BIF under low-grade conditions; or both.

Ore stage 3: hydrothermal/contact metamorphic magnetite in D_{2b}–D_4 structures

Iron ore stage 3 includes the mineralization of magnetite in brittle and brittle–ductile structures, such as D_{2b}-faults, -fractures, and -breccias; in reactivated D_{2a}-fold cores, and locally in wall rock and quartz veins adjacent to mineralized brittle structures. Main structures that control the ore stage 3 mineralization in the K deposit are the boundary fault between massive sulfide and quartz-, and carbonate–magnetite BIF (Fig. 38c). The main process of magnetite formation during ore stage 3 involved replacement of quartz and localized carbonate.

The granular magnetite ore in the K deposit was modified by pressure-solution deformation and mineral growth during ore stage 3. In magnetite BIF, only minor and centimetre- to decimetre-scale brittle–ductile shear zones or mineralized fold cores contain stage 3 magnetite mineralization. The stage of specularite replacement (ore stage 4), associated with D_4 faults, represents the likely minimum age for ore stage 3.

Ore stage 4: specularite mineralization and first martitization (syn-D_4)

Specularite mineralization controlled by steep D_4 faults is defined as ore stage 4 (Fig. 38d). Major controlling structures are large strike-slip faults with a north-northwesterly to west-northwesterly trend (Fig. 33). Mineralized faults at the deposit-scale include second-order strike-slip faults, such as the footwall and horse faults of the duplex system, and strike-slip and reverse shear zones in the eastern lithon (Fig. 36).

Specularite formation is characterized by the replacement of gangue in laminated micro-specularite–martite ore and medium-grade BIF, and by coarse-crystalline massive and disseminated specularite in brittle faults, breccias, and voids. Specularite formation is also locally associated with hydrothermal quartz–Fe-dolomite–talc–chlorite–pyrite–magnetite alteration associated with breccia pods, brittle faults, and tension gashes, which all crosscut magnetite ore. This carbonate-rich alteration may be associated to a second metasomatic event, but to some extent remobilization of early carbonate (stage 1) may have also taken place. The precipitation of this hydrothermal assemblage in BIF was not an effective ore upgrading process; in fact, it caused downgrading of magnetite ore. However, any carbonate replacement of quartz in siliceous BIF was important ground preparation for weathering-related leaching during ore stage 5 (see below).

Hydrothermal martitization related to specularite overprint has been observed in some magnetite ore (cf. Lobato et al., 2008). In the weathering zone, it is not distinguishable from the ubiquitous martitization related to weathering (cf. Morris, 1980; Morris, 1985).

Ore stage 5: recent supergene ore stage

Supergene ore stage 5 produced two generalized weathering profiles, which: a) overprinted preferably altered BIF; and b) much more importantly, overprinted hypogene ore (Fig. 38e). Whereas weathering in quartz–magnetite BIF does not show significant ore formation, unless it was strongly carbonate altered, weathering of hypogene ore exhibit the following main zones, from the base to the top: a) a magnetite ore showing no weathering; b) a martite zone, which indicates partial to complete gangue leaching; c) a goethite-rich martite zone, which shows partial to complete pseudomorphic gangue replacement from carbonate(–siliceous) BIF and breccias, and goethite replacement of martite forming goethite–martite ore; d) a massive to vuggy, clay- and secondary silica-rich goethite zone, which represents a hard cap. In these zones, which are similar to vertical depth profiles of supergene modifications in iron ore deposits in the Hamersley Basin, relative and absolute thicknesses strongly depend on the extent of vadose and phreatic zones (Clout, 2003). The maximum age of this weathering-related overprint in the KGB may be as old as Permian, corresponding to regolith ages throughout the Yilgarn (Anand and Paine, 2002).

Summary and exploration significance

Hydrothermal BIF alteration in the K deposit and iron ore formation took place in several stages, commencing with an early Fe–Mg(±Ca?) metasomatism, which caused localized alteration of quartz–magnetite BIF to Fe-rich carbonate–magnetite BIF. This was followed by a synorogenic mobilization of gangue minerals producing residual enrichment of mostly magnetite protore (i.e. a partially mineralized or carbonate-altered rock, which was subject to further alteration) and talc alteration surrounding the protore. Localized hydrothermal quartz–magnetite mineralization in reverse fault breccias and fractures occurred afterwards and was followed by strike-slip fault-controlled late hydrothermal alteration that involved the formation of specular hematite and martitization. The P–T–X characteristics, fluid sources and timing and evolution of the hydrothermal (mineralizing) fluids and associated hydrothermal alteration, is the subject of current investigations.

The results of this study may influence exploration for iron ore in Archean BIF because the strong structural control of iron ore that has been described for the KGB implies the general necessity of evaluating the structural features and evolution of an exploration district to fully understand its prospectivity. The close spatial relationship of the surface-related upgrade by goethite precipitation and gangue leaching to existing medium- to high-grade magnetite–martite–specularite ore, clearly indicates the possibility of existing blind magnetite or specularite-rich

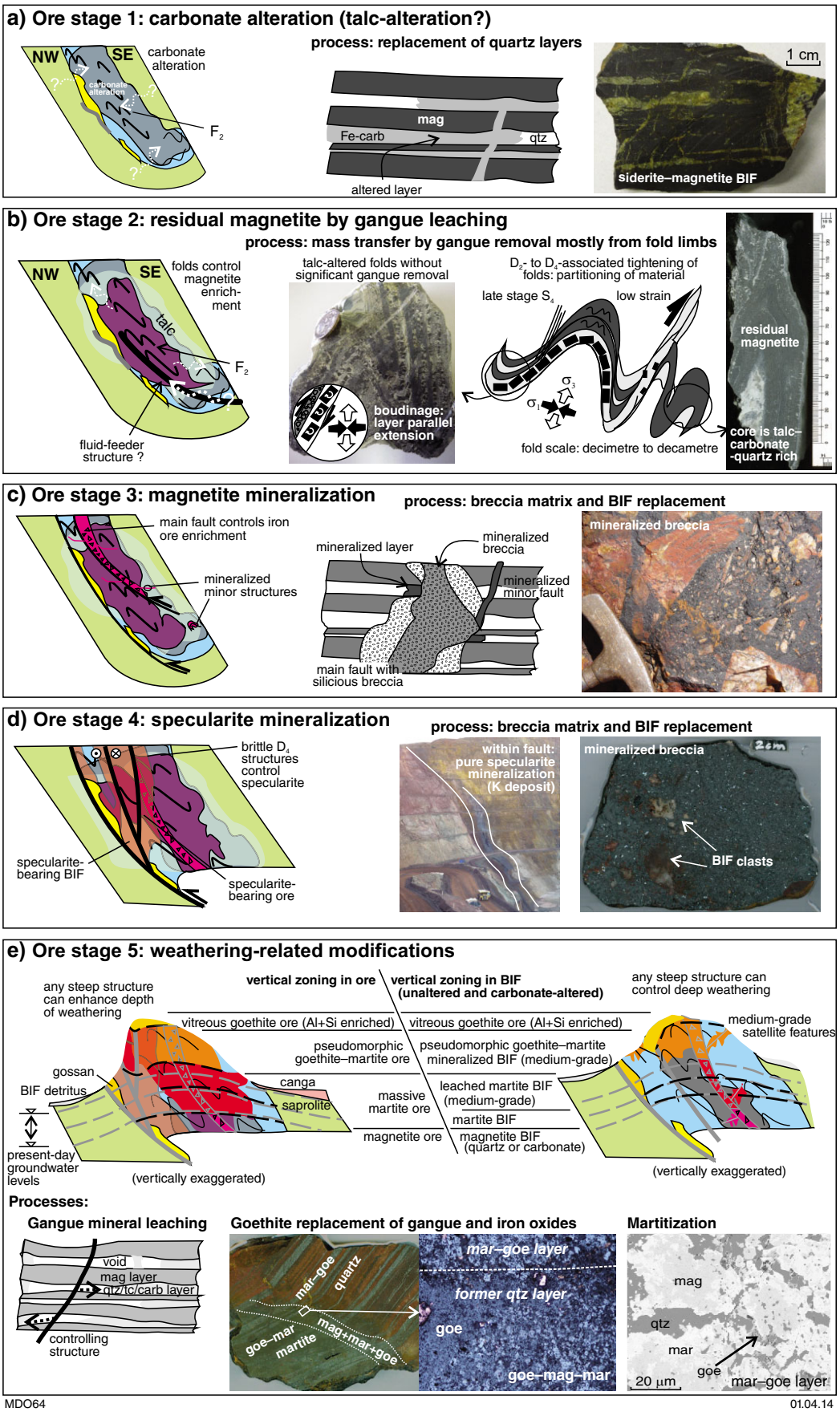

Figure 38. Summary of ore-forming stages at Koolyanobbing (modified after Angerer and Hagemann, 2010)

ore bodies within the BIF units. The martitization during specularite stage may also have produced localized high-grade specularite–martite ore. The occurrence of talc and carbonate proximal to high-grade ore may be used as footprint indicators for high-grade magnetite-, martite-, and specularite-rich ore types. In order to delineate concealed ore bodies and alteration footprints, an evaluation of the prospectivity of structures in the BIF unit, combined with the application of geophysical — that is, gravity, magnetic, and reflectance spectral surveys — are essential.

Koolyanobbing excursion stops

Locality 3a: K deposit

Two Lookout provides an excellent overview of the entire pit. Afterwards, we enter the pit and stop at two localities.

The first stop is within the 'K deeps' zone, the carbonate(–talc)-rich magnetite ore zone. Here, the intense, isoclinal, folding and shearing in BIF is observable, as well as syndeformational upgrade textures (thinned BIF oxide layers in fold limbs and mineralized breccias) with talc-altered BIF haloes. Shear zone hosted talc–magnetite schists and hematite veins and breccias are mostly related to subsequent D_4-reactivation.

The second stop in the pit is farther up, in the oxidized martite ore zone. Here we walk along the footwall mafic rocks, intensely sheared chlorite schists (weakly Fe-enriched), into BIF, crossing the high-grade hematite (specularite) mineralized footwall D_4-shear zone. Martite–specularite ore in BIF is only patchily distributed, as here we are at the edge of the deposit.

Locality 3b: supergene zone in A deposit

Supergene-altered quartz–martite BIF with martite–goethite ore, lies within the weathering zone of A deposit. BIF does not show any carbonate here but deeper in the deposit Mg-siderite is the dominating gangue mineral. Quartz and siderite have been replaced by goethite in the ore.

Locality 3c: core farm with KPDD017 core

Rock textures of — and transitions between — variably altered BIF and ore types (goethite–martite–specularite and magnetite–carbonate–talc), as well as the footwall massive pyrite zone and chlorite schists below BIF, can be observed in the very informative drillcore KPDD017.

Additional locality (not visited): D deposit

The abandoned D deposit is a smaller and relatively shallow 'satellite' deposit, a few kilometres south of K deposit. Here, we study the goethite-richer supergene zones. Walking down the ramp to the bottom of the pit, we observe the transition from: a) supergene detrital to; b) in-situ, remobilized, vitreous goethite ore to; c) footwall mafic rocks to; d) fracture controlled patchy saprolitic martite–goethite ore in BIF to; e) fault-related hypogene specularite-rich martite ore.

Acknowledgements

This study has been funded by Cliffs Natural Resources Asia Pacific Iron Ore. Their financial and logistical support is very much appreciated.

Locality 4: the geological setting of the Marvel Loch gold mine

by S Shenton, St Barbara Limited

Introduction

Marvel Loch is the largest of the many shear-hosted gold deposits found within the Southern Cross greenstone belt. The Marvel Loch gold mine is located 600 m east of the Marvel Loch township and 35 km south of Southern Cross. Prospectors Lenneburg, Williamson and Marksman first discovered gold there in 1905.

St Barbara Ltd purchased the Yilgarn operations from Sons of Gwalia in August 2004. Marvel Loch has produced in excess of 2.5 Moz Au.

Geological setting

The Southern Cross Province comprises several greenstone belts with one of the larger ones being the Southern Cross – Forrestania greenstone belt, running from north of Bullfinch, through Southern Cross town, Marvel Loch, Nevoria, Forrestania, and southeast of Hyden (Fig. 39a). Like many of the other greenstone belts, this is strongly attenuated in the north-northwesterly direction. Rock units near Marvel Loch trend north-northwesterly parallel to the greenstone belt margins, and are inferred to young away from the Ghooli granite dome. Multiple periods of folding have shortened the greenstone belt, generated district-scale folds, and accompanied faulting that has juxtaposed rock units at slightly oblique angles across the fault zones.

Marvel Loch geology

The Marvel Loch gold deposit is hosted by a steep westerly dipping package of ultramafic, mafic, and sedimentary rocks to the west, with gabbro, dolerite, and sedimentary rocks to the east (Fig. 39b). In places, units are overturned and may dip steeply to the east. Rock type identification is based on textures, mineralogy, and whole rock geochemistry. In many greenstone belts, all three are well preserved and useful. However, around Marvel Loch high strain has overprinted some early textures, high-grade metamorphism has developed new minerals, and alteration has modified rock chemistry. All of the stratigraphy has been overprinted by amphibolite facies metamorphism and deformed by a major shear zone (the Marvel Loch Shear Zone).

Gold mining is focused in 10 steeply plunging ore pipes: four in the north, and three each in the central and southern areas (Figs 40 and 41). These pipes generally

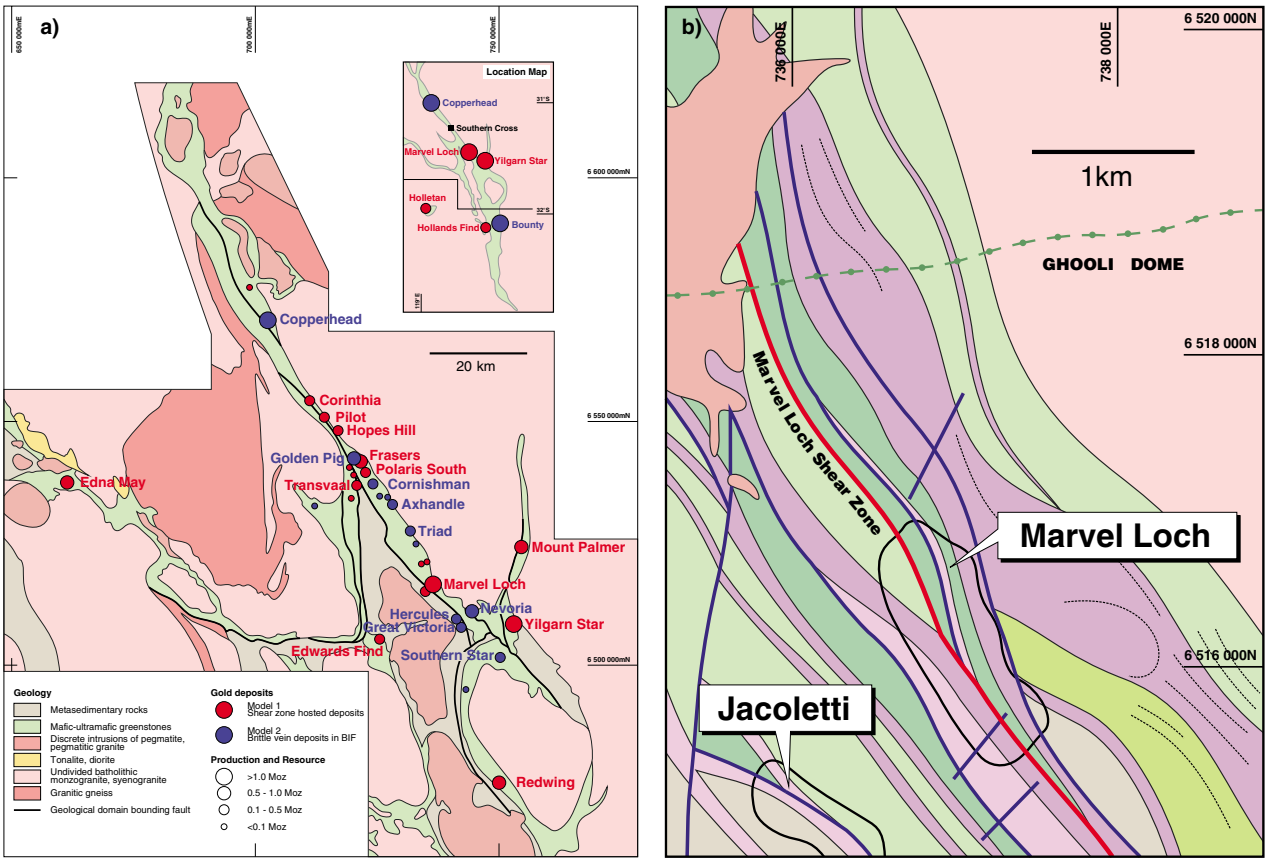

Figure 39. a) Simplified geology of the Southern Cross greenstone belt showing the distribution of gold deposits; b) detailed geology of the Marvel Loch mine area

plunge 60–80° south, have dimensions of tens of metres on a horizontal mine level and are continuous down plunge for more than 500 m. Gold occurs in quartz veins and in altered wallrocks with sulfide minerals. The dominant sulfides are pyrrhotite, arsenopyrite, and pyrite.

The greatest challenge facing the Marvel Loch geology team today is the presence of large granitoid sills that crosscut mineralization in all areas of the mine (Fig. 42). Their intrusion was guided by pre-existing faults, and they are themselves faulted along chlorite-bearing surfaces. At the current mining level in the south (650 m below the pit surface), a large pegmatite approximately 80–100 m thick has displaced mineralization. This pegmatite layer has been interpreted to affect the centre and south lodes below 200 mRL and, therefore, drilling has commenced to determine the geological setting below this pegmatite.

Locality 5: Nevoria gold deposit

by MP Doublier

Introduction

The Nevoria group of deposits is located at the southern closure of the Ghooli dome, about 40 km south-southeast of Southern Cross, and about 10 km southeast of Marvel Loch. The deposit was first mined in the 1930s by Nevoria Gold Mining Co, and by Great Western Consolidated NL in the 1950s (Cullen et al., 1990).

Geology

The Nevoria deposits belong to the BIF-hosted Model 2 deposits, where the rheological contrast between the competent BIF and the surrounding mafic and ultramafic rocks is essential for deposit formation (see ‘Styles of gold mineralization’; Figs 22 and 23). The deposits are at the moderately dipping southern limb of the regional ‘Nevoria Anticline’ (Fig. 43). This doubly plunging anticline is refolded around the southern closure of the Ghooli dome, and delineated by two to three beds of grunerite–quartz BIFs, which are traditionally termed ‘BIF-1’ to ‘BIF-3’. They vary in thickness between 0.2 and 20 m (Cullen et al., 1990; Mueller et al., 2004), and show a sinistral offset along brittle northeast-trending faults (Fig. 44). The major rock types within the deposit are tholeiitic amphibolites in the footwall and a mixed volcanic sequence dominated by metakomatiites in the hangingwall of the BIF horizon (Mueller et al., 2004). The Nevoria geology is intruded by a granite–pegmatite complex, whose main body is exposed to the north of the mines, and has a U–Pb age of 2634 ± 4 Ma (Qiu et al., 1999). Related pegmatitic dykes cut and postdate the Nevoria ore bodies (see cross-section in Fig. 44).

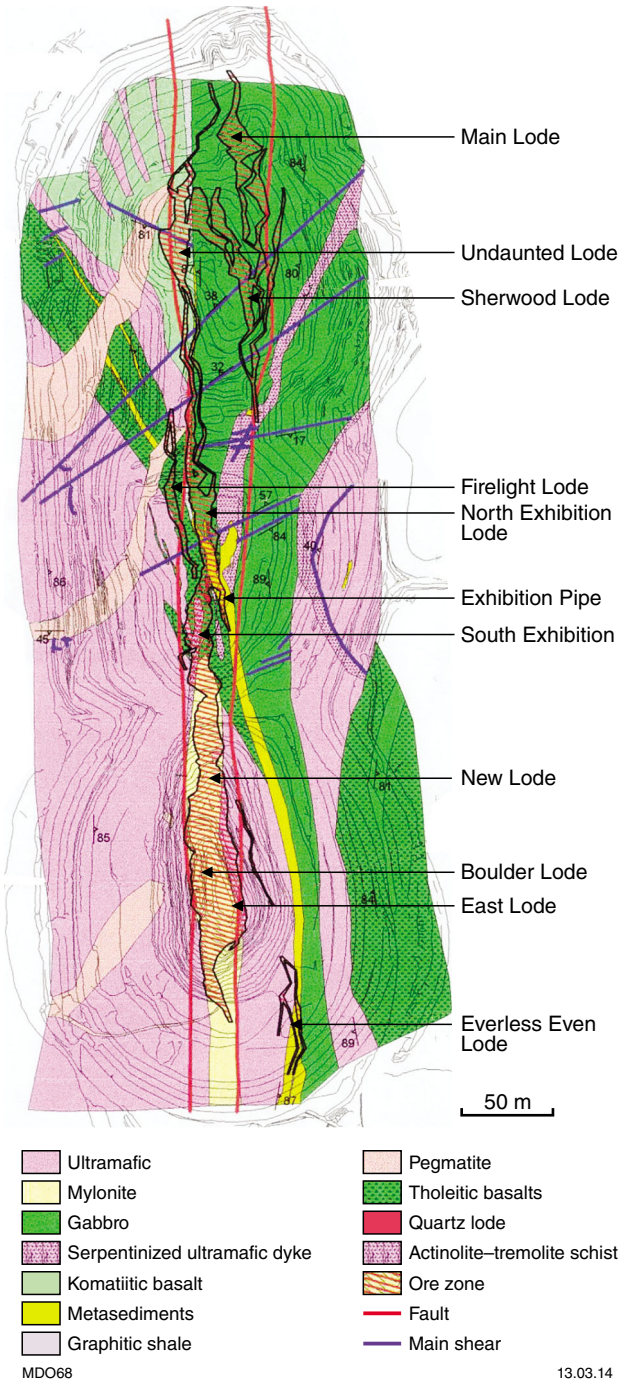

Figure 40. Plan geology of the Marvel Loch mine showing the positions and names of the main orebodies with the pit contours shown for reference

Mineralization

The Nevoria deposit has been studied in detail by Mueller (1997) and Mueller et al. (2004), who characterized the gangue as calcic and highly reduced, and distinguished a hedenbergite–actinolite and almandine–hornblende type in the iron formation (so-called 'skarns'; e.g. Mueller 1997). The amphibolites and komatiites adjacent to the BIFs typically show wide zones of biotite alteration. According to Mueller (1997), 'the calc silicates are intergrown with abundant pyrrhotite (10 vol. %) and with accessory (≤0.5%) pyrite, arsenopyrite–loellingite, and chalcopyrite. Native gold is enclosed in hedenbergite, actinolite, almandine, and quartz, and occurs together with the alloy maldonite (Au_2Bi) and a suite of bismuth tellurides'. Mueller et al. (2004) estimated the peak fluid temperature at 550–600°C, and corresponding pressures at 300–400 MPa.

Locality 6: granite–greenstone contact south of Southern Cross

by MP Doublier and N Thébaud

From the town centre of Southern Cross, turn south at the Palace Hotel onto the road to Marvel Loch. Follow the road for about 300 m, and park on the right-hand side of the road in front of the water pipeline.

This locality provides a cross-section through the granite–greenstone contact between the Ghooli dome to the east and the easternmost part of the Southern Cross greenstone belt to the west (Fig. 25).

Locality 6.1: medium- to coarse-grained gneiss within Ghooli dome

Outcrop about 10 m north of the road (MGA 722217E 6542126N).

The locality is a shallow pavement outcrop of medium- to coarse-grained gneiss (Fig. 45a). This rock type forms wide parts of the northern, western and southern Ghooli dome. There is no age from this particular outcrop, but within the Ghooli dome this rock type yields magmatic ages between c. 2775 and 2720 Ma. In the outcrop, the rocks have a foliation that dips steeply towards the southwest. Microstructures indicate that the deformation occurred under mid- to high-amphibolite facies conditions with no retrograde overprint. The rocks show a mineral assemblage of quartz, feldspar, muscovite and biotite (Fig. 45b).

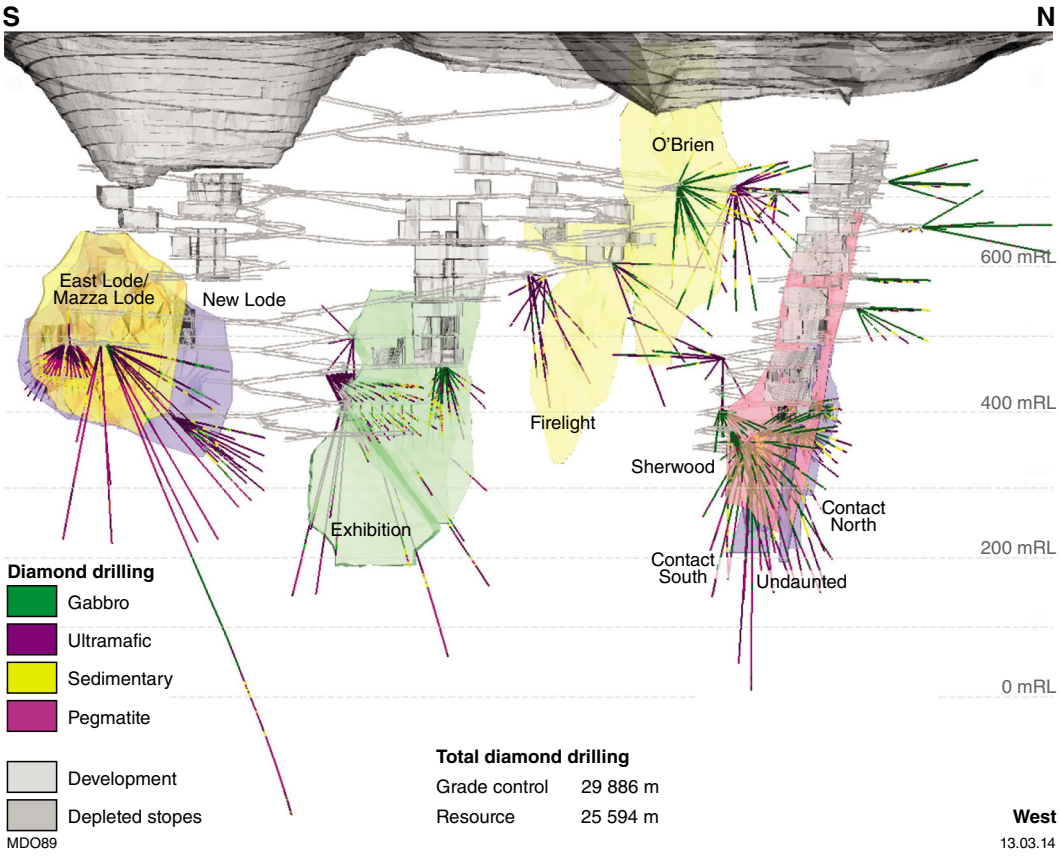

Figure 41. Long section looking west through the Marvel Loch 3D model showing the depth extent of pits, underground development, stopes, and positions and shapes of orebodies

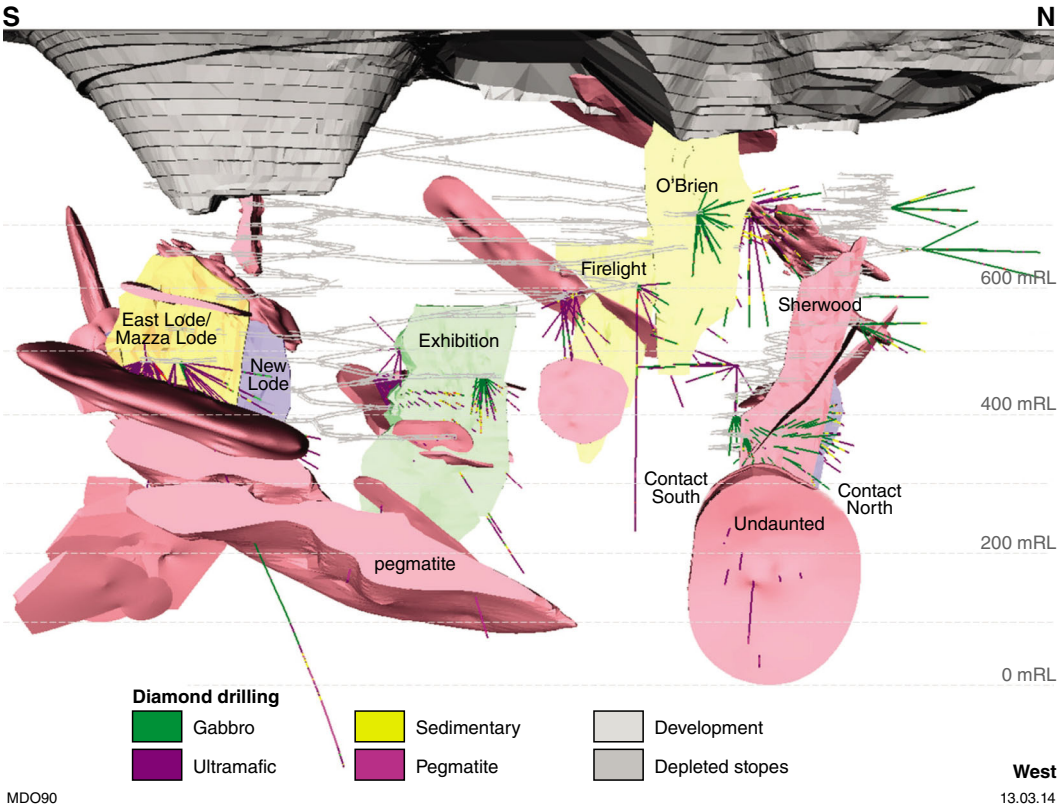

Figure 42. Same long section as for Figure 41, with the interpreted shape of postmineralization pegmatites shown

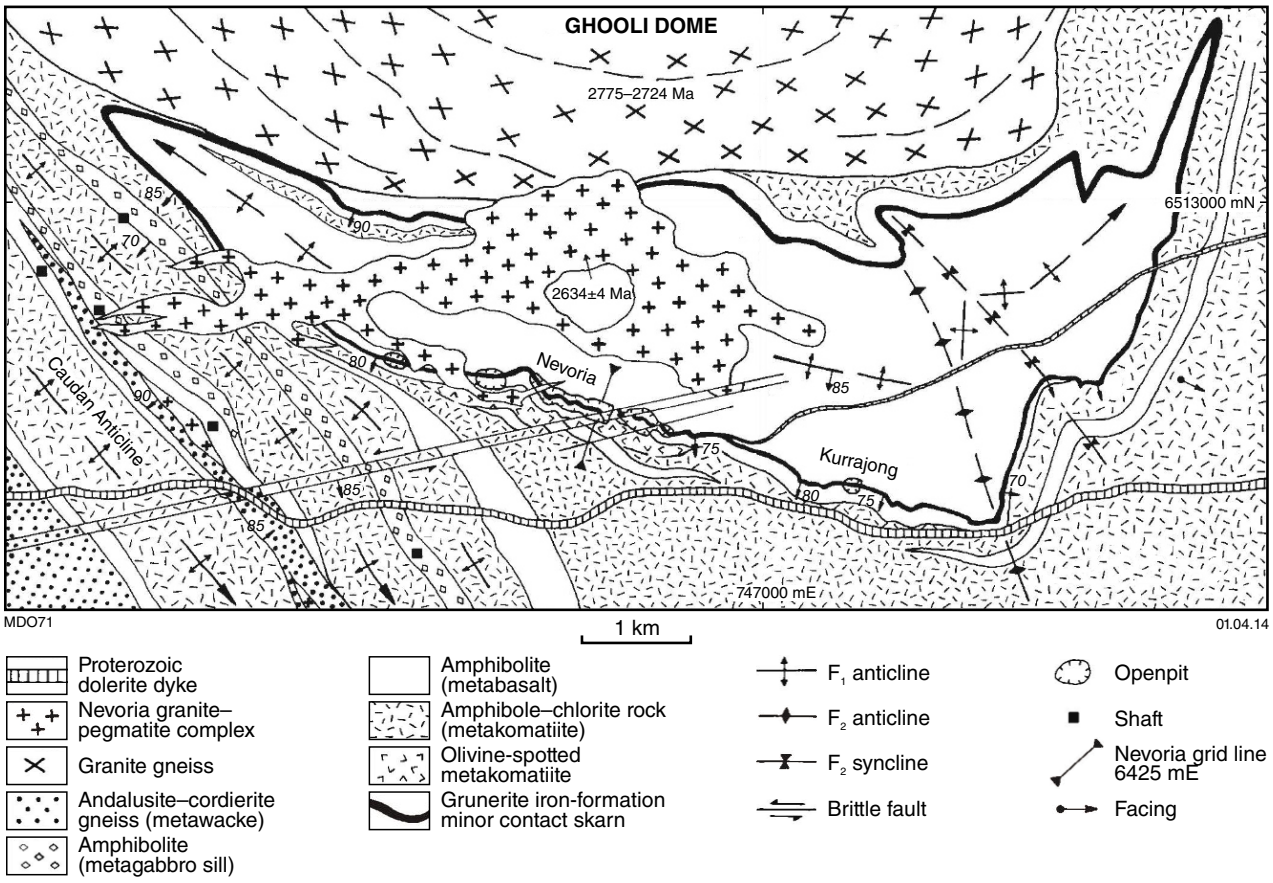

Figure 43. Bedrock geological map from southern closure of the Ghooli dome and adjacent greenstones, showing the regional context of the Nevoria group of deposits (after Mueller et al., 2004)

Locality 6.2: traverse through the granite–greenstone contact

The following traverse through the granite–greenstone contact starts about 50 m further towards Marvel Loch, on a little ridge on the southern side of the road (MGA 722271E 6542041N).

In the little gully on the northeastern side of the ridge are small outcrops of the coarse-grained gneiss from Locality 7.1, in contact with fine-grained felsic gneiss (Fig. 46a). The latter shows an intense foliation dipping moderately towards the southwest. Microstructures indicate ductile deformation of feldspar and a chessboard pattern in quartz, corresponding to temperatures of about 650°C (Stipp et al., 2002). The mineral content is quartz, feldspar, muscovite and garnet (Fig. 46b). The contact relationship between the gneisses and the finer grained material is not always easy to characterize but is at least partly tectonic (Fig. 46c). However, outcrops in a similar structural position further north show that the gneisses are intruded by fine-grained granite, which is possibly the protolith of the intensely foliated, fine-grained gneiss in this outcrop (Fig. 46d). The latter unit is about 10 m wide and marks the boundary of the greenstone succession that crops out on the southwestern side of the ridge.

The greenstone sequence begins with a well-foliated, fine-grained amphibolite, which becomes locally variolitic farther away from the contact. (Fig. 46e: varioles show stretching lineation plunging shallowly towards the south-southeast). The amphibolites are followed by komatiitic metabasalts with well-preserved pyroxene-spinifex texture (Fig. 46f). The traverse ends with ultramafic schists, which are exposed in a costean. The greenstone succession has been affected by folding and faulting. There is at least one generation of folds that refolds the penetrative foliation, ranging from centimetre to metre scale. The folds are characterized by moderately south-plunging fold axes, steep east–west-trending axial planes, and some S-type asymmetry. In parts of the outcrop, these folds are mirrored by a macrocrenulation (mm up to cm scale; Fig. 46g). However, small-scale S-folds with steep fold axes have also been observed (Fig. 46h). It is not clear whether they reflect a separate deformation event.

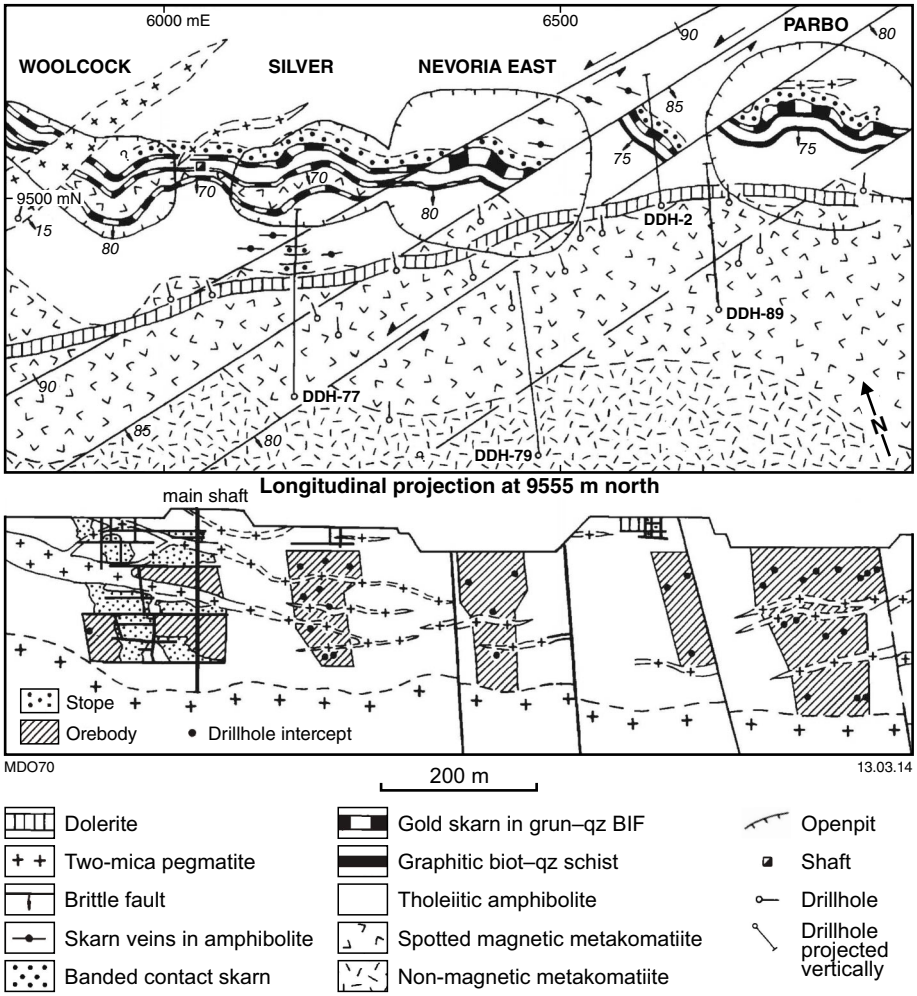

Figure 44. Geological map and long section from the Nevoria mine area, illustrating the crosscutting relationship between orebodies and pegmatitic dykes

Locality 7: greenstone rafts and komatiites east of Southern Cross

by MP Doublier and N Thébaud

From the Great Eastern Highway in the town centre of Southern Cross, turn north onto Antares Street towards Bullfinch. Follow the road for about 800 m until the turn-off to Koolyanobbing. Follow the road to Koolyanobbing for about 550 m until the beginning of a track to the northeast in the salt lake (MGA 721833E 6543205N). Follow the track for 400 m, and park off the road on the little ridge (MGA 721850E 6543620N). The outcrops are east and west of the car park on the northern and northwestern edge of the salt lake.

This lake section traverses from west to east across two greenstone remnants east of the main greenstone belt (Figs 25 and 47). They are separated from the latter and from each other by gneisses and granites, and presumably represent rafts.

Locality 7.1: fine-grained granite close to the granite–greenstone contact

From the car park, go 200 m to the west-southwest to the edge of the salt lake (MGA 721626E 6543508N).

This boulder-like outcrop on the edge of the salt lake (Fig. 48a) exposes fine- to medium-grained granite (quartz, feldspar, biotite, muscovite, iron oxide). The deformation is partitioned, which results in both largely undeformed zones and zones with a solid state fabric that dip steeply to the southwest (Fig. 48b). These granites occupy a similar structural position to the fine-grained gneisses exposed at locality 6.2, but have a different mineralogy.

Locality 7.2: Komatiite flows (MGA 721695E 6543530N)

The area between locality 7.1 and the car park is dominated by thin komatiite flows, with a few outcrops of

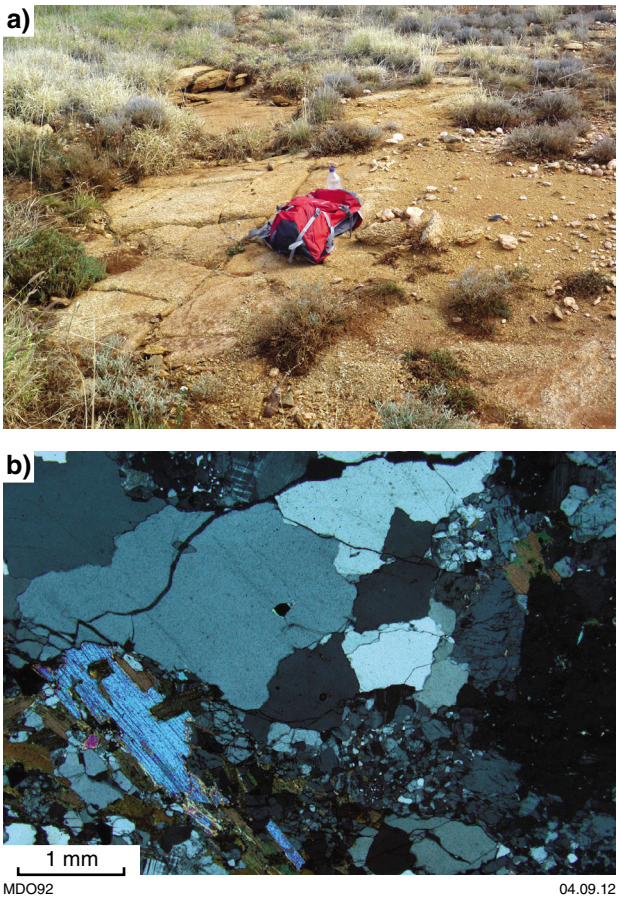

Figure 45. Locality 6.1: a) outcrop of gneisses on the edge of the salt lake; b) mineral assemblage in the gneiss (x2.5 cpl)

foliated granite and tremolitic schist. Thin komatiite flows are exposed on the sides of the small ridge (Fig. 49a). The flows are typically thinner than 50 cm. This type of komatiite allows the determination of stratigraphic younging, because the flows typically consist of an upper zone characterized by olivine–spinifex texture and a lower cumulate-rich zone (Fig. 50). In the upper part of the spinifex zone, the orientation of the plates is typically random, and becomes more organized towards the bottom (Fig. 49b; pen points in younging direction). Stratigraphic younging of the succession — as indicated by the komatiites — is towards the southwest, that is, towards the greenstone belt. The komatiites locally contain a patchy texture in the cumulate zone that is reminiscent of porphyroblasts (Fig. 49c). This texture is caused by widespread chlorite replacement of olivine, which appears to delineate an early fracture pattern in the lower part of the flow.

There are several small komatiite outcrops on the northern edge of the lake.

Locality 7.3: granite, gneiss, and amphibolite separating the two greenstone rafts (MGA 721819E 6543625N)

Fine- to medium-grained granites and coarse-grained gneisses are exposed on and adjacent to the track. They mark the end of the western greenstone raft. The foliation in the gneisses and a small sliver of mafic amphibolite dips steeply towards the south-southwest.

The traverse continues to the southeast of the track, along the edge of the salt lake.

Locality 7.4: fine-grained granite

From the last outcrop, go about 150 m to the southeast (MGA 721931E 6543513N).

This outcrop consists of fine- to medium-grained granite, which forms boulders on the edge of the salt lake (Fig. 51a). The rocks have a moderately west-dipping foliation, which varies in intensity. In thin section, the foliation is delineated by biotite, and is possibly magmatic. Other minerals present are plagioclase, K-feldspar, quartz, muscovite after K-feldspar, chlorite after biotite, and iron oxides (Fig. 51b).

Locality 7.5: coarse-grained gneisses and komatiite

Go 40 m to the east from locality 7.4 (MGA 721980E 6543521N).

The gneisses are cut by quartz veins, and exhibit a steeply southwesterly dipping foliation. Aligned quartz aggregates define a shallow stretching lineation, which plunges towards the south-southeast. The shear sense is ambiguous. Asymmetric clasts are dominantly sinistral and there are also sinistral shear bands. However, there are also clasts that show a dextral shear sense.

A 5 m wide komatiite unit with well-preserved olivine–spinifex texture lies 10 m east of the gneisses (MGA 721985E 6543529N). The stratigraphic younging appears to be towards the southwest (Fig. 52).

Locality 7.6: laminated BIF

From the last outcrop, go about 160 m to the east along the edge of the salt lake (MGA 722130E 6543496N).

The last stop on the traverse is a laminated BIF. The rocks show local very fine banding at mm to 0.5 cm scale (Fig. 53a), but layers can also reach a thickness up to 2 cm (Fig. 53b). The structural inventory is not very complex. The bedding typically dips steeply towards the southwest, and folds are only locally developed (Fig. 53c; fold axes plunge 305/30°). However, felsic intrusions appear to splay and fold the bedding (Fig. 53d).

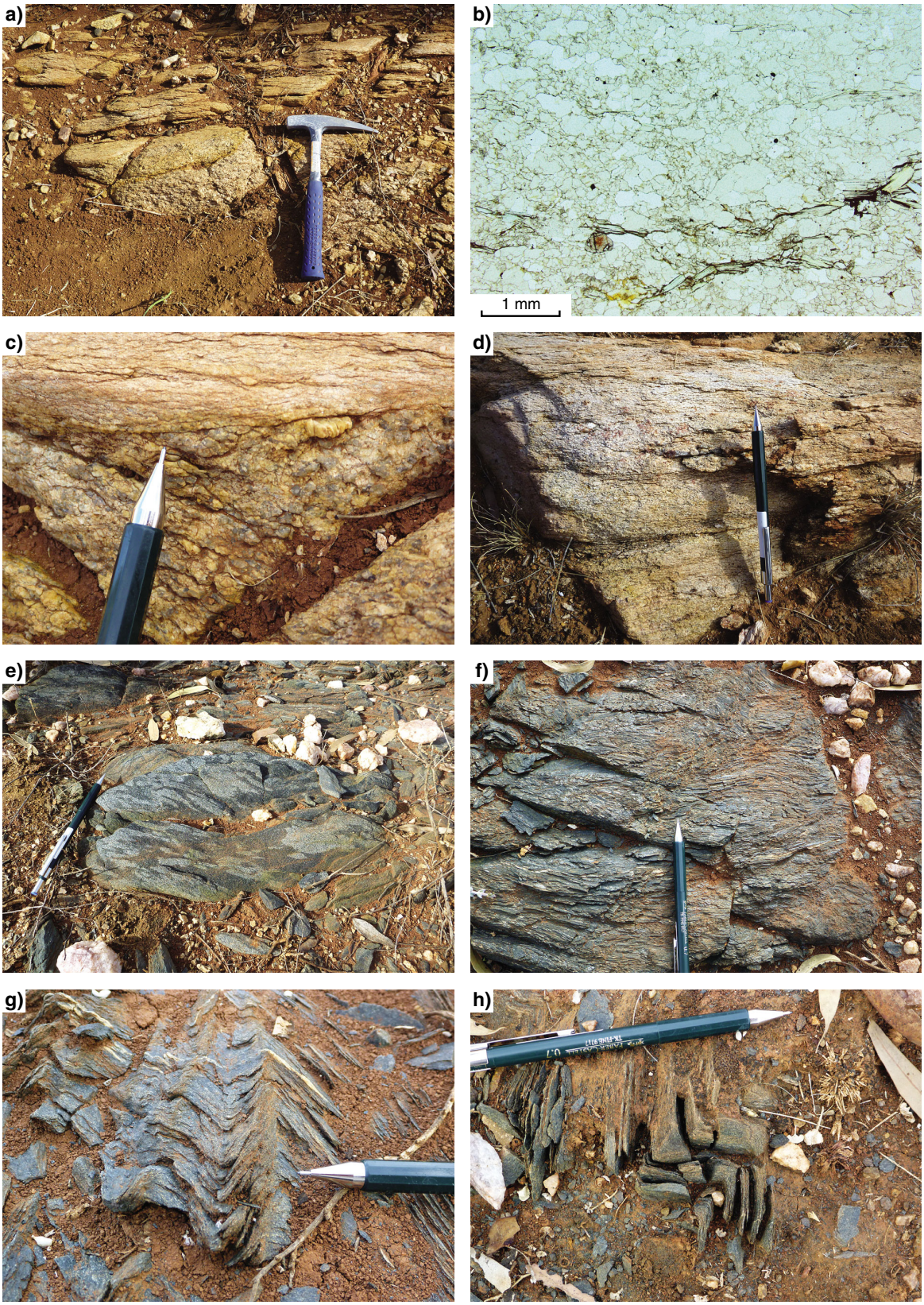

Figure 46. **Locality 6.2: a) outcrop of the contact between coarse- and fine-grained felsic gneisses (hammer as scale); b) mineral assemblage in the fine-grained gneiss (x2.5 ppl); the foliation is delineated by the aligned muscovite; c) detail of tectonic contact between coarse- and fine-grained felsic gneisses (pen as scale); d) outcrop of the well-foliated, fine-grained gneisses, which mark the boundary between Ghooli dome and greenstones (pen as scale); e) vesicular metabasalt; stretched vesicles plunge south-southeast (pen as scale); f) pyroxene-spinifex texture in komatiitic metabasalt (pen as scale); g) small-scale folds with moderately south-plunging fold axes (pen as scale); h) S-type folds with steep fold axes (pen as scale)**

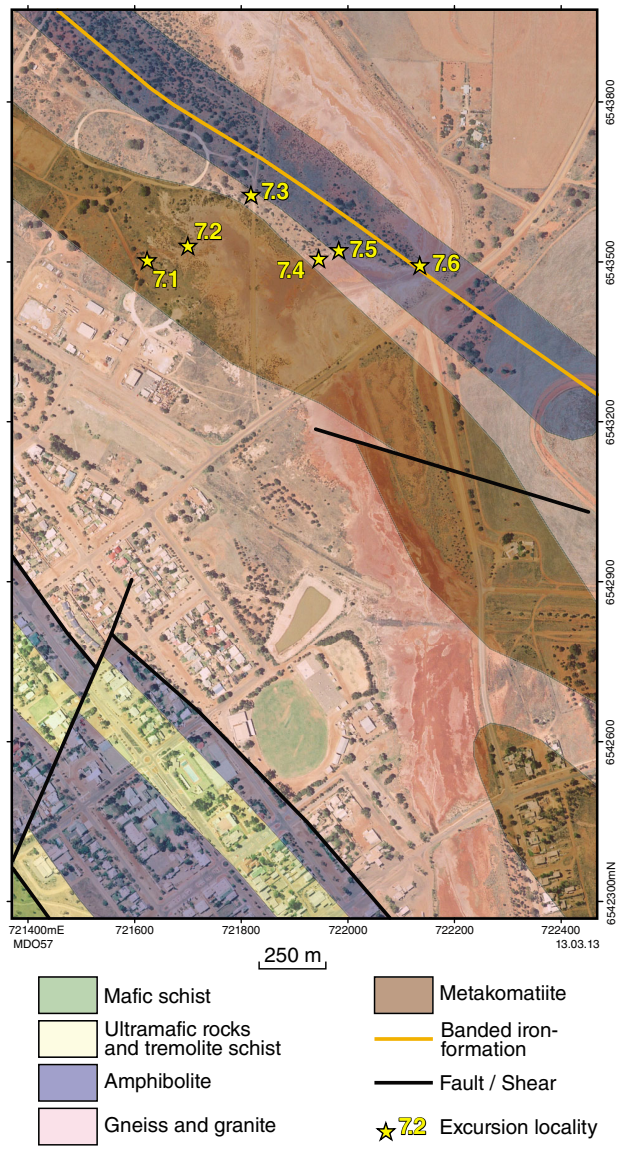

Figure 47. Geological context of Locality 7 with outcrop stops

Locality 8: lake traverse through central part of the greenstone belt north of Southern Cross

by MP Doublier and N Thébaud

From the Great Eastern Highway at Southern Cross, turn north onto Antares Street towards Bullfinch. Follow the road for about 1.9 km and then turn left on a bitumen road following the signage for the cemetery. Go straight ahead at the next intersection (after about 700 m) and cross the railway line. Stay on the road, which becomes a gravel road north of the railway line, for 1.3 km, until the road bends towards the west. Here, turn off to the right, and follow a gravel road that runs along the eastern side of the pipeline. Stay on this road for 1.4 km and then park next to the track (MGA 718263E 6546220N).

The traverse runs along the northern edge of the salt lake west of the water pipeline to Bullfinch and goes right through the middle of the Southern Cross greenstone belt (Figs 25 and 54). It crosses the zone where the eastern and western branches of the belt converge, in the 'bottleneck' of the belt where it is very narrow. Hence, the geology is characterized by intense deformation and high tectonic strain.

Locality 8.1: foliated amphibolite

From the car park, cross the water pipeline and go about 60 m to the west-southwest to the outcrop at the edge of the lake (MGA 718229E 6546179N).

The outcrop is dominated by grey to black, fine- to medium-grained amphibolites that have an intense, steeply southwesterly dipping foliation (Fig. 55a). The structural inventory of the outcrop includes folds, boudinage of quartz veins and amphibolite, and tension gashes. Both boudins and tension gashes are commonly symmetric and indicate an amount of coaxial deformation (Fig. 55b; note that the tension gashes crosscut the sheared and boudinaged quartz veins, indicating their formation during a later increment of the deformation).

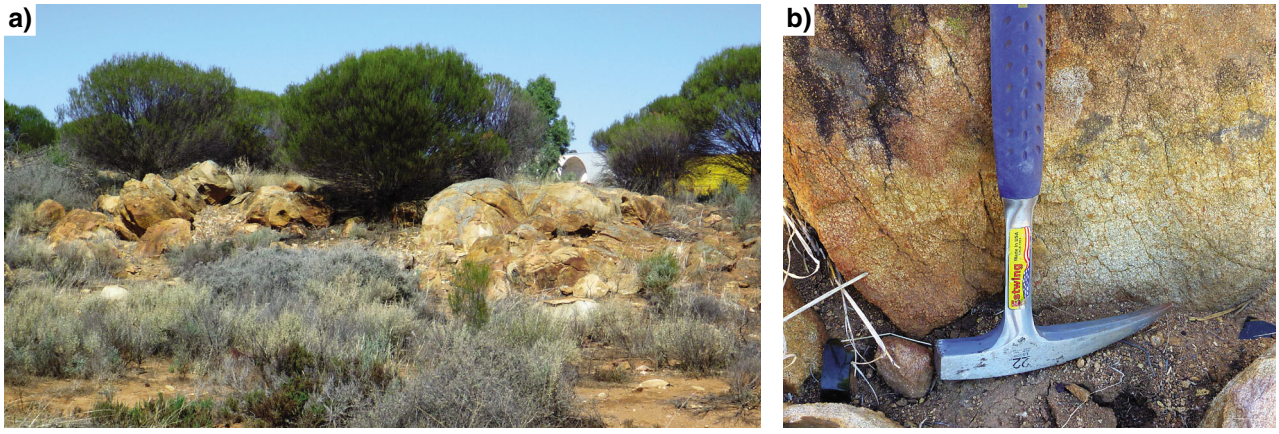

Figure 48. Locality 7.1: a) granite outcrop east of Southern Cross; b) in places, the granites show a steep southwest-dipping solid state fabric (hammer as scale)

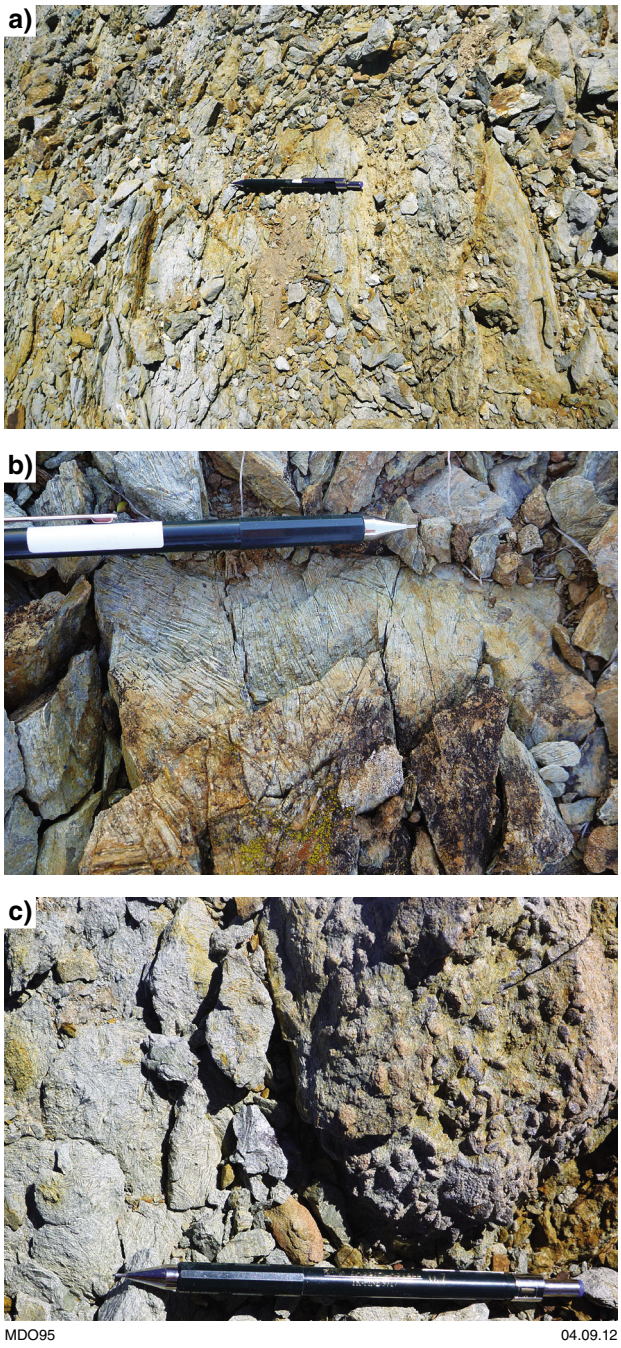

Figure 49. Locality 7.2: a) rubbly outcrop of komatiite flows (pen as scale); b) upper part of a komatiite flow with olivine–spinifex texture becoming less regular towards the top of the flow (pen points up section); c) chlorite porphyroblasts in the basal cumulate part of a komatiite flow (pen as scale)

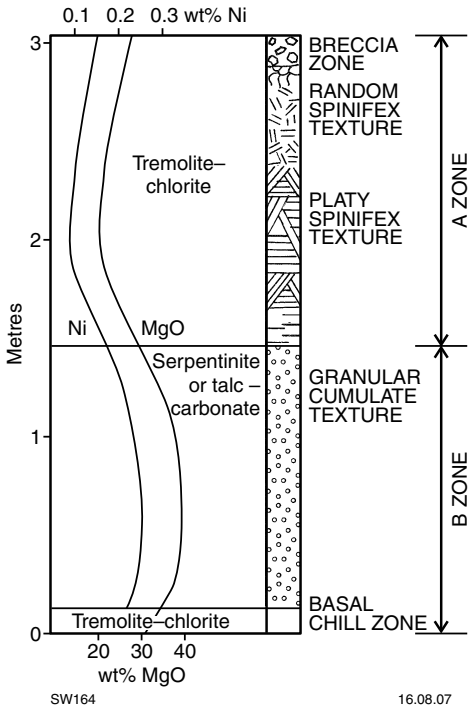

Figure 50. Diagrammatic section and geochemical trends through a thin komatiite unit (after Mason, 1984)

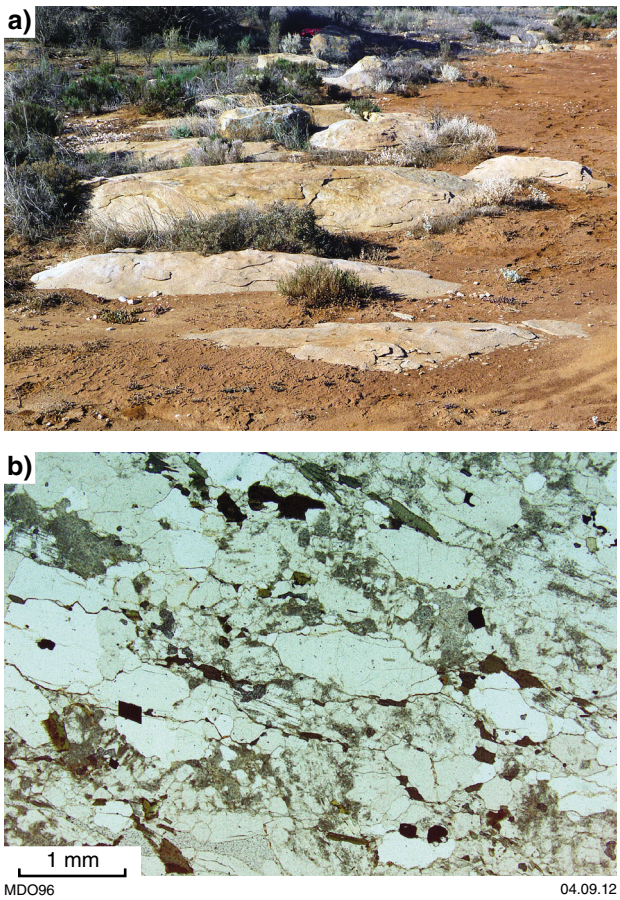

Figure 51. Locality 7.4: a) outcrop of fine-grained granite at the edge of the salt lake; b) mineral assemblage of fine-grained granite (x2.5 ppl)

MDO97 04.09.12

Figure 52. Locality 7.5: olivine–spinifex texture within a komatiite flow indicates younging towards the southwest (pen points up section)

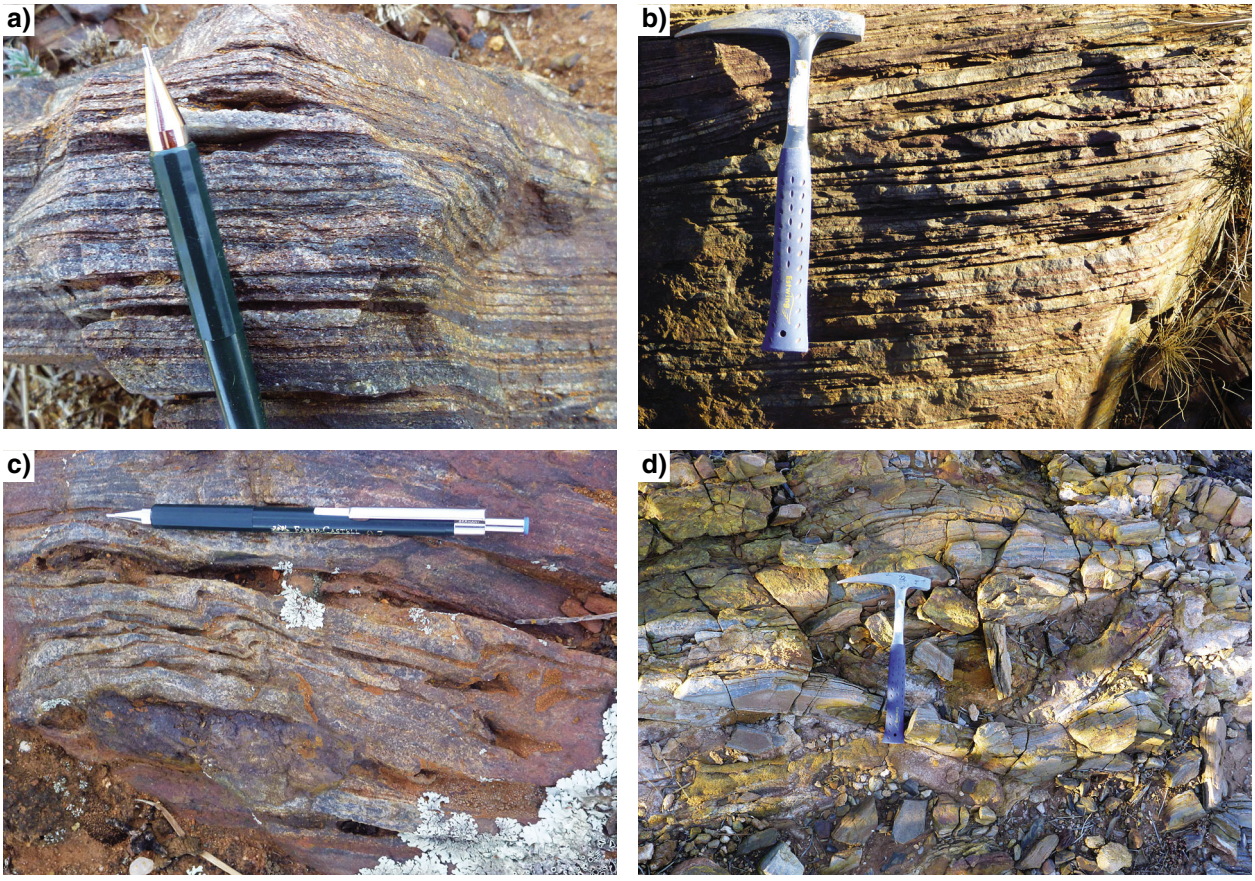

MDO98 04.09.12

Figure 53. Locality 7.6: a) fine-banded BIF (pen as scale); b) layers up to 2 cm thickness in BIF (hammer as scale); c) small-scale folds with northwest-plunging fold axes (pen as scale); d) felsic intrusions introduce complexity in the BIF (hammer as scale)

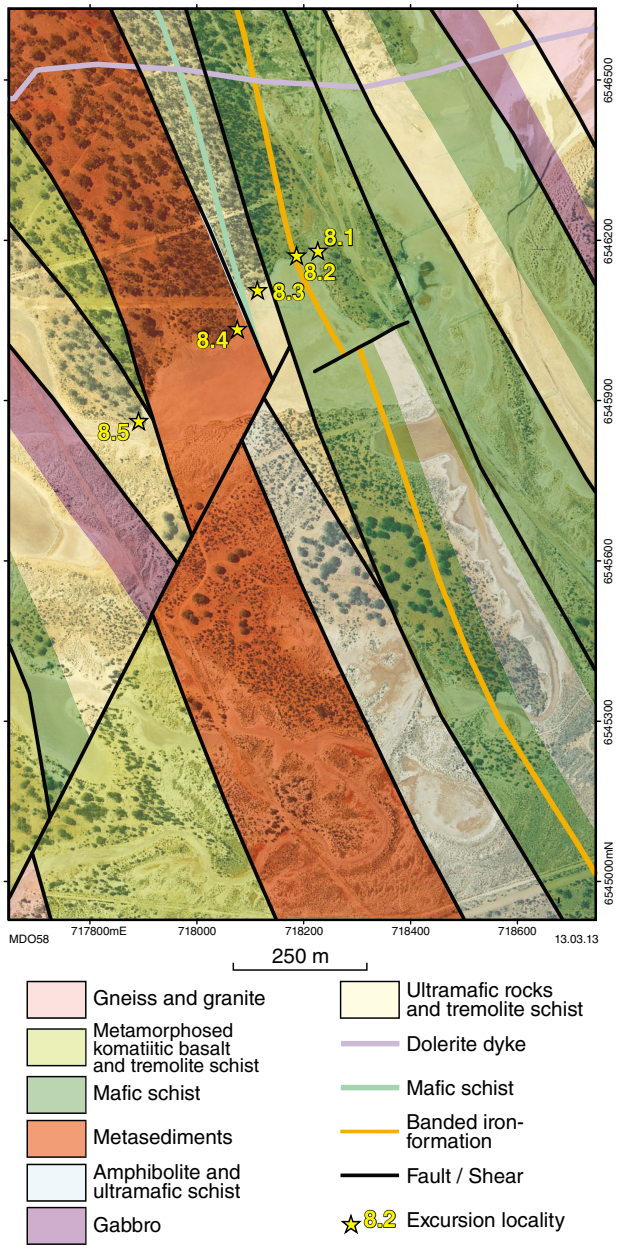

Figure 54. Geological context of Locality 8 with outcrop stops

Locality 8.2: medium-grained boudinaged amphibolite

Go along the edge of the salt lake to the west for 50 m (MGA 718188E 6546173N).

Between Localities 8.1 and 8.2, the dominant rock type is well-foliated amphibolite with minor intercalations of ferruginous chert. At Locality 8.2, there are fine- to medium-grained amphibolites, with an intense steeply southwest-dipping foliation (Fig. 56a). The outcrop exposes spectacular structures, which are quite complex due to the interplay of disharmonic folding, boudinage and shearing (Fig. 56b and c). The folding seems to pre-date the latter events (Fig. 56d). Determination of the shear sense is difficult: symmetric boudinage and clasts indicate some flattening. Asymmetric shear-sense indicators (clasts, shear bands, mica fish) are dominantly sinistral, although dextral examples are readily evident.

Locality 8.3: folded ultramafic schists

From the last outcrop, go along the edge of the salt lake to the southwest for about 100 m.

This outcrop is dominated by tremolitic and ultramafic schist, characterized by mainly talc-, chlorite-, and tremolite-bearing mineral assemblages. Local magnetite porphyroblasts are up to 1 cm in size. The rocks exhibit a steeply southwesterly dipping foliation (Fig. 57a) and are, in places, intensely folded (Fig. 57b). In some of the hinges, an axial-planar spaced cleavage dips steeply towards the north-northeast (Fig. 57c). The fold axes show some orientation variation but mainly plunge towards the northwest. The ultramafic rocks are flanked to the west by amphibolites, before the outcrop is interrupted by a valley, which is also marked by a large quartz vein. The rocks to the east of the little valley belong to the eastern branch of the belt, that is, the branch that lies between Marvel Loch and Southern Cross. The sedimentary rocks on the western side of the valley (see Locality 8.4) and all rocks farther to the west represent the continuation of the western branch of the greenstone belt, from the Transvaal deposit to the west (Fig. 17). The area where both branches converge is located in the valley (Fig. 57d).

Locality 8.4: garnet-bearing metasedimentary rocks

From the last outcrop, go along the edge of the salt lake to the southwest for about 70 m (MGA 718074E 6546046N).

At this locality, sedimentary rocks locally contain abundant garnets (Fig. 58a). The rocks have a range of dip directions but it is difficult to tell whether the rocks are in situ. A prominent 10 m wide metachert unit (MGA 718055E 6546003N) has subvertical bedding and a southwest strike (Fig. 58b). The area between Localities 8.4 and 8.5 is dominated by sedimentary rocks with possible local intercalations of mafic rocks.

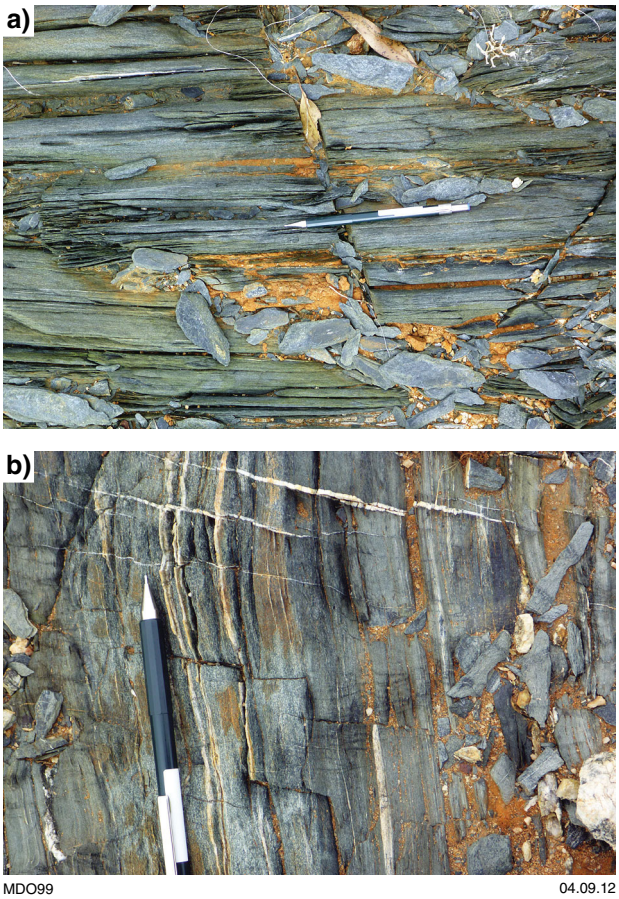

Figure 55. Locality 8.1: a) amphibolites show a steeply southwest-dipping foliation (pen as scale); b) boudinaged quartz veins and tension gashes in fine-grained amphibolite (pen as scale)

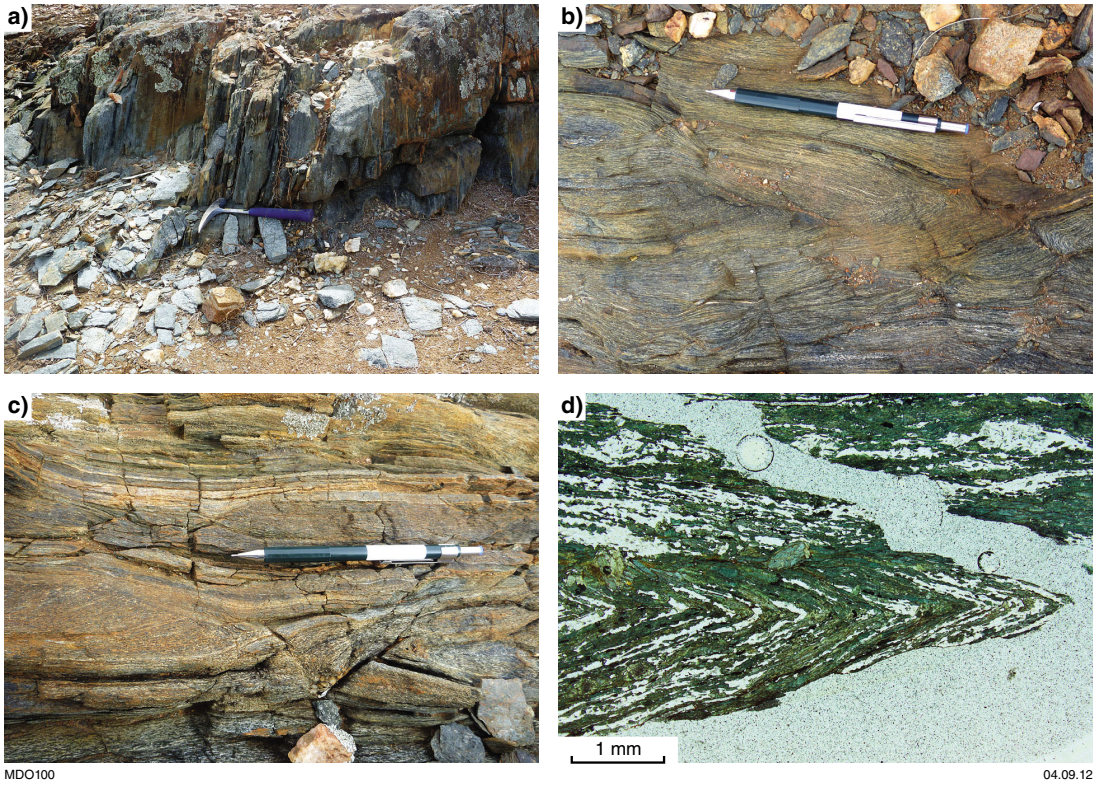

Figure 56. Locality 8.2: a) outcrop of foliated amphibolite (hammer points west); b) complex geometries due to the interplay of folding, boudinage and shearing within amphibolites (pen points south); c) boudinage within amphibolites; note the control of grain size on rheology (pen points south); d) small-scale fold in fine-grained amphibolite with sheared fold limb (x2.5 ppl)

Locality 8.5: amphibolites and tremolite schist

From the metachert outcrop, go along the edge of the salt lake to the southwest for about 220 m (MGA 717903E 6545849N).

Fine-grained amphibolite (Fig. 59a) and tremolite schist (Fig. 59b) mark the end of the sedimentary package. The rocks have a steep southwest-dipping foliation (235/75°), and form part of the western ultramafic–mafic package of the greenstone belt. The pale rocks east of the amphibolite represent quartz-rich metasediments (Fig. 59c).

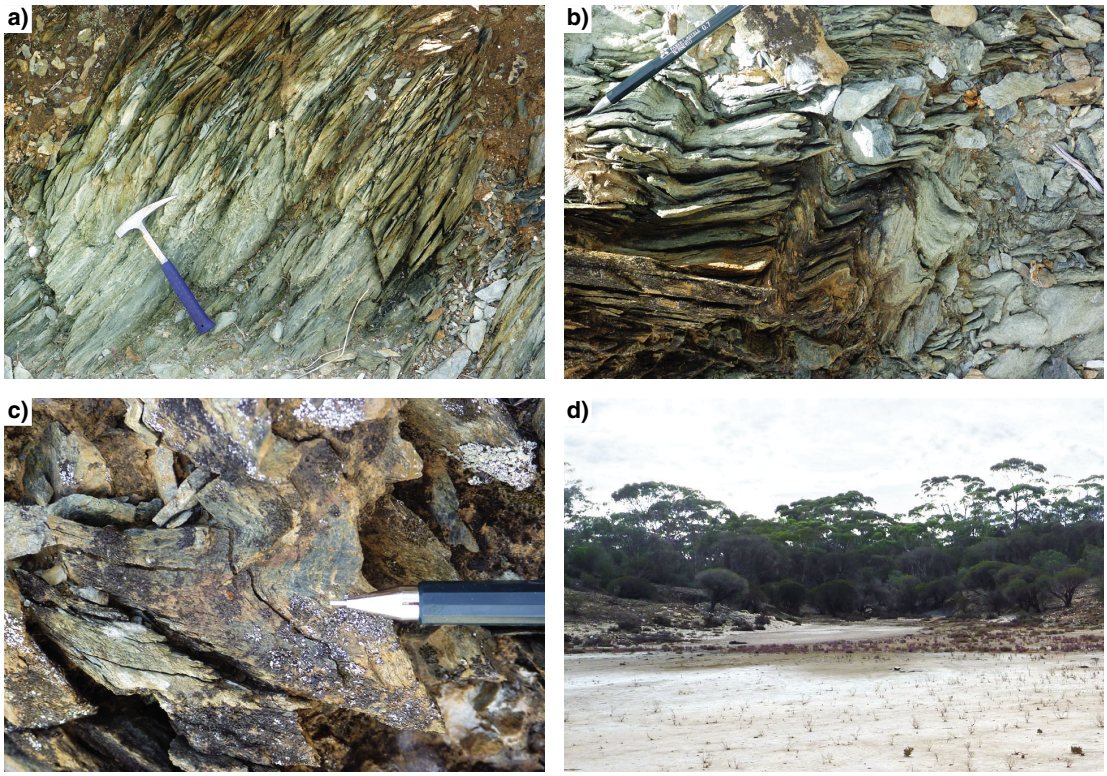

Figure 57. Locality 8.3: a) outcrop of ultramafic schist with a southwest-dipping foliation (hammer as scale); b) folds within ultramafic schist refold the main foliation (pen as scale); c) a second spaced axial plane cleavage to the folds is developed within fold hinges (pen as scale); d) valley on the northern edge of the salt lake where the eastern and western branches of the Southern Cross greenstone belt converge (photo taken to the north)

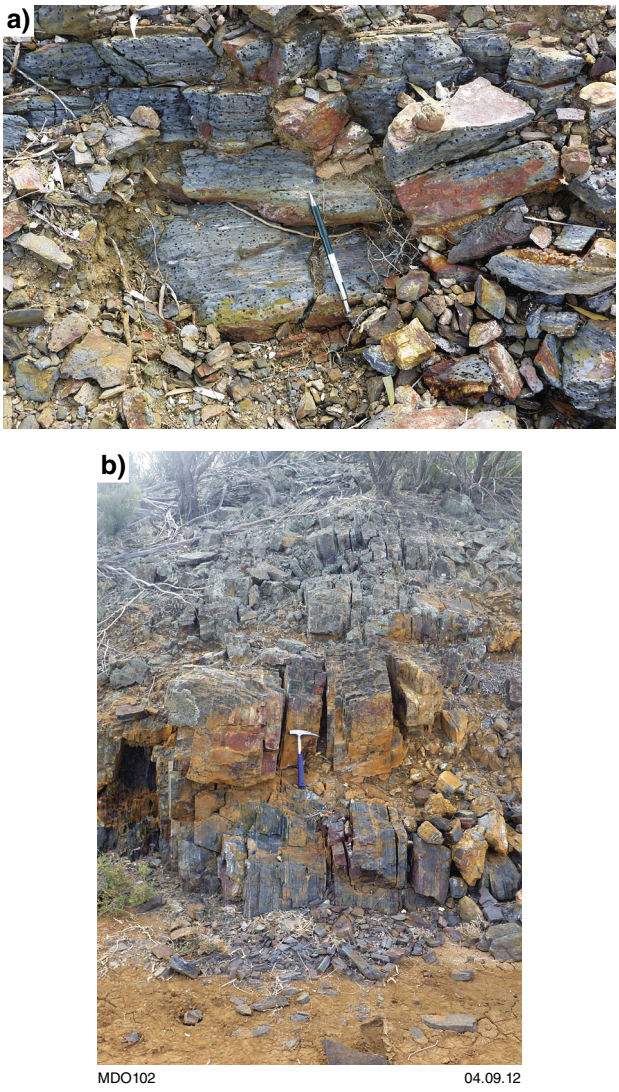

Figure 58. Locality 8.4: a) outcrop of fine-grained, garnet-bearing clastic sediments (pen as scale); b) metachert outcrop with subvertical bedding (hammer as scale)

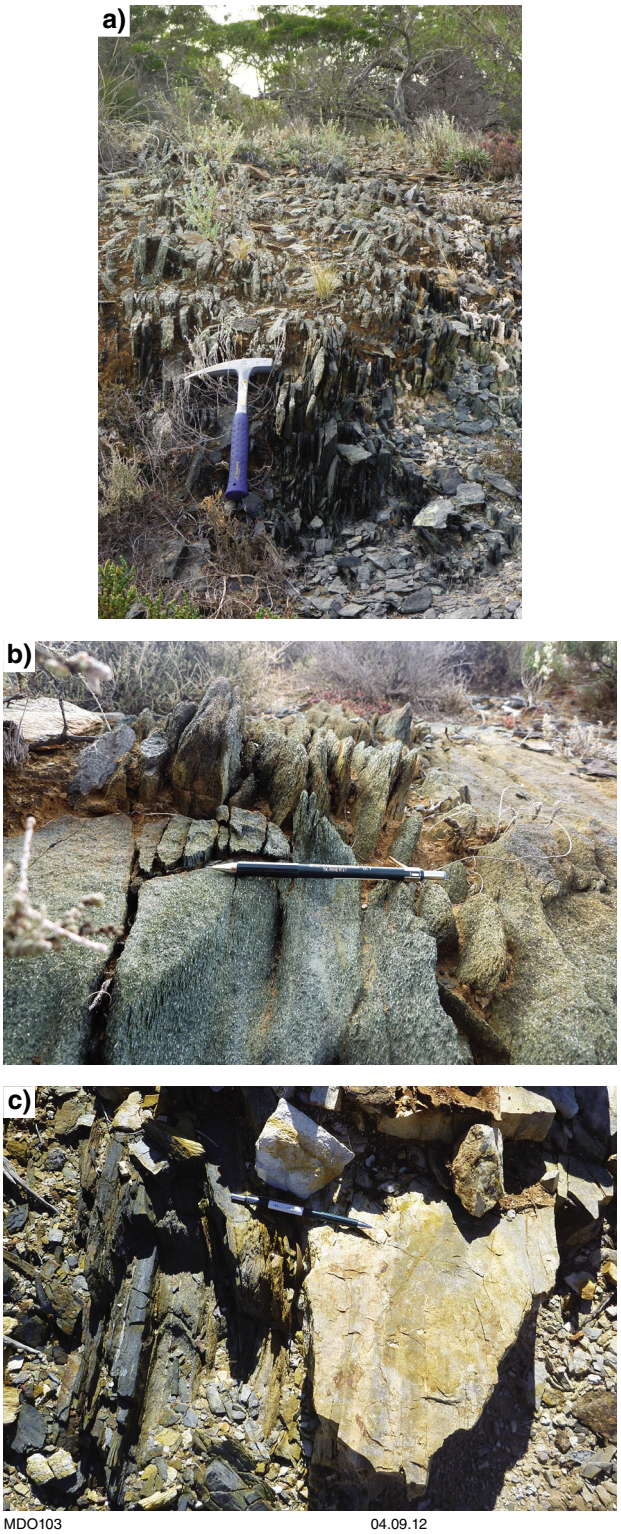

Figure 59. Locality 8.5: a) outcrop of fine-grained, foliated amphibolite (hammer as scale); b) outcrop of tremolite schist with a southwest-dipping foliation (pen as scale); c) contact between fine-grained amphibolite (to the east) and quartz-rich clastic sediments (to the west; pen as scale)

References

Ahmat, AL 1986, Metamorphic patterns in the greenstone belts of the Southern Cross Province, Western Australia, in Professional papers for 1984: Geological Survey of Western Australia, Report 19, p. 1–21.

Allibone, AH, Windh, J, Etheride, MA, Burton, D, Anderson, G, Edwards, PW, Miller, A, Graves, C, Fanning, CM and Wysoczanski, R 1998, Timing relationships and structural controls on the location of Au–Cu mineralisation at the Boddington gold mine: Economic Geology, v. 93, p. 245–270.

Anand, R and Paine, M 2002, Regolith geology of the Yilgarn Craton, Western Australia: implications for exploration: Australian Journal of Earth Sciences, v. 49, p. 3–162.

Angerer, T, Duuring, P, Lascelles, DF and Hagemann, SG 2010, BIF-related iron ore in the Yilgarn Craton, Western Australia: geological setting and ore forming processes, *in* Fifth International Archean Symposium Abstracts *edited by* IM Tyler and CM Knox-Robinson: Geological Survey of Western Australia, Record 2010/8, p. 277–280.

Angerer, T and Hagemann, SG 2010, The BIF-hosted high-grade iron ore deposits in the Archean Koolyanobbing Greenstone Belt, Western Australia: structural control on synorogenic- and weathering-related magnetite-, hematite-, and goethite-rich iron ore: Economic Geology, v. 105, p. 917–945.

Angerer, T, Hagemann, SG and Danyushevsky, LV 2012, Geochemical evolution of the banded iron formation-hosted high-grade iron ore system in the Koolyanobbing greenstone belt, Western Australia: Economic Geology, v. 107, p. 599–644.

Angerer, T, Hagemann, SG and Danyushevsky, L (2012), High-grade iron ore at Windarling, Yilgarn craton: a product of synorogenic deformation, hydrothermal alteration, and supergene modification in an Archean BIF–basalt lithostratigraphy: Mineralium Deposita, v. 48, p. 697–728

Angerer, T, Kerrich, R and Hagemann, SG 2013, Geochemistry of a komatiitic, boninitic, and tholeiitic basalt association in the Mesoarchean Koolyanobbing greenstone belt, Southern Cross Domain, Yilgarn craton: Implications for mantle sources and geodynamic setting of banded iron formation: Precambrian Research, v. 224, p. 110–128.

Barley, ME, Brown, SJA, Krapež, B and Kositcin, N 2008, Physical volcanology and geochemistry of a Late Archaean volcanic arc: Kurnalpi and Gindalbie Terranes, Eastern Goldfields Superterrane, Western Australia: Precambrian Research, v. 161, p. 53–76.

Barley, ME, Pickard, AL, Hagemann, SG and Folkert, SL 1999, Hydrothermal origin for the 2-billion-year-old Mount Tom Price giant iron ore deposit, Hamersley Province, Western Australia: Mineralium Deposita, v. 34, p. 784–789.

Barnes, SJ 2006, Komatiites: petrology, volcanology, metamorphism and geochemistry: Society of Economic Geologists, Special Publication, v. 13, p. 13–49.

Barnes, SJ, Coats, CJA and Naldrett, AJ 1982, Petrogenesis of a Proterozoic nickel-sulfide – komatiite association: the Katinniq sill, Ungava, Quebec: Economic Geology, v. 77, p. 413–429.

Bloem, EJM, Dalstra, HJ, Groves, DI and Ridley, JR 1994, Metamorphic and structural setting of amphibolite-hosted gold deposits near Southern Cross, Southern Cross Province, Yilgarn Block: Ore Geology Reviews,v. 9, 183–208.

Bloem, EJM, Dalstra, HJ, Ridley, JR and Groves, DI 1997, Granitoid diapirism during protracted tectonism in an Archaean granitoid – greenstone belt, Yilgarn Block, Western Australia: Precambrian Research,v. 85, 147–171.

Bloem, EJM, McNaughton, NJ, Grove, DI, Ridley, JR 1995, An indirect lead isotope age determination of gold mineralization at the Corinthia mine, Yilgarn Block, Western Australia: Australian Journal of Earth Sciences, v. 42, p. 447–451.

Buck, PS, Vallance, SA, Perring, CS, Hill, RE and Barnes, SJ 1998, Maggie Hays nickel deposit, *in* Geology of Australian and Papua New Guinean mineral deposits *edited by* DA Berkman and DH Mackenzie: The Australasian Institute of Mining and Metallurgy, Melbourne, Australia, p. 357–364.

Campbell, IH and Hill, RI 1988, A two-stage model for the formation of the granite–greenstone terrains of the Kalgoorlie–Norseman area, Western Australia: Earth and Planetary Science Letters, v. 90, p. 11–25.

Cassidy, KF, Champion, DC, Krapež, B, Barley, ME, Brown, SJA, Blewett, RS, Groenewald, PB and Tyler, IM 2006, A revised geological framework for the Yilgarn Craton, Western Australia: Geological Survey of Western Australia, Record 2006/8, 8p.

Champion, DC and Cassidy, KF 2002, Granites of the northern Eastern Goldfields: their distribution, age, geochemistry, petrogenesis, relationships with mineralisation, and implications for tectonic environment, *in* The characterisation and metallogenic significance of Archean granitoids in the Yilgarn Craton *edited by* KF Cassidy, DC Champion, NJ McNaughton, IR Fletcher, AJ Whitaker, IV Bastrakova and AR Budd: Minerals and Energy Research Institute of Western Australia (MERIWA), Project no. M281/AMIRA Project no. 482 (unpublished report no. 222), p. 2.1–2.49.

Champion, DC and Cassidy, KF 2007, An overview of the Yilgarn and its crustal evolution, *in* Kalgoorlie '07 *edited by* FP Bierlein and CM Knox-Robinson: Geoscience Australia; Geoconferences (WA) Inc., Conference Proceedings, Kalgoorlie, Western Australia, 25 September 2007; Record 2007/14, p. 8–13.

Champion, DC, Cassidy, KF and Budd, A 2002, Overview of the Yilgarn magmatism: implications for crustal development in The characterisation and metallogenic significance of Archean granitoids in the Yilgarn Craton *edited by* KF Cassidy, DC Champion, NJ McNaughton, IR Fletcher, AJ Whitaker, IV Bastrakova and AR Budd: Minerals and Energy Research Institute of Western Australia (MERIWA), Project no. M281/AMIRA Project no. 482 (unpublished report no. 222), p. 8.1–8.21.

Champion, DC and Sheraton, JW 1997, Geochemistry and Nd isotope systematics of Archaean granites of the Eastern Goldfields, Yilgarn Craton, Australia: implications for crustal growth processes: Precambrian Research, v. 83, p. 109–132.

Chen, SF, Libby, JW, Greenfield, JE, Wyche, S and Riganti, A 2001, Geometry and kinematics of large arcuate structures formed by impingement of rigid granitoids into greenstone belts during progressive shortening: Geology, v. 29, p. 283–286.

Chen, SF, Libby, JW, Wyche, S and Riganti, A 2004, Kinematic nature and origin of regional-scale ductile shear zones in the central Yilgarn Craton, Western Australia: Tectonophysics, v. 394, p. 139–153.

Chen, SF, Riganti, A, Wyche, S, Greenfield, JE and Nelson, DR 2003, Lithostratigraphy and tectonic evolution of contrasting greenstone successions in the central Yilgarn Craton, Western Australia: Precambrian Research, v. 127, p. 249–266.

Chin, RJ, Hickman, AH and Thom, R 1984, Hyden, WA Sheet SI50-4: Geological Survey of Western Australia, 1:250 000 Geological Series Explanatory Notes, 21p.

Clout, JMF 2003, Upgrading processes in BIF-derived iron ore deposits: implications for ore genesis and downstream mineral processing: Transactions of the Institution of Mining and Metallurgy Section B-Applied Earth Science, v. 112, p. B89–B95.

Collins, JE, Barnes, SJ, Hagemann, SG, McCuaig, TC and Frost, KM 2012b, Postmagmatic variability in ore composition and mineralogy in the T4 and T5 ore shoots at the high-grade Flying Fox Ni–Cu–PGE deposit, Yilgarn Craton, Western Australia: Economic Geology, v. 107, p. 859–879.

Collins, JE, Hagemann, SH, McCuaig, TC and Frost, KM 2012a, Structural controls on sulfide remobilization at the Flying Fox Ni–Cu–PGE deposit, Forrestania greenstone belt, Western Australia: Economic Geology, v. 107, p. 1433–1455.

Cooper, RW and Flint, DJ 2009, Iron ore deposits of the Pilbara region (1:500 000 scale): Geological Survey of Western Australia.

Cullen, I, Jones, M and Baxter, JL 1990, Nevoria gold deposits, *in* Geology of the mineral deposits of Australia and Papua New Guinea *edited by* FE Hughes: Australian Institute of Mining and Metallurgy, Melbourne, p. 301–305.

Czarnota, K, Champion, DC, Goscombe, B, Blewett, RS, Cassidy, KF, Henson, PA and Groenewald, PB 2010, Geodynamics of the eastern Yilgarn Craton: Precambrian Research, v. 183, p. 175–202.

Dalstra, HJ 1995, Metamorphic and structural evolution of greenstone belts of the Southern Cross – Diemals region of the Yilgarn Block, Western Australia, and its relationship to gold mineralisation: The University of Western Australia, PhD thesis, 219p. (unpublished).

Dalstra, H 2011, From banded iron-formation to iron ore – genetic models and their application in iron ore exploration in the Hamersley Province, Western Australia, The Australian Institute of Mining and Metallurgy, Iron Ore Conference 2011, Perth, WA, Publication Series 6/2011, p. 73–84.

Dalstra, HJ, Bloem, EJM., Ridley, JR and Groves, DI 1998, Diapirism synchronous with regional deformation and gold mineralisation, a new concept for granitoid emplacement in the Southern Cross Province, Western Australia: Geologie en Mijnbouw, v. 76, p. 321–338.

Dalstra, HJ and Ridley, JR 1995, Structural and metamorphic controls on gold mineralisation in the Southern Cross and Marda–Diemals greenstone belts, Yilgarn Block, Western Australia, *in* Southern Cross greenstone belt, geology and gold mines *edited by* PJ Schwebel: Geoconferences (WA) Inc., Southern Cross, WA, March 1995, Extended Abstract Volume, p. 21–27.

Dalstra, HJ, Ridley, JR, Bloem, EJM and Groves DI 1999, Metamorphic evolution of the central Southern Cross Province, Yilgarn Craton, Western Australia: Australian Journal of Earth Sciences, v. 46, p. 765–784.

Dalstra, HJ and Rosière, CA 2008, Structural controls on high-grade iron ores hosted by banded iron-formation: a global perspective, *in* Banded iron formation-related high-grade iron ore *edited by* SG Hagemann, CA Rosière, J Gutzmer and NJ Beukes: Reviews in Economic Geology, v. 15, Society of Economic Geologists, p. 73–106.

Doublier, MP, Thébaud, N, Mole, D, Wingate, MTD, Kirkland, CL, Romano, SS, Wyche, S and Duclaux, G 2012, New data on the geological evolution and gold mineralization of the Southern Cross greenstone belt, *in* GSWA 2012 Extended abstracts: promoting the prospectivity of Western Australia: Geological Survey of Western Australia, Record 2012/2, p. 1–2.

Drummond, BJ, Goleby, BR and Swager, CP 2000, Crustal signature of Late Archean tectonic episodes in the Yilgarn Craton, Western Australia: evidence from deep seismic sounding: Tectonophysics, v. 329, p. 193–221.

Duuring, P and Hagemann, SG 2012a, Genesis of superimposed hypogene and supergene Fe ore bodies in BIF at the Madoonga deposit, Yilgarn Craton, Western Australia: Mineralium Deposita, doi:10.1007/s00126-012-0429-0.

Duuring, P and Hagemann, SG 2012b, Leaching of silica bands and concentration of magnetite in Archean BIF by hypogene fluids: Beebyn Fe ore deposit, Yilgarn Craton, Western Australia: Mineralium Deposita, doi:10.1007/s00126-012-0428-1.

Ewers, WE, Hudson, DR and Davis, CES 1972, Interpretive study of a nickel–iron sulfide ore intersection, Lunnon Shoot, Kambalda, Western Australia — analytical methods used in study of an ore intersection from Lunnon Shoot, Kambalda: Economic Geology, v. 67, p. 1075–1092.

Findlay, D 1994, Diagenetic boudinage, an analogue model for the control on hematite enrichment iron ores of the Hamersley Iron Province of Western Australia, and a comparison with Krivoi Rog of Ukraine, and Nimba Range, Liberia: Ore Geology Reviews, v. 9, p. 311–324.

Frost, KM 2003, Forrestania nickel sulphide deposits, Western Australia, in MSc short course — New frontiers in research on magmatic NiS–PGE mineralisation: Centre for Global Metallogeny, The University of Western Australia, Perth, Western Australia, p. 110–115.

Frost, KM, Black, AP, Amann, W and Hanna, J 2006, The Flying Fox nickel sulphide deposit, Forrestania, WA, *in* Outcrop to orebody – innovative geoscience in exploration and mining *edited by* P Neumayr, The Australian Institute of Geoscientists, AIG Conference, Kalgoorlie, WA, 2006, Bulletin 44, p. 59–60.

Gee, RD 1979, Structure and tectonic style of the Western Australian Shield: Tectonophysics, v. 58, p. 327–369.

Gee, RD 1995, Regional geology of the Southern Cross greenstone belt, in Southern Cross greenstone belt, geology and gold mines edited by PJ Schwebel: Geoconferences (WA) Inc., Southern Cross, WA, March 1995, Extended abstracts, p. 11–16.

Gower, CF and Bunting, JA 1976, Lake Johnston, Western Australia: Geological Survey of Western Australia, 1:250 000 Geological Series Explanatory notes, 27p.

Greentree, MR and Lord, D 2007, Iron mineralization in the Yilgarn Craton and future potential, *in* Proceedings *edited by* FP Bierlein and CM Knox-Robinson: Geoscience Australia; Geoconferences (WA) Inc. Kalgoorlie '07, Kalgoorlie, Western Australia, 25 September 2007; Record 2007/14, p. 70–73.

Guarin Jr, CP, Angerer, T, Maund, NH, Cowan, DR and Hagemann, SG 2009, The K deeps magnetite mineralisation at Koolyanobbing, Western Australia, *in* Iron ore conference edited by AusIMM, 2009, Conference Proceedings, Perth, Western Australia, 27–29 July 2009, p. 95–104.

Heggie, GJ, Fiorentini, ML, Barnes, SJ and Barley, ME 2012, Maggie Hays nickel deposit: Part 1. Stratigraphic control on the style of komatiite emplacement in the ~2.9 Ga Lake Johnston greenstone belt, Yilgarn Craton, Western Australia: Economic Geology, v. 107, p. 797–816.

Ivanic, TJ, Wingate, MTD, Kirkland, CL, Van Kranendonk, MJ and Wyche, S 2010, Age and significance of voluminous mafic–ultramafic magmatic events in the Murchison Domain, Yilgarn Craton: Australian Journal of Earth Sciences, v. 57, p. 597–614.

Keats, W 1991, Geology and gold mines of the Bullfinch – Parker Range region, Southern Cross Province, Western Australia: Geological Survey of Western Australia, Report 28, 44p.

Krapež, B, Barley, ME and Brown, SJA 2008, Late Archaean synorogenic basins of the Eastern Goldfields Superterrane, Yilgarn Craton, Western Australia. Part I. Kalgoorlie and Gindalbie Terranes: Precambrian Research, v. 161, p. 135–153.

Krapež, B and Hand, JL 2008, Late Archaean deep-marine volcaniclastic sedimentation in an arc-related basin: the Kalgoorlie Sequence of the Eastern Goldfields Superterrane, Yilgarn Craton, Western Australia: Precambrian Research, v. 161, p. 89–113.

Lascelles, DF 2007, Black smokers and density currents: a uniformitarian model for the genesis of banded iron-formations: Ore Geology Reviews, v. 32, p. 381–411.

Lesher, CM 2007, Ni–Cu–(PGE) deposits in the Raglan area, Cape Smith belt, New Quebec, *in* Mineral resources of Canada: a synthesis of major deposit-types, district metallogeny, the evolution of geological provinces, and exploration methods *edited by* WD Goodfellow: Geological Survey of Canada and Mineral Deposits Division of the Geological Association of Canada, Special Publication, p. 351–386.

Lesher, CM and Keays, RR 2002, Komatiite-associated Ni–Cu–(PGE) deposits: geology, mineralogy, geochemistry and genesis, *in* The geology, geochemistry, mineralogy and mineral beneficiation of the platinum group elements *edited by* LJ Cabri: Canadian Institute of Mining, Metallurgy and Petroleum, Special Volume 54, p. 579–617.

Lobato, LM, Figueiredo e Silva, RC, Hagemann, SG, Thorne, WS and Zuchetti, M 2008, Hypogene alteration associated with high-grade banded iron formation-related iron ore, *in* Banded iron formation-related high-grade iron ore *edited by* SG Hagemann, CA Rosière, J Gutzmer and NJ Beukes: Reviews in Economic Geology, v. 15, Society of Economic Geologists, p. 107–128.

Maskell, A, Duuring, P and Hagemann, SG (in press), Iron ore in the Matthew Ridge prospect, Jack Hills greenstone belt: Australian Journal of Earth Sciences.

Mole, DR, Fiorentini, M, Thébaud, N, McCuaig, C, Cassidy, KF, Kirkland, CL, Romano, SS, Doublier, MP, Belousova, EA and Barnes, SJ 2011, 4D imaging of an Archean craton: implications for the localisation of komatiite-hosted nickel camps: SGA2011 conference proceedings, September 2011, Antofagasta, Chile, 4p.

Mole, DR, Fiorentini, M, Thébaud, N, McCuaig, TC, Cassidy, KF, Kirkland, CL, Wingate, MTD, Romano, SS, Doublier, MP and Belousova, EA 2012, Spatio-temporal constraints on lithospheric development in the southwest-central Yilgarn Craton, Western Australia: Australian Journal of Earth Sciences, v. 59, p. 625–656.

Morris, PA, Riganti, A, Chen SF 2007, Evaluating the provenance of Archean sedimentary rocks of the Diemals Formation (central Yilgarn Craton) using whole-rock chemistry and precise U–Pb zircon chronology: Australian Journal of Earth Sciences, v. 54, p. 1123–1136.

Morris, RC 1980, A textural and mineralogical study of the relationship of iron-ore to banded iron-formation in the Hamersley Iron Province of Western Australia: Economic Geology, v. 75, p. 184–209.

Morris, RC 1985, Genesis of iron ore in banded iron-formation by supergene and supergene-metamorphic processes – a conceptual model, edited by KH Wolf: Handbook of strata-bound and stratiform ore deposits: Amsterdam, Elsevier, p. 73–235.

Morris, RC, Thornber, MR and Ewers, WE 1980, Deep-seated iron ores from banded iron-formation: Nature, v. 288, p. 250–252.

Mueller, AG 1991, The Savage Lode magnesian skarn in the Marvel Loch gold–silver mine, Southern Cross greenstone belt, Western Australia: Part I. Structural setting, petrography and geochemistry: Canadian Journal of Earth Sciences, v. 28, p. 659–685.

Mueller, AG 1997, The Nevoria gold skarn deposit in Archean iron-formation, Southern Cross greenstone belt, Western Australia: I. Tectonic setting, petrography, and classification: Economic Geology, v. 92, p. 181–209.

Mueller, AG and McNaughton, NJ 2000, U–Pb ages constraining batholith emplacement, contact metamorphism, and the formation of gold and W–Mo skarns in the Southern Cross area, Yilgarn Craton, Western Australia: Economic Geology, v. 95, p. 1231–1258.

Mueller, AG, Nemchin, AA and Frei, R 2004, The Nevoria gold skarn deposit, Southern Cross reenstone Belt, Western Australia: II. Pressure–temperature–time path and relationship to postorogenic granites: Economic Geology, v. 99, p. 453–478.

Naldrett, AJ 1973, Nickel sulfide deposits: their classification and genesis with special emphasis on deposits of volcanic association: Transactions of the Canadian Institute of Mining and Metallurgy, v. 76, p. 183–201.

Nelson, DR 1995, 112163: rhyolite, Bandalup; Geochronology Record 490: Geological Survey of Western Australia, 4p.

Nelson, DR 2001, 168960: meta-ignimbrite, Marda Tank; Geochronology Record 194: Geological Survey of Western Australia, 4p.

Pawley, MJ, Wingate, MTD, Kirkland, CL, Wyche, S, Hall, CE, Romano, SS and Doublier, MP, 2012, Adding pieces to the puzzle: episodic crustal growth and a new terrane in the northeast Yilgarn Craton, Western Australia: Australian Journal of Earth Sciences, v. 59, p. 603–623.

Perring, CS, Barnes, SJ and Hill, RET 1995, The physical volcanology of Archaean komatiite sequences from Forrestania, Southern Cross Province, Western Australia: Lithos, v. 34, p. 189–207.

Perring, CS, Barnes, SJ and Hill, RET 1996, Geochemistry of komatiites from Forrestania, Southern Cross Province, Western Australia: evidence for crustal contamination: Lithos, v. 37, p. 181–197.

Perring, CS, Barnes, SJ and Hill, RET 1997, The geology and volcanological setting of komatiite-hosted nickel sulphide ore shoots from Forrestania, Southern Cross greenstone belt, *in* Geology and mineralization of the south central Yilgarn Craton, Western Australia — a field guide: Kalgoorlie '97 *compiled by* WK Witt: Geological Survey of Western Australia, Record 1997/8, p. 42–63.

Pidgeon, RT, Wingate, MTD, Bodorkos, S and Nelson, DR 2010, The age distribution of detrital zircons in quartzites from the Toodyay – Lake Grace Domain, Western Australia: implications for the early evolution of the Yilgarn Craton: American Journal of Science, v. 310, p. 1115–1135.

Porter, DJ and McKay, KG 1981, The nickel sulfide mineralization and metamorphic setting of the Forrestania area, Western Australia: Economic Geology, v. 76, p. 1524–1549.

Portman, 2008, Annual report 2007, p. 12 (unpublished).

Powell, CM, Oliver, NHS, Li, Z-X, Martin, DM and Ronaszeki, J 1999, Synorogenic hydrothermal origin for giant Hamersley iron oxide ore bodies: Geology, v. 27, p. 175–178.

Pyke, DR, Naldrett, AJ and Eckstrand, OR 1973, Archean ultramafic flows in Munro township, Ontario: Geological Society of America Bulletin, v. 84, p. 955–978.

Ramanaidou, ER 2009, Genesis of lateritic iron ore from banded iron-formation in the Capanema mine (Minas Gerais, Brazil): Australian Journal of Earth Sciences, v. 56, p. 605–620.

Rasmussen, B, Fletcher, IR, Muhling, JR and Wilde, SA 2010, In situ U–Th–Pb geochronology of monazite and xenotime from the Jack Hills belt: implications for the age of deposition and metamorphism of Hadean zircons: Precambrian Research, v. 180, p. 26–46.

Riganti, A, Wyche, S, Wingate, MTD, Kirkland, CL and Chen, SF 2010, Constraints on ages of greenstone magmatism in the northern part of the Southern Cross Domain, Yilgarn Craton, *in* Fifth International Archean Symposium abstracts *edited by* IM Tyler and CM Knox-Robinson: Geological Survey of Western Australia, Record 2010/8, p. 119–122.

Romano, SS, Doublier, MP, Mole, DR, Thébaud, N, Wingate, MTD and Kirkland, CL 2010, Age constraints in the southern part of the Southern Cross Domain of the Yilgarn Craton, *in* Fifth International Archean Symposium abstracts *edited by* IM Tyler and CM Knox-Robinson: Geological Survey of Western Australia, Record 2010/8, p. 206–208.

Romano, SS, Thébaud, NJM, Mole, DR, Wingate, MTD, Kirkland, CL and Doublier, MP (2013), Geochronological constraints on nickel metallogeny in the Lake Johnston belt, Southern Cross Domain: Australian Journal of Earth Sciences, doi:10.1080/08120099.2013.812579.

Qiu, YM, McNaughton, NJ, Groves, DJ and Dalstra, HJ 1999, Ages of internal granitoids in the Southern Cross region, Yilgarn Craton, Western Australia, and their crustal evolution and tectonic implications: Australian Journal of Earth Sciences, v. 46, p. 971–981.

Squire, RJ, Allen, CM, Cas, RAF, Campbell, IH, Blewett, RS and Nemchin, AA 2010, Two cycles of voluminous pyroclastic volcanism and sedimentation related to episodic granite emplacement during the Late Archean: eastern Yilgarn Craton, Western Australia: Precambrian Research, v. 183, p. 251–274.

Stipp, M, Stünitz, H, Heilbronner, R and Schmid, SM 2002, The eastern Tonale fault zone: a 'natural laboratory' for crystal plastic deformation of quartz over a temperature range from 250°C to 700°C: Journal of Structural Geology, v. 24, p. 1861–1884.

Taylor, D, Dalstra, HJ, Harding, AE, Broadbent, GC and Barley, ME 2001, Genesis of high-grade hematite orebodies of the Hamersley Province, Western Australia: Economic Geology and the Bulletin of the Society of Economic Geologists, v. 96, p. 837–873.

Taylor, SR, McLennan, SM, Armstrong, RL and Tarney, J 1981, The composition and evolution of the continental crust: rare earth element evidence from sedimentary rocks [and discussion]: Philosophical Transactions of the Royal Society of London, Series A, Mathematical and Physical Sciences, v. 301, p. 381–399.

Thébaud, N and Barnes, SJ 2012. Geochemistry of komatiites in the Southern Cross belt, Youanmi Terrane, Western Australia: Australian Journal of Earth Sciences, v. 59, 695–706.

Thébaud, N, Doublier, MP, Mole, D, Wingate, MTD, Kirkland, CL, Romano, SS and Wyche, S (in prep.): New constraints on stratigraphy and magmatism of the Southern Cross – Forrestania area.

Thébaud, N, Fiorentini, M, McCuaig, C, Barnes, S, Joly, A, Doublier, MP 2009, Tectonostratigraphic controls on the localization of Archean komatiite-hosted nickel–sulfide deposits and camps in the Yilgarn Craton, Goldschmidt Conference, Davos.

Thébaud, N and Miller, J 2009, U–Pb age constraints on the siliciclastic sediments from the upper supracrustal cover in the Southern Cross greenstone belt, Youanmi Terrane, Western Australia, *in* Smart science for exploration and mining *edited by* PJ Williams et al., Proceedings of the 10th Biennial SGA Meeting, Townsville, Queensland, p. 960–962.

Thorne, WS, Hagemann, SG and Barley, ME 2004, Petrographic and geochemical evidence for hydrothermal evolution of the North Deposit, Mt Tom Price, Western Australia: Mineralium Deposita, v. 39, p. 766–783.

Van Kranendonk, MJ and Ivanic, TJ 2009, A new lithostratigraphic scheme for the northeastern Murchison Domain, Yilgarn Craton, in Geological Survey of Western Australia annual review 2007–08: Geological Survey of Western Australia, Perth, Western Australia, p. 34–53.

Van Kranendonk, MJ, Ivanic, TJ, Wingate, MTD, Kirkland, CL and Wyche, S 2013, Long-lived, autochthonous development of the Archean Murchison Domain, and implications for Yilgarn Craton tectonics: Precambrian Research, v. 229, p. 49–92.

Wang, Q, Schiøtte, L and Campbell, IH 1996, Geochronological constraints on the age of komatiites and nickel mineralisation in the Lake Johnston greenstone belt, Yilgarn Craton, Western Australia: Australian Journal of Earth Sciences, v. 43, p. 381–385.

Wilde, SA 2001, Jimperding and Chittering metamorphic belts, southwestern Yilgarn Craton, Western Australia: a field guide: Geological Survey of Western Australia Record 2001/12, 24p.

Wilde, SA and Pidgeon, RT 1986, Geology and geochronology of the Saddleback Greenstone Belt in the Archaean Yilgarn Block, southwestern Australia: Australian Journal of Earth Sciences, v. 33, p. 491–501.

Wingate, MTD, Kirkland, CL and Doublier, MP 2012b, 199043: metamonzogranite dyke, Marvel Loch; Geochronology Record 1076: Geological Survey of Western Australia, 4p.

Wingate, MTD, Kirkland, CL, Riganti, A and Wyche, S 2011, 185990: metagabbro, Grass Flat Bore; Geochronology Record 868: Geological Survey of Western Australia, 4p.

Wingate, MTD, Kirkland, CL, Wyche, S and Riganti, A 2012a, 185988: metasandstone, Kim Bore; Geochronology Record 1082: Geological Survey of Western Australia, 5p.

Witt, WK 1997, Geology of the Ravensthorpe and Cocanarup 1:100 000 sheets: Geological Survey of Western Australia, 1:100 000 Geological Series Explanatory Notes, 26p.

Witt, WK 1998, Geology and mineral resources of the Ravensthorpe and Cocanarup 1:100 000 sheets: Geological Survey of Western Australia, Report 54, 152p.

Witt, WK 1999, The Archaean Ravensthorpe Terrane, Western Australia: synvolcanic Cu–Au mineralization in a deformed island arc complex: Precambrian Research, v. 96, p. 143–181.

Witt, WK, Drabble, M and Bodycoat, FM 2001, Yilgarn Star gold deposit, Southern Cross greenstone belt, Western Australia: geological setting and characteristics of an amphibolites facies orogenic gold deposit, *in* World-class gold camps and deposits in the eastern Yilgarn Craton, Western Australia, with special emphasis on the Eastern Goldfields Province *edited by* SG Hagemann, P Neumayr and WK Witt: Western Australia Geological Survey, Record 2001/17, p. 45–62.

Wyche, S, Kirkland, CL, Riganti, A, Pawley, MJ, Belousova, E and Wingate, MTD 2012, Isotopic constraints on stratigraphy in the central and eastern Yilgarn Craton, Western Australia: Australian Journal of Earth Sciences, v. 59, p. 657–670.

Wyche, S, Nelson, CS and Riganti, A 2004, 4350–3130 Ma detrital zircons in the Southern Cross Granite–Greenstone Terrane, Western Australia: implications for the early evolution of the Yilgarn Craton: Australian Journal of Earth Sciences, v. 51, p. 31–45.

RECORD 2013/11

GEOLOGICAL SETTING OF MINERAL DEPOSITS IN THE SOUTHERN CROSS DISTRICT — A FIELD GUIDE

This Record is published in digital format (PDF) and is available as a free download from the DMP website at <http://www.dmp.wa.gov.au/GSWApublications>.

Further details of geological products produced by the Geological Survey of Western Australia can be obtained by contacting:

Information Centre
Department of Mines and Petroleum
100 Plain Street
EAST PERTH WESTERN AUSTRALIA 6004
Phone: (08) 9222 3459 Fax: (08) 9222 3444
http://www.dmp.wa.gov.au/GSWApublications

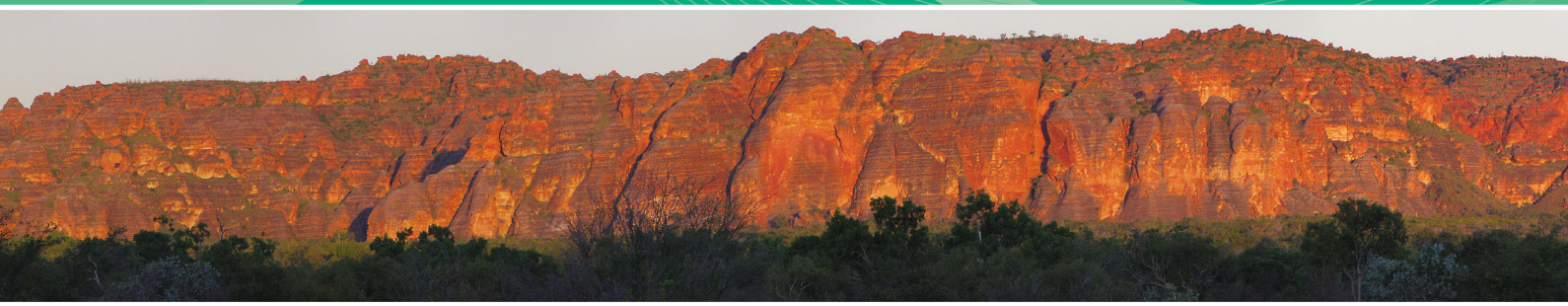

Doublier et al.